Fabrication of Ceramic Filtration Membrane Using Suspension Plasma Spray Process

Elnazsadat Ale ebrahim

A Thesis

In

The Department

of

Mechanical, Industrial and Aerospace Engineering

Presented in Partial Fulfillment of the Requirements

For the Degree of Master of Applied Science (Mechanical Engineering) at

Concordia University

Montreal, Quebec, Canada

Summer 2018

CONCORDIA UNIVERSITY
School of Graduate Studies

This is to certify that the thesis prepared

By: Elnazsadat Ale ebrahim

Entitled: Fabrication of Ceramic Filtration Membrane Using Suspension Plasma Spray Process

and submitted in partial fulfillment of the requirements for the degree of

Master of Applied Science (Mechanical Engineering)

complies with the regulations of the University and meets the accepted standards with respect to originality and quality.

Signed by the final examining committee:

_____ Chair

R. Wuthrich

_____ Examiner

M. Pugh

_____ Examiner

A. De Visscher

_____ Thesis Supervisor(s)

C. Moreau

_____

A. Dolatabadi, S. Rahaman

Approved by _____

Chair of Department or Graduate Program Director

_____

Dean,

Date _____

Abstract

Fabrication of Ceramic Filtration Membrane Using Suspension Plasma Spray Process

Elnazsadat Ale ebrahim

Suspension plasma spraying (SPS) is an emerging versatile and scalable coating technology for deposition of sub-micron sized particles on different substrates to generate coatings with fine microstructures and high mechanical and physical properties. This work, was the first attempt to fabricate ceramic filtration membrane with SPS technique.

Porous pressure driven ceramic filtration membranes with asymmetric micro structures are effective tools for removing pollutants in many industries. Depending on the contaminants of concern, submicron to a few micron-sized pores are essential for this application. Suspension plasma spray enables deposition of a few microns to nano-sized particles to generate such a microstructure. Titanium dioxide membrane has gained interest as water treatment filter due to its mechanical, chemical and thermal stability, its nontoxicity, availability and photocatalytic property.

The promising results of this study confirmed the potential of suspension plasma spray technique as an emerging process in ceramic membrane manufacturing. Porous water permeable titanium dioxide membrane with 14% of open porosity and considerable water flux was produced, in which the network of open pores was generated by accumulation of un-melted and re-solidified particles. In addition, SPS titanium dioxide membrane exhibited photocatalytic property.

Acknowledgments

I would like to express my sincere gratitude to my supervisor, Dr. Christian Moreau, and to my co supervisors, Dr. Ali Dolatabadi and Dr. Saifur Rahaman, for their professional guidance, insightful comments, immense knowledge and continuous encouragement throughout my research work. It has been a great honor to have the chance of working under their supervision.

My sincere thanks also goes to Dr. Fariba Tarasi who supported me thoroughly with her knowledge and experience. My special thanks also goes to Dr. Fadhel Ben Ettouil, to Ali Nozari, Dr. Navid Sharifi and to all my fellow labmates in thermal spray and multiphase flow laboratory at Concordia University who helped and supported me unconditionally through my thesis work.

Last but not the least, I would like to thank my family, for supporting me spiritually throughout writing this thesis and my life in general. This accomplishment would not have been possible without them.

Contents

List of Figures

List of Tables

1. Introduction and literature review

Removing hazardous pollutants is a major concern of many industries such as chemical, petrochemical, mechanical, automotive, textile, pulp and paper, biotechnology, cosmetic, pharmaceutical and food and beverages. Filtration using membranes is known as an effective, sustainable, inexpensive and eco-friendly technique to remove contaminants. Water treatment is another major area, in which filtration plays an important role.

71% of the surface on earth is covered with water. However, 97.5% of the water cycle on earth is dominated by oceans. Water resources directly usable for humans , fresh liquid and atmospheric water, include less than 1% of the existing resources [1]. During the last century, global water demand has increased drastically due to the growth in global population resulting in increase in water demand by sevenfold [2]. Around 4 billion people live under conditions of severe water scarcity for at least 1 month of the year, while 0.5 billion people experience severe water scarcity through the whole year [3][4]. Beside the global water shortage, poor water quality in many parts of the world is the main cause for diseases such as cholera and diarrhea. Managing the current water challenge requires better protection of the remaining water resources as well as development of affordable and modern water treatment methods.

Porous ceramic membrane are considered as effective tools to remove pollutants and are used in liquid filtration process in many industries. Compared to polymeric membranes, which are widely used in industrial applications due to their low manufacturing prices and their acceptable performance, ceramic membranes show more reliability in terms of their higher mechanical, thermal and chemical stability. However, due to their complex and expensive manufacturing processes, their application is restricted to the areas in which improved properties cannot be provided by polymer membranes [2].

Ceramic filtration membranes are conventionally fabricated by methods such as sol-gel and slip casting. However, an improvement in membranes properties such as productivity, selectivity, fouling resistance and stability are needed [2]. New membrane materials as well as new manufacturing methods need to be developed to produce inexpensive and more efficient membranes.

Thermal spraying includes a group of melting- spraying processes in which small particles of almost all types of materials including, metals, ceramics and polymers can be deposited through melting the particles and accelerating them to impact a substrate. This can be carried out by combustion flame or a dc or rf plasma arc. Depending on the thermal spray process, the feedstock could be in the form of powder, wire or rod. Coating is generated by successive impact of melted and semi melted particles to the substrate in the form of splats [5]. In addition, high deposition rate and relatively low operation cost were the drivers for their further development [6]. Suspension plasma spray is an emerging thermal spray technique, in which using a liquid media such as water and ethanol to carry the feedstock powder allows to deposit sub-micron size particles. As far as we know, this work was the first attempt in order to manufacture ceramic filtration membranes with suspension plasma spray process.

1.1. Liquid filtration membranes

A membrane is basically a selective barrier between two environments [7]. Industrial use of membranes started in early 20th century in petroleum industries [8]. Between 1977 and 1993 organic membrane units was used in refinery applications such as H_2 recovery, adjustment of H_2/CO ratio in stream methane reformers and for separation of CO_2 from light hydrocarbon streams [9]. Successful achievements in using membranes in gas separation technologies led to efforts to employ them for liquid- liquid and solid- liquid separation purposes. Using pressure driven membranes started in mid 1980s by the introduction of low-pressure nano- filtration membranes, which was followed by the first industrial use of membranes to separate organic solvent mixtures by employing reverse osmosis membranes to separate a solution of methyl ethyl ketone and lube oil [10]. The development of porous ceramic membranes started in early 1940s for the enrichment of U235 [11]. In 1980s, micro filtration and ultra-filtration inorganic membranes were used industrially [2]. Nowadays, gas separation, pervaporation and electrochemical processes are used for separation purposes. However, Pressure driven membranes have remained the most dominant in the field of water treatment technologies [2]. Table 1 shows the classification of pressure driven membranes in four groups, namely micro filtration, ultra-filtration, nano filtration and reverse osmosis, based on the pore size, permeability, pressure under which they perform and their selectivity [12].

Table 1. Classification of filtration membranes [12].

	Micro- filtration	Ultra-filtration	Nano- filtration	Reverse Osmosis
Permeability (L/h.m².bar)	>1000	10-1000	1.5-3	0.005-1.5
Pressure (bar)	0.1- 2	0.1- 5	3- 20	5- 120
Pore size (nm)	100- 10,000	2- 100	0.5- 2	< 0.5
Rejected species:	-	-	-	+
Monovalent ions	-	-/+	+	+
Multivalent ions	-	-	-/+	+
Small organic compounds	-	+	+	+
Macromolecules Particles	+	+	+	+
Separation mechanism	Sieving	Sieving	Sieving, Charge effects	Solution diffusion
Applications	Clarification, Pre-treatment, Removal of bacteria	Removal of multi molecules, bacteria, viruses	Removal of multivalent ions and relatively small organics	Ultrapure water, desalination

Based on the material used to manufacture membranes, they are classified in four groups, namely organic polymer, inorganic, organic- inorganic (mixed matrix); and biological membranes [10][13].

1.1.1. Organic membranes

Most of the technically used membranes are produced from organic polymer membranes [13] [14].

Conventional organic membranes are made with a single membrane material, in which a thin porous skin is placed on top of a porous support with larger pores and higher number of pores compared to the skin [10][13]. In this structure, the separation is performed by the top layer, while the bottom layer provides a low- resistant path for water. Thin film composite membranes, illustrated in Fig. 1, are another group of these membranes, in which the skin and the support are made of two types of polymers. In this case, the properties of the support and the skin can be chosen separately in order to optimize the performance and the cost of membrane [15][16].

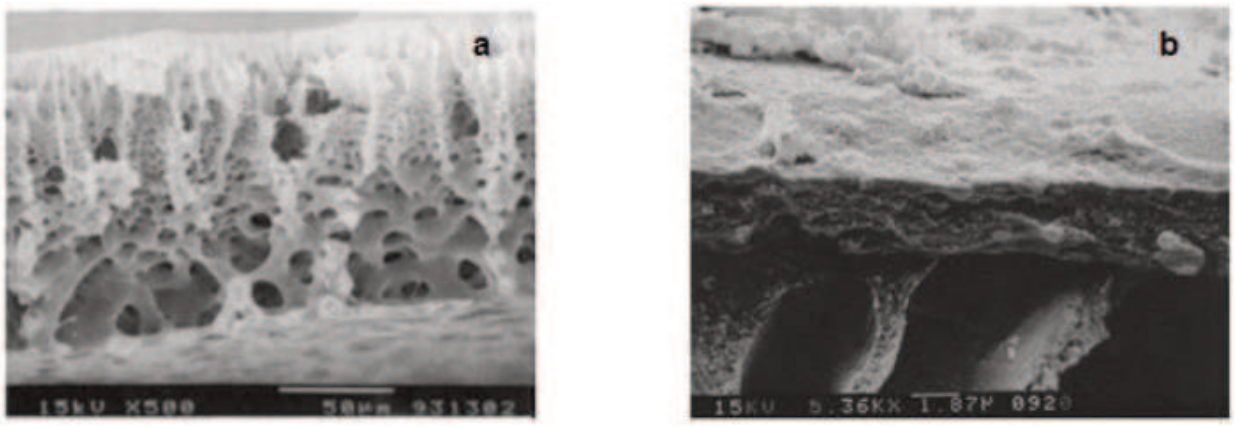

Fig. 1. a) Cross-section of an anisotropic microporous membrane and b) cross- section of a thin-film composite membrane [16].

The most common materials for organic membranes are cellulose acetate and its other derivations [10]. Other membrane materials include polysulfone (PSf), polyethersulfone (PES), sulfonated PSf or PES, polyacrylonitrile (PAN), polypropylene (PP), polytetrafluoroethylene (PTFE), and polyvinylidine fluoride (PVDF) [2] [16].

1.1.2. Inorganic membranes

Enhanced mechanical, thermal, and chemical stability of ceramics makes them an ideal material to produce separation membranes especially to be employed in aggressive environments. Ceramic membranes are commercially fabricated by slip casting-sintering method and to a more limited level by sol-gel technique. However, their application has been limited to those areas in which polymer membranes cannot be used, due to their higher price which has been made them unsuitable for large scale applications [10] [12].

Ceramic water treatment membranes, their characteristics and fabrication methods will be discussed in detail in the next sections.

1.1.3. Organic- inorganic membranes

Introducing nano particles to membrane technology has provided the possibility of combining enhanced functional properties of inorganic membranes with lower cost more available and more easily produced organic membranes in order to increase the flux and decrease fouling. In these

group of membranes an inorganic filler is usually combined with a polymeric matrix [2] [17]. Nano particles have been used as filler include TiO_2 [18], $Al_2\ O_3$ [19], SiO_2 [20], ZrO_2 [21] and Ag [22].

1.2. Ceramic water treatment membranes

Ceramic membranes with their superior properties propose an interesting solution for liquid filtering purposes in many industries [23]. Polymer membranes are not reliable in aggressive acidic or basic environments, would dissolve in many solvents and cannot be used in temperatures over 100 ^{o}C. Ceramic membranes can be cleaned by back flush, by high temperature sterilization or by chemical agents and they do not swell or deform. In addition some ceramic materials such as titanium dioxide, have anti fouling property, which makes them to be able to photodegrade organic pollutants [11][13].

On the other hand, compared to polymer membranes ceramic membranes are more expensive and sealing them in metallic housing is not easy. In addition, they are brittle, much heavier and have lower packing density [10].

1.2.1. Microstructural features of ceramic water treatment membranes

Ceramic water treatment membranes have been traditionally produced by slip casting technique and to a more limited level by sol- gel method with an asymmetric microstructure, which is illustrated in Fig. 2. This structure is built of multiple porous layers on top of each other, in which pore size and thickness of the layers decrease respectively from the bottom layer to the top layer. The bottom layer with the largest pore size provides the mechanical support for the membrane system as well as a low- resistance path for water to pass [17].

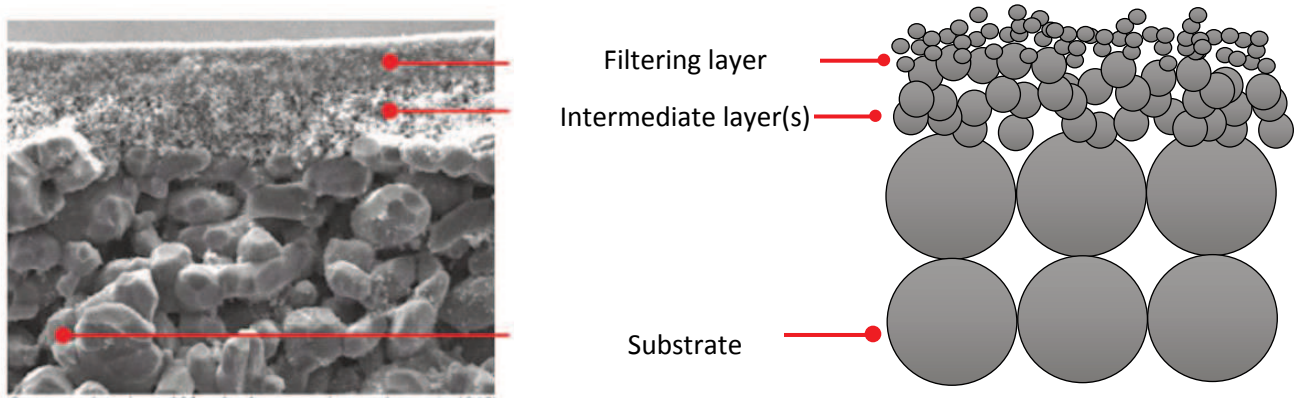

Fig. 2. Asymmetric microstructure of ceramic water treatment membranes [17].

The substrate is usually manufactured using a mixture of metal oxide powders and binders by extrusion or slip-casting with the thickness of the order of mm and have pore sizes larger than 1 μm [24][25]. The intermediate layer(s) with medium pore size is to prepare the surface for applying the filtering layer by preventing the top layer material to penetrate into the large pores of the support and also to provide a smoother surface for the application of mush thinner filtering layer during the synthesis process. Furthermore, it adjusts the pressure gradient through the membrane system. However, in many cases this layer can be removed. The top layer, which is the filtering layer owns the smallest pore size. The filtering layer needs to be uniform, defect free with a narrow pore size distribution and it has to be very thin [26]. This is the configuration that serves both quality and quantity purposes, since it provides a highly selective barrier with elevated flux. However, producing a defect free filtering layer is not easy with commercial manufacturing methods. A too thick layer is more prone to crack during drying and sintering process and a too thin layer is more likely to form incompletely, which would not cover the whole surface of the substrate [27]. The ideal thickness for the filtering layer is still not clear. However, it has been suggested that the thickness should be more than 50 times the diameter of the particles used for fabricating that [17]. Since the flux is inversely proportional to the thickness of the separation layer, it should be thin enough to obtain a reasonably high flux. On the other hand, it should be

thick enough to allow the filtering process to take place. Figure. 3 illustrates slip casting and sol-gel processes for manufacturing inorganic membranes.

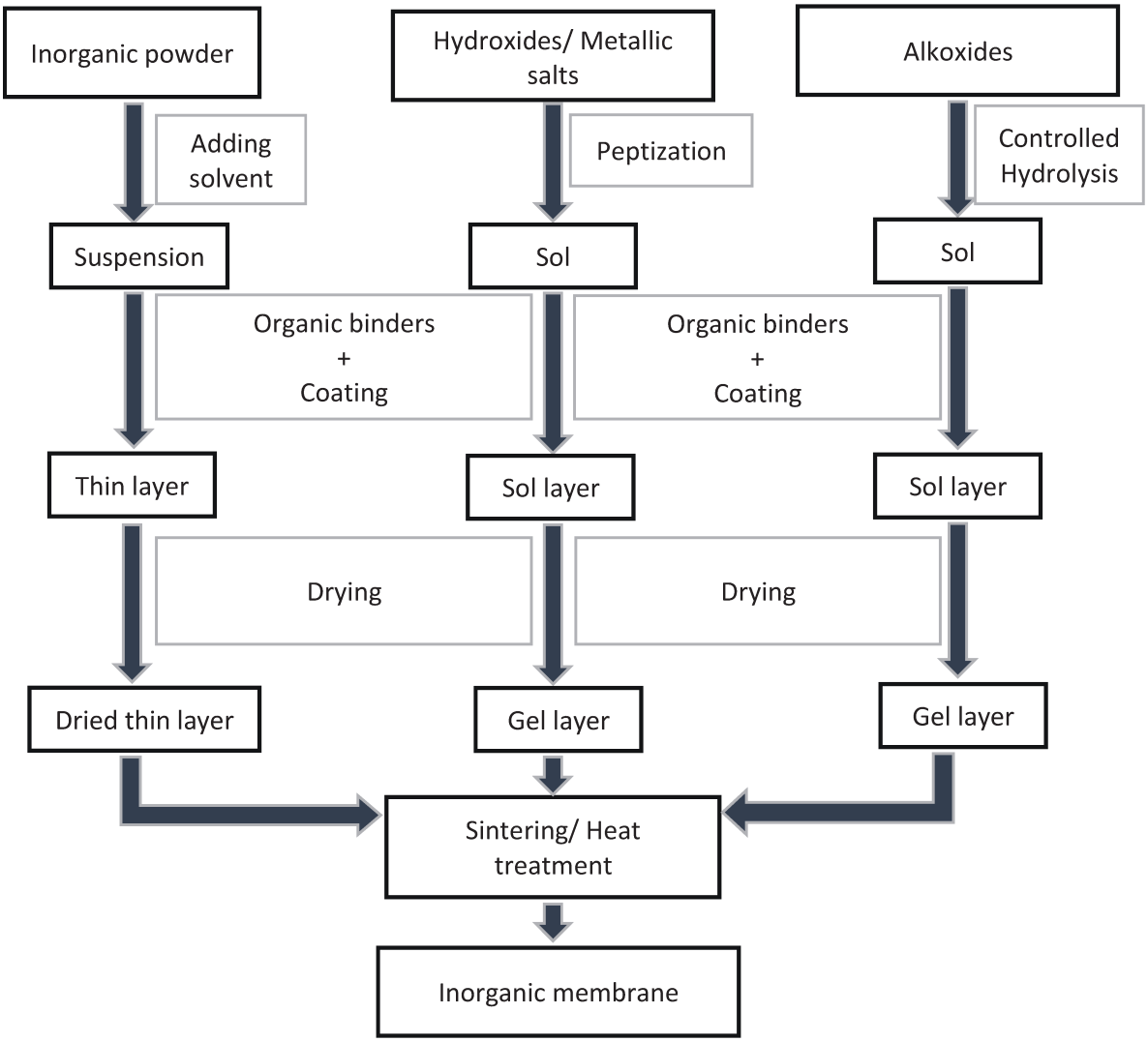

Fig. 3. Summary of ceramic membranes manufacturing techniques. Adapted from [38].

In all these methods, the fabrication process includes several steps in which ceramic nano particles are deposited on the surface of a porous substrate and are heat treated in order to produce a chemically attached membrane. However, application of nano particles in ceramic membranes is not easily possible due to difficulty of immobilization of these particles on commercial ceramic membranes [17]. There have been several efforts to find an organic binder or other connecting elements in order to overcome this issue [28][29][30]. It has to be underlined that before the sintering process the pore size of the membrane is depended on the particle size of the precursor

[17]. However, it has been shown that the sintering process drastically influences the pore size of the membrane. Bhave et al. found that the pore size of TiO_2 based membranes increased 30 times by increasing the sintering temperature from 550 °C to 1100 °C [26]. Examples of commercial ceramic membranes are shown in Fig. 4.

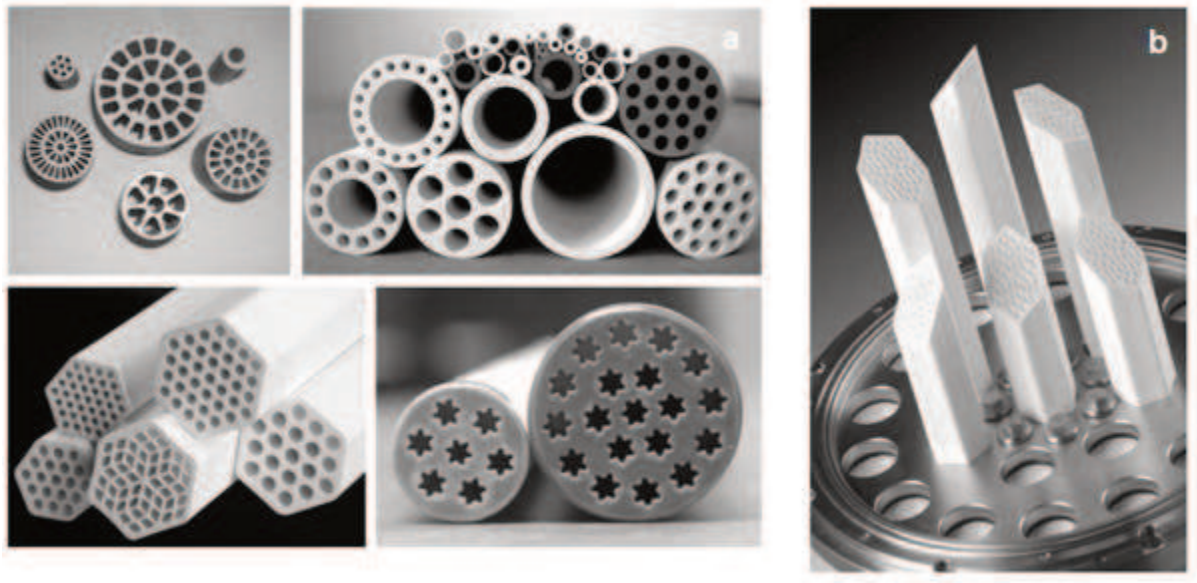

Fig. 4. a) Examples of commercial ceramic membranes. b) A stainless steel housing for ceramic membranes holding 23 modules [2].

1.2.2. Photocatalytical property of titanium dioxide particles

Water treatment systems based on photocatalytic disinfection are commercially available [31], in which the pathogen deactivation is performed by germicidal UV irradiation. With wavelength of 200- 280 nm, UVC light has the capacity to mutate DNA eventually resulting in cell death [32]. The process is simple and ecofriendly. In addition, there is no need to transport or store chemicals, no harmful by products are generated and it does not affect aquatic life negatively. There are also commercial air purifying systems available working based on only UV light illumination [33] and also based on a combination of UV light and TiO_2 catalysts [34].

Choosing titanium dioxide for water filtration purpose is based on its abundance, chemical stability and non-toxicity. In addition, TiO_2 nano particles are highly photo reactive and show anti- fouling activity under UV irradiation [35][36][37][38][39][40]. Using titanium dioxide as a photocatalytic

agent in water treatment has been discussed first in 1976, where an aqueous suspension of TiO_2 was used to degrade polychlorobiphenyls [41]. It is capable of degrading pollutants such as benzene, dyes, and many other chemical contaminants and micro- organism to carbon dioxide, water, and mineral acids [42][43][44].

Figure. 5 illustrates a schematic of the photocatalytic reaction. When a semiconductor is exposed to a photon with energy greater than its band gap energy, an electron in the valence band is excited and by the jump of this excited electron to the conduction band an electron-hole pair is created. At this point three routes are possible. The electron-hole pairs may be recombined, which mostly occurs in the bulk of semiconductor and does not affect the photocatalytic activity. In the case of semiconductors with small particle size, these very reactive species can be transferred to the surface and react with the surrounding environment and two other reactions may also happen. Holes may react with water in order to form hydroxyl $OH^{\cdot}$ Radicals, which are the main cause of photo degradation of organic pollutants [37]. Electrons may react with oxygen molecules to form super excited O^{2-} ions, which are also active towards organic contaminants. In reaction with water molecules they produce hydroxide ions OH^{-} and peroxide radicals $OOH^{\cdot}$. Peroxide radicals then combine with H^{+} ions to form $OH^{\cdot}$ and OH^{-}. Thus, all reactions finally lead to the formation of hydroxyl radicals [44].

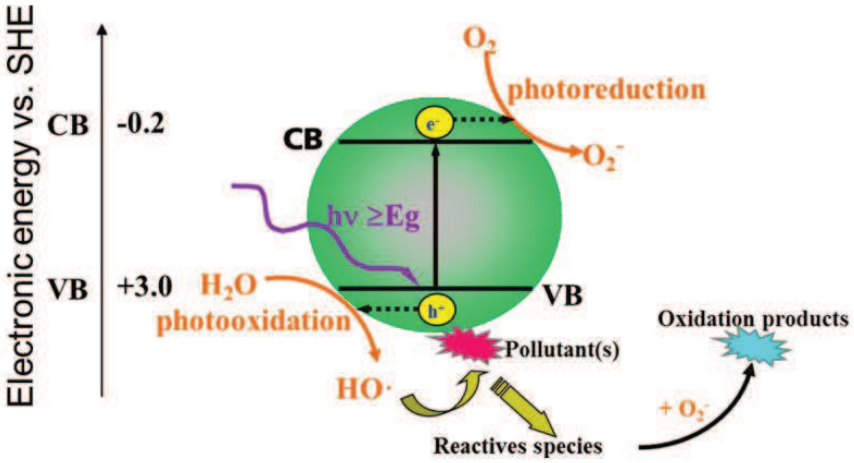

Fig. 5. Schematic of the photocatalytic reaction [42].

Generation of $OH^{\cdot}$ radicals and super excited O^{2-} ions occurs in semiconductors with bandgap energy of around 3 eV, which makes TiO_2 in the form of anatase with bandgap energy of 3.2 eV and with appropriate valence and conduction band positions, the most favorable photocatalytically active candidate [45][46].

Titanium dioxide has three polymorphs, rutile, anatase and brookite. Photocatalytic property of TiO_2 has been mainly associated with the anatase content of the catalyst, due to the higher levels of radicals adsorbed on the its surface resulting in significantly higher photoacatalytical activity compared to rutile.

In order to perform the decontamination process, TiO_2 nanoparticles can be employed directly, which provides maximum activity due to the high reactive surface area [37]. However, recovering the nano-catalyst particles would be an issue adding a post treatment process to the filtration process.

As a solution, magnetic nanoparticles were coated with anatase TiO_2 nano particles enabling the removal of the catalyst by application of a magnetic field [47]. Another approach was to immobilize the TiO_2 nanoparticles on the surface of the membrane.

The drawback of immobilization of catalyst particles was the decrease in photo degradation activity due to the reduction of active surface area [47]. Various methods were used to immobilize the catalyst nanoparticles. The surface of commercial polymer membranes was modified by infiltration of porous polymer membranes with a TiO_2 suspension [48]. TiO_2 nanoparticles were binded on thin film composite membranes by using polydopamine with the capacity of self-polymerization on the surface of both the membranes and the nanoparticles [49]. However, polymeric membranes are not stable under UV irradiation [50]. TiO_2 nanoparticles has been applied to the surface of ceramic membranes as well. Alumina substrates were coated by a mesoporous nano structured TiO_2 film with narrow poresize distribution via sol- gel method with anatase crystalline size of 9 nm [51]. In general, photocatalitycal TiO_2 coatings can be deposited by various methods such as sol-gel, spray pyrolysis, chemical vapor deposition and physical vapor deposition [52]. Photocatalytical property of thermal spray coatings will be discussed in section 2.5.

1.2.3. Ceramic membranes manufactured by thermal spray method

As mentioned in previous sections, wet ceramic methods are used to fabricate ceramic membranes conventionally. All these techniques include several production steps resulting in the process to be time consuming and expensive. Furthermore, they require a high temperature heat treatment step at the end, which is an energy consuming process and can take a long time to complete [53]. Moreover, the pore size of the ceramic membrane depends greatly on the sintering process as well as on the primary powder size [17]. In addition, in the case of using metallic porous substrates, the sintering process may result in densification of the substrate and its oxidation [53].

Numerous coating production techniques have been explored for deposition of thin and thick films, including thermal-spray technologies such as combustion flame spray (CFS), atmospheric plasma spray (APS), vacuum plasma spray (VPS), high- velocity oxygen fuel (HVOF), suspension plasma spray (SPS) and solution precursor plasma spray (SPPS) [6]. Thermal spray technology, provides the possibility to generate coating in a single step process, in which the crystalline structure of the feedstock could be retained [54], which may eliminate the necessity of a post heat treatment process. In addition, it has the potential to create less expensive coatings because of the much higher deposition rate and the ease of automation of the process for mass production compared to wet-ceramic techniques [55]. Depending on the method, a high temperature and high velocity flame, such as a plasma jet or an oxy-fuel jet is used to melt the feedstock particles in the form of powder, suspension and rod (or wire). The molten particles are accelerated toward the substrate and upon their impact, splats are formed. The coating is built by piling up the splats [56]. A schematic of thermal spray process is shown in Fig. 6a. The process can be applied on a wide range of materials such as polymers, metals, alloys, cermets and ceramics [6]. Compared to thin film deposition techniques such as CVD, thermally sprayed coatings may be developed with higher deposition rate and lower process costs. On the other hand, as it is marked in Fig. 6b, the microstructures of these coatings may contain features such as intera- lamellar cracks, macro pores, inter-lamellar cracks, which might be considered as defects in some applications [57].

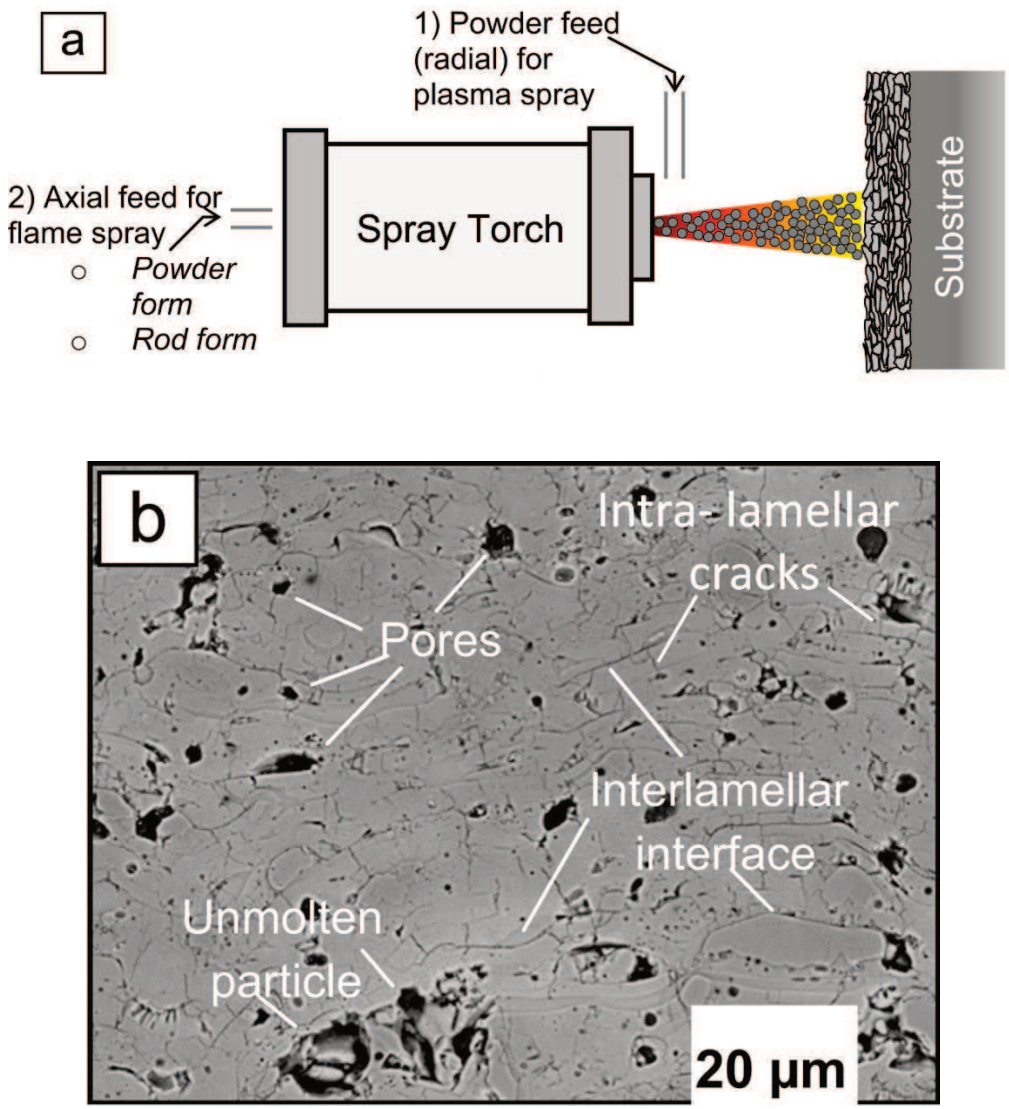

Fig. 6. a) Schematic of the thermal spray process, b) SEM image of the cross section of a sprayed coating showing various features [57].

Coatings generated by thermal spray methods have been used in many industries such as aerospace, automotive, biomedical, steel, pulp and paper [5]. However, there is a limited knowledge in evaluation of the capacity of this group of techniques for ceramic membrane manufacturing. For example, producing solid oxide fuel cells (SOFC) with thermal spray process is an emerging area of investigation. Ma et al. produced multi layers in SOFC by APS and SPPS methods as shown in Fig. 7 [58]. Porous cathode layer as oxygen/air electrode deposited by APS providing a favorable structure for air transportation to the cathode/ electrolyte interface. A gas tight perovskite electrolyte layer was produced with APS and the crystalline microstructure was

retained by a post heat treatment process. The highly porous anode layer was deposited by SPPS[58].

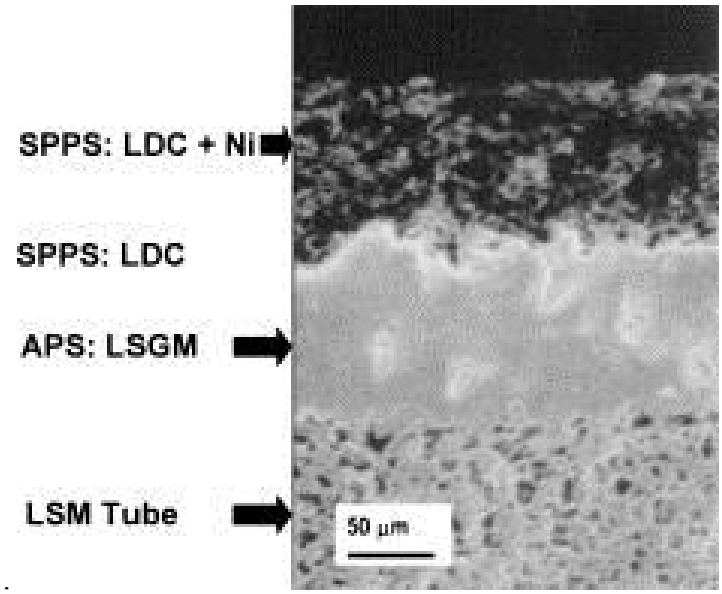

Fig. 7. Structure of multi- layer SOFC produced by thermal spray method [58].

In another study, Kulkarni et al. employed APS and VPS processes in order to produce dense YSZ gas separation membranes. The results they obtained, which is shown in Fig. 8a for APS and in Fig. 8b for VPS coating, determined the generation of much denser coatings with VPS process with about 2.3% of open pores and less defects such as micro cracks [59].

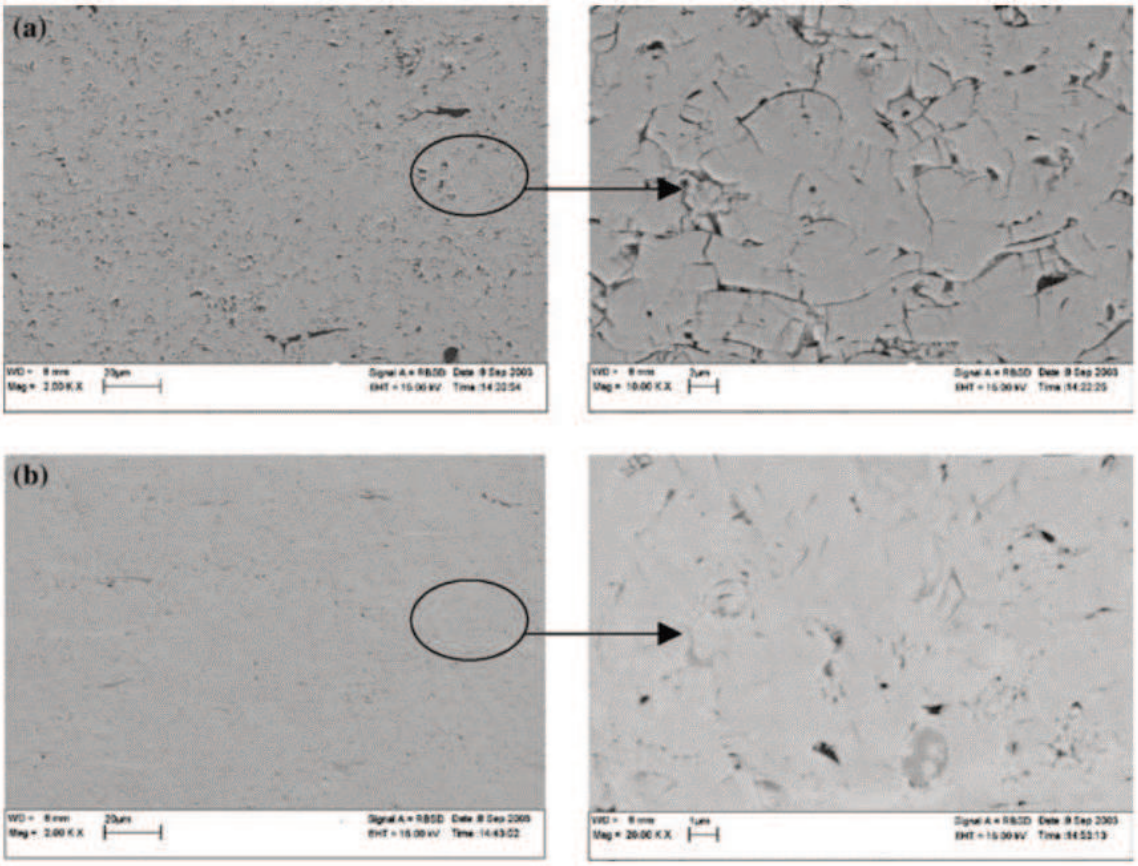

Fig. 8. SEM micrograph of the two coatings with high magnification images (on the right) showing detailed microstructure: (a) APS and, (b) VPS coatings [59].

In another example, Kesler et al. used SPS process to generate dense lanthanum strontium cobalt ferrite oxygen separation membranes. In that study, the coating was deposited on porous metal substrates and smooth dense membranes were obtained at longer stand off distance with very low gas leakage [53].

There have also been some attempts in order to produce filtration membranes with thermal spray techniques. Madaeni et al. produced relatively thick porous stainless steel membranes (0.5mm to 1.25mm), by wire arc spraying [60]. An average pore size of 6.7 µm was obtained at the optimum gun distance with 63% with the mean size smaller than 5 µm (functional in filtration), and 16% with the mean size larger than 10 µm (defects). In their case, increasing the standoff distance more than an optimum value resulted in a decrease in the number of pores. Increasing the gun distance also increased the oxide content of the coating. Water permeability of the membrane was reduced

by increasing the thickness. On the other hand, ion rejection was improved in membranes with higher thickness [60].

In another work, Tung et al. used APS to generate $Al_2O_3/Ni-Cr$ cermet microfiltration membranes with the pore size, porosity and water flux of the cermet membranes in the range of 0.2–0.4 μm, 8–16% and 100–500 LMH/bar, respectively [61].

Ramakrishnan et al. used APS and combustion flame spray (CFS) methods to produce Al_2O_3 microfiltration membranes. They were able to produce filtration coatings with the thickness in the range of 100 – 300 μm, pore sizes in the range of 0.8- 2.6 μm and porosity in the range of 8.5 – 30% [57].

2. Suspension plasma spray process

Suspension plasma spray is an emerging thermal spray technology in which, a liquid such as water or various alcohols are used to carry nano to sub- micron sized particles in the form of colloidal suspension through the injecting system and into the plasma jet [54]. This process has the capacity of generating a tailored coating structure, in which the crystalline phases of the starting powder may be preserved [62].

In thermally sprayed coatings, the pore size depends on the feedstock particle size beside other parameters. For example, in conventional atmospheric plasma spraying, the size of feed stock powder is kept between 10 and 100 μm in order to preserve the followability of the powder [63]. Small particles tend to form larger agglomerates due to electrostatic forces, which may lead to clogging the injecting system. In addition, it is more difficult for the fine particles to penetrate the plasma jet. It means that fine particles may travel in the colder parts of the plasma jet with less heat transfer [64]. As a result, spraying submicron sized particles with APS method requires a carrier gas flow rates as high as 80 slm, which greatly perturbs and intensively cools down the plasma jet [65]. Also, limitation in choosing the minimum particle size used in conventional plasma spray process imposes a limit on the minimum splat size and consequently on minimum thickness of the coating [63], since larger particles are deposited in the form of larger splats with higher thickness.

On the other hand, in SPS process the size of the molten particles are typically in the range of 0.1 – 3 μm, the diameter of the splats are in the range of 0.2 - 6μm and their thickness is between 20 to 300 nm. Consequently, compared to APS, much smaller pore sizes can be obtained and much thinner coatings can be deposited [66].

2.1. Plasma initiation

A schematic of a suspension plasma process is illustrated in Fig 9.

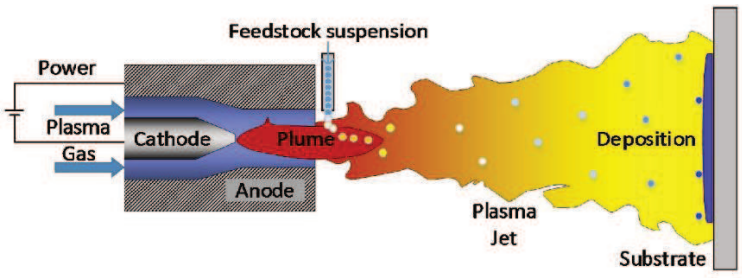

Fig. 9. Schematic of suspension plasma spray process [67].

Plasma is initiated by the struck of an electrical arc between the anode and the cathode. Generation of the electric arc occurs as the result of a voltage breakdown between two electrodes [6]. Plasma gas is usually a combination of gas with a high atomic weight (Ar, N_2) as primary gas and a gas with a high thermal conductivity (H_2, He) or with a high viscosity (He) as the secondary gas [68].

Plasma jet has been described in three sections based on the momentum and the temperature transfer to the particles: *(i)* the hot core, where the particles may have the highest heat and momentum transfers; *(ii)* the plume, where the heat and momentum transfers to the particles are drastically lower compared to the plasma core; and *(iii)* fringe around the plasma core, where the particles might obtain enough momentum but not enough heat transfer [69]. Consequently, the microstructural features of the each layer of the coating depends on the trajectory of the particles in the plasma jet, which itself can be manipulated by the process parameters such as stand- off distance, feeding rate, torch speed and torch power.

Traverse of the torch over the substrate is considered as over lapping of plasma beads. Fully melted particles are those present in the plasma core (center of the bead) and poorly treated particles are those traveled in the fringes. Overlapping the beads, makes it possible for poorly treated particles to attach to the well treated preceding pass and vice versa [69]. A well adjustment of the overlapping plasma beads in the torch raster pattern allows the generation of a uniform well-adhered coating.

2.2. Suspension transport phenomena within the plasma jet

Figure. 10 illustrates a schematic of a series of physical phenomenon, which occurs upon penetration of the feedstock suspension into the plasma jet.

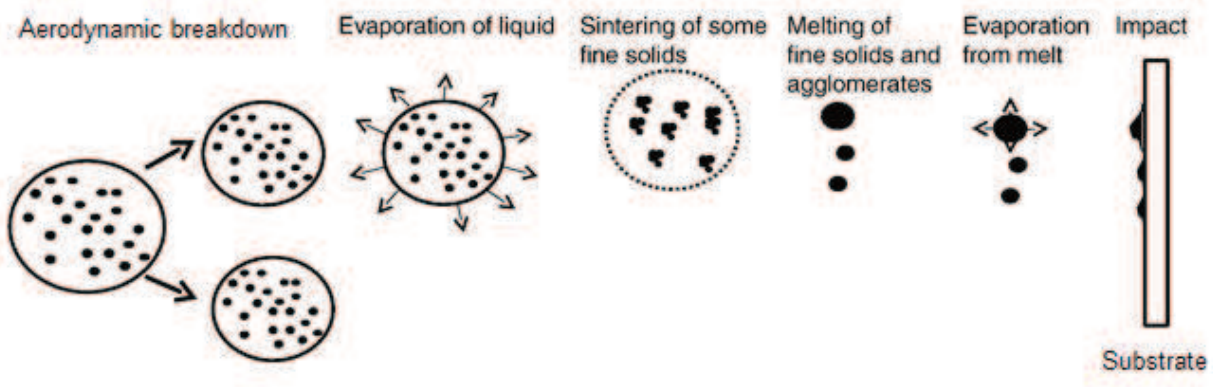

Fig. 10. Physical phenomenon involved in SPS process [39].

When the suspension penetrate the plasma jet aerodynamic drag forces generated by the plasma flow fragments them into smaller droplets. Following the fragmentation process, the liquid containing the particles evaporates because of the high heat flux of the plasma jet [70]. Depending on their size, temporal, spatial and temperature history, inflight particles may sinter, melt or partially melt or evaporate, and some particles may remain un- molten. These particles are accelerated toward the substrate at a velocity ranging from one hundred to several hundred meters per second and upon impinging on the substrate form flattened solidified splats. The formation of the coating results from the successive pile-up of the lamellae formed by these splats on the substrate surface or on the top of the previously deposited lamellae [68].

2.3. Parameters influencing the SPS process

In order to preserve the repeatability of the SPS process and reproducibility of the coatings, many factors need to be taken into consideration.

- Properties of the suspension is one of the important factors influencing the stability and reliability of the process. Suspensions need to be uniform, stable and free of large agglomerates in order to provide a good flowability, to avoid clogging of the injecting system and to produce a uniform coating. In addition, high solid content of the suspension can increase the deposition rate [62]. Particle size distribution of the suspension may affect the heat treatment of the inflight particles and as a result the microstructure of the coating [65].

- The solvent used to prepare the suspension can influence the microstructure of the coating. For example, the higher enthalpy of evaporation of water (2.3×10^6J/kg) compared to other

solvents for example ethanol (0.8×10^6 J/kg), means that it would take a longer time for the solvent carrying the inflight particles to evaporate [39]. As a result, the duration of time that the particles are exposed to high temperature is reduced and so does the heat transfer from the plasma to the particles. This may cause the presence of un-melted particles in the coating that is generated from water based suspension.

- Standoff distance is another parameter that plays a role in the microstructure of the coating. Compared to conventional plasma spraying, the standoff distance in SPS process is shorter. One of the characteristics of conventional plasma torches is the fast decrease of axial velocity of the jet with its expansion out of the torch due to the decrease of the temperature of the plasma jet. As mentioned, in SPS process, the particle size of the feedstock is much smaller compared to the conventional plasma spray methods. When injected into the plasma jet, these small particles are heated and accelerated rapidly. Reaching the colder areas of the plasma jet, they also cool down and decelerate rapidly. As a result, in order to avoid re- solidification of the melted particles before they impact the substrate, the substrate needs to be located closer to the torch [71].

- Another element which highly influences the quality of the coating in SPS process is the arc root fluctuations of the torch due to the voltage fluctuations, which impacts the trajectory and fragmentation of the particles. Heat transfer and composition of the plasma gas influence the arc stability [66].

2.4. Shadow effect

Figure. 11 shows columnar microstructure, which is one of the microstructural features that can be often found in SPS coatings. These features are formed in the shape of cones and their endings appear as bumps on the surface of the coating.

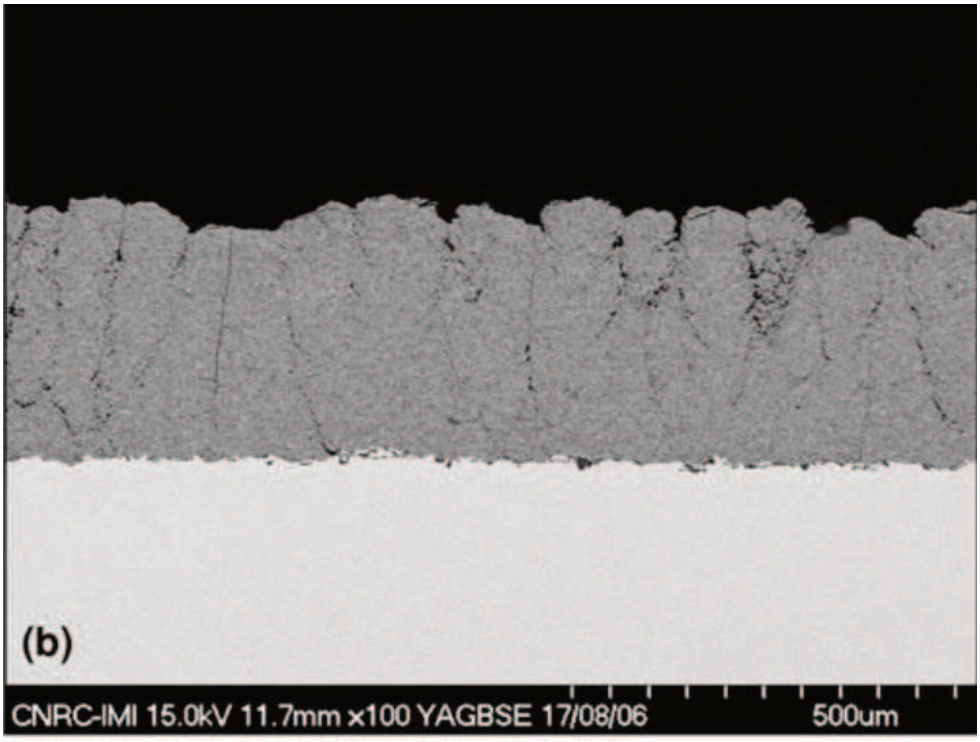

Fig. 11. Columnar microstructure in SPS coating [72].

It has been shown the smaller particles have more sensitivity to gas velocity changes. For these particles, the effect of the velocity component parallel to the substrate become more important than the normal velocity component, resulting them to be dragged parallel to the substrate and more likely to deposit on the sides of surface asperities and create a region of porosity as the coating build up [73]. When the cones grow further, they shadow the underlying porous region and prevent the particles impingement on those areas. Some factors that may possibly promote the shadow effect have been mentioned to be high surface roughness, by providing asperities on the surface and large substrate size and diversion of the plasma jet, by exposing the substrate to the periphery of the plasma jet [72].

2.5. Photocatalytic properties of titanium dioxide thermally sprayed coatings

Thermal spray methods including SPS, have been used to generate photocatalitycally active TiO_2 coatings. By using this group of manufacturing techniques, the catalyst particles form a naturally immobilized layer on the surface of the substrate in a single step manufacturing process.

Toma et al. deposited TiO_2 nano particles by both high velocity oxy fuel (HVOF) and suspension plasma spray (SPS) methods on stainless steel substrates, where SPS coatings showed higher photocatalytical activity. In their study, the higher photocatalytical activity of SPS coating corresponded to the higher content of anatase present in it [74]. A comparison among TiO_2 coatings obtained by APS, SPS and HVOF determined the SPS process to be the most suitable method to generate coatings with a higher photocatalytic activity [75]. This conclusion was also corresponded to the higher anatase content in SPS coatings. However, the influence of anatase content on photocatalytical property of thermal sprayed coatings is still not clear. In another study, Toma et al. found that microstructure and photocatalytical behavior of SPS TiO_2 coatings could be influenced by the type of injecting system (internal or external injecting systems). In that work, coatings sprayed with external injector were more uniform with higher content of anatase, while those sprayed with internal injecting system showed a bimodal microstructure consisting of molten and non- molten areas with lower anatase content. The results of photo degradation of methylene blue on these coatings did not show a direct relation with their anatase content [39].

Studies conducted on TiO_2 thermally sprayed coatings have shown that rutile content of the coating also influences the photocatalitical property of the coatings. Toma et al. found that thermal sprayed coatings with anatase content of 20 vol. % to 65 vol. % exhibited a significant organic pollutants degradation, which increased with increasing the anatase content [59]. The results of a study on 11 SPS TiO_2 coatings deposited by Bannier et al. on various substrates did not show a direct relation between anatase content of the coating and its photocatalytical activity as well [76]. Kozerski et al. showed that the photocatalytic property of SPS TiO_2 coatings did not correlate with the anatase content, since coatings mainly containing rutile had photocatalytical property. They suggested that properties of the thermal spray coating such as porosity, roughness and thickness may also influence its photocatalitycal activity [39]. It has also been suggested that rutile may improve photocatalytical activity by improving the charge carrier separation by trapping the electrons and preventing the electron- hole recombination [77]. In thermal sprayed coatings, anatase content of the coating has been suggested to be the result of the presence of un-melted anatase particles from the feedstock [39], since Anatase transforms to rutile irreversibly at around 900K (~ 600 ^{o}C) [77]. However, In SPS there may also be a possibility for anatase nucleation.

As it is shown in Fig. 12, rutile is the more stable phase compared to anatase with its lower Gibbs free energy.

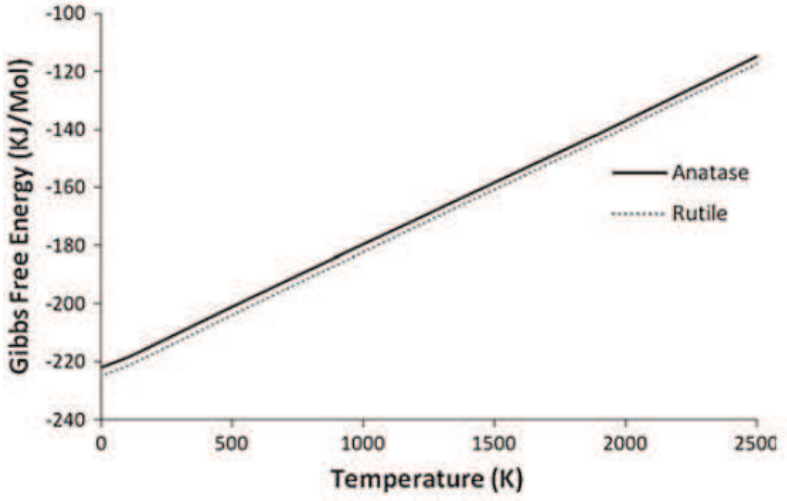

Fig. 12. Gibbs free energy of anatase and rutile versus temperature[77].

However, anatase is often the majority product of TiO_2 films that are synthesis by methods such as sol–gel. It has been suggested that the nucleation of anatase is because of its lower surface free energy compared to rutile, which at small crystallite sizes becomes more influential [77][78]. In SPS, since sub- micron sized particles can be used the nucleation of anatase may be possible.

It has also been calculated that based on free energy of nucleation and interfacial energy between liquid and solid phase, preferential nucleation of metastable anatase during SPS process may occur at high cooling rates. Figure. 13 shows anatase to rutile ratio of critical nucleation free energies as a function of solidification temperature. Anatase may nucleate at the temperatures under 1870 K while rutile may nucleate above this temperature and up to the melting point of titanium dioxide at 2130 K [78].

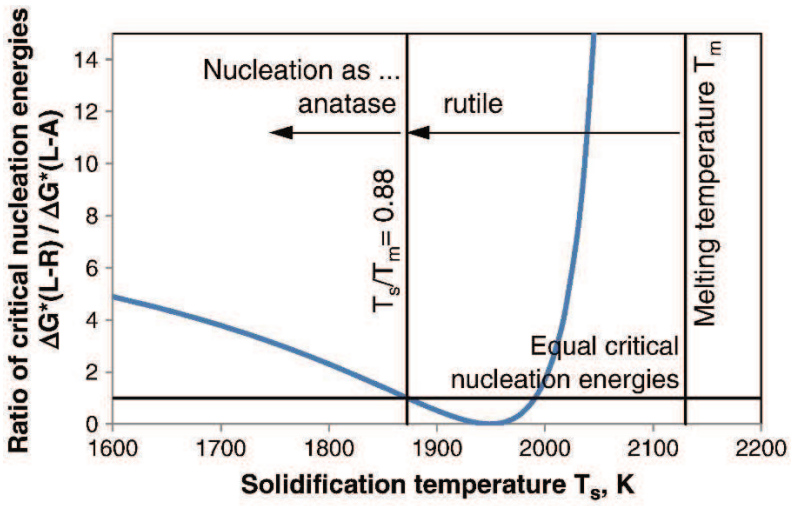

Fig. 13. Anatase to rutile ratio of critical nucleation free energies as a function of solidification temperature Ts [78].

2.6. Objectives

Commercial ceramic membranes for filtration purposes are mainly manufactured by slip casting and sol-gel techniques. Some efforts has been made in the field of producing dense gas separation membranes with atmospheric plasma spray [59] and suspension plasma spray [79]. A few studies were conducted to manufacture microfiltration membranes with atmospheric plasma spray and flame spray[57]. Photocatalytic behavior of titanium dioxide coating fabricated by APS, HVOF and SPS [80][78][38][75] has also been investigated. However, to our knowledge, there has been no studies in order to investigate the potential of SPS process as a new manufacturing method for producing water permeable membranes. The possibility of generating a coating using sub- micron sized particles in suspension plasma spray, brings interesting characteristics in terms of the smaller size of the droplets, which leads to the possibility of generating membrane coatings with smaller pore size and lower thickness that cannot be achieved with other thermal spray techniques. In addition, the possibility to manufacture the membrane in a single step process without further heat treatment provides another advantage compared to conventional ceramic membrane manufacturing processes. The main objective of the current work was to evaluate the capacity of suspension plasma spray for deposition of liquid permeable membranes, which was carried out through:

- Developing SPS titanium dioxide coatings based on different spray parameters and optimization of some parameters.
- Developing SPS titanium dioxide membrane system.
- Characterization of the SPS membrane and evaluation of its performance.

3. Experimental procedures

In this chapter, the experimental procedures for producing suspension plasma sprayed ceramic membrane, characterization of microstructure and evaluation of service performance of the ceramic membranes will be discussed in detail.

The experimental approach followed for deposition of suspension plasma sprayed ceramic membrane on porous ceramic substrate was as follows:

- Preliminary experiment by deposition of a coating on stainless steel substrate. The spray parameters and the suspension used in this experiment was chosen based on a previous work on titanium dioxide hydrophobic thin coatings [67]. The result of the preliminary coating, sample SPS-W-0, showed the presence of columnar features in the micro structure and sedimentation of suspension during SPS process occurred.

- Optimization of the suspension parameters in order to find a suspension with reliable stability that could last throughout the spray process and with a rather low viscosity.

- Designing a full matrix of experiment by evaluation of three parameters at two levels. The resulting 8 spray conditions was used to deposit 8 coatings on stainless steel substrates. The best set of parameters was chosen for producing the final membrane.

- Deposition of ceramic membrane on porous alumina substrate.

- Characterization of the membrane including microstructural characterization, phase analysis and porosity measurement.

- Evaluation of service performance of the membrane including water permeability measurement and photocatalitycal activity evaluation.

As a general rule the coatings generated in this work were identified by the spray process name, solvent and number of experiment. For example, in SPS- W+ E- 1; SPS stands for suspension plasma spray, W stands for water, E stands for ethylene glycol and 1 stands for the number of experiment.

3.1. Procedure of suspension plasma spray process

3.1.1. Plasma generation

In this work, a 3MB plasma torch (Oerlikon-Metco, Switzerland), mounted on a six-axis robot was used for plasma generation. In order to initiate the plasma, Ar was used as the primary gas and H_2 was used as secondary gas.

3.1.2. Suspension feeding

In the suspension feeding system used in this work, the suspension was injected radially into the plasma through an external injection (from outside of the nozzle).

A schematic of the feeding system is described in Fig. 14. The suspension and water, are stored in separate containers. Suspension is introduced to the plasma plum by the means of an injector, which is oriented toward the plasma torch by a 15° angle with respect to y axis. This angle had been chosen in order to keep the particles in the hot core of plasma jet for a longer time. The distance between the tip of the injector and the plasma torch orifice is 20 mm, which is adjusted with micrometers. In this study, an injector with the internal diameter of 0.2 mm was used to inject the suspension into the plasma jet.

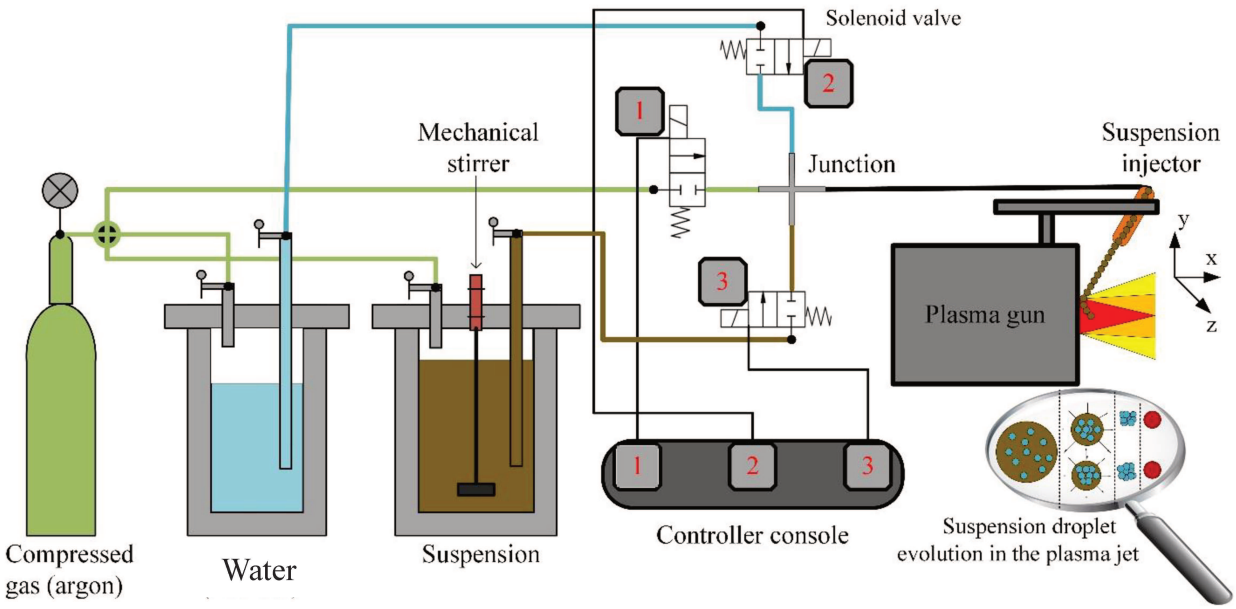

Fig. 14. Schematic of the suspension feeding system in suspension plasma spray [81].

A mechanical stirrer was positioned in the suspension container in order to avoid the sedimentation of the suspension during the spray process. A compressed gas (Ar, 50 psi), is used to force the suspension through the route and to the injector and the suspension flow rate was 33 mL/min. The flow rate was measured by Coriolis flow meter. The pressure could be switched between the suspension container and the water container by the means of a set of solenoid valves through the controlling console. In the feeding system used in this work, suspension was introduced to the system by opening valve number 3.

At the end of each experiment the injection system was cleaned by interval switching between valves number 1 (pressured gas) and valve number 2 (water).

3.2. Feedstock powder characterization

Particle size distribution in the suspension was measured with a laser light scattering technique (Spraytec, Malvern, UK), with the average particle of Dv (50) = 0.3 μm, as it is shown in Fig. 15.

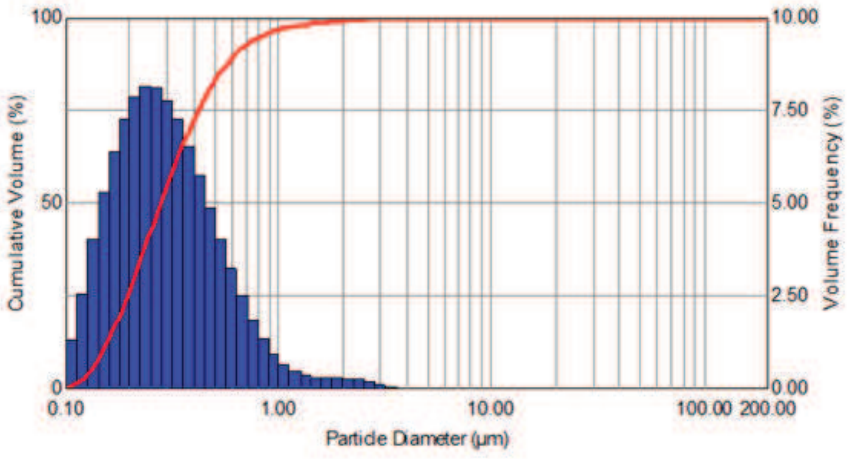

Fig. 15. Particle size analysis of titanium dioxide powder.

Powder particle size was also measured based on SEM images of the feedstock powder with an Image analyzing software (Olympus Stream basic, Canada) and the average powder particle size of 137 nm was obtained by measuring 150 particles. SEM micrograph of TiO_2 powder is shown in Fig. 16.

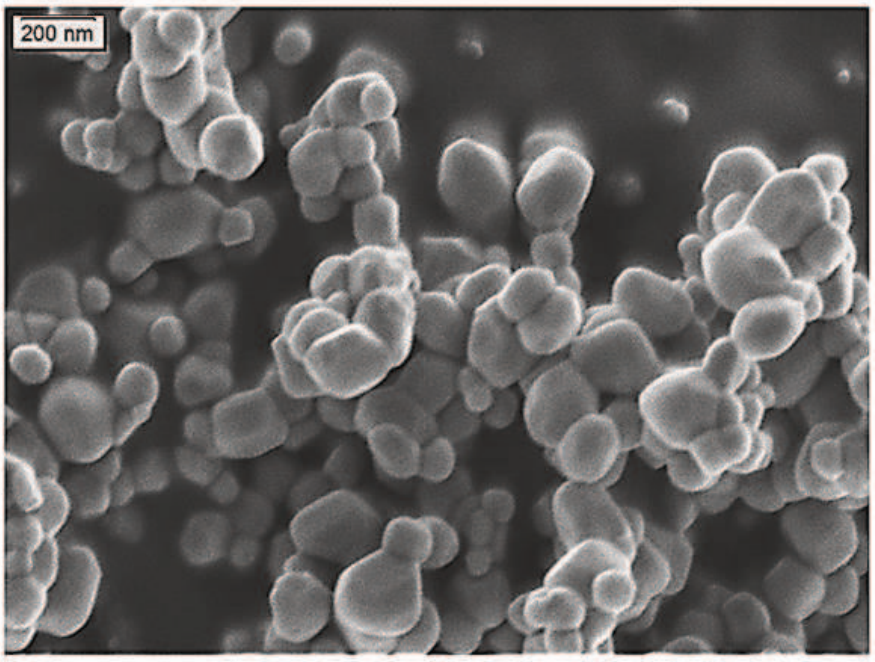

Fig. 16. SEM micrograph of titanium dioxide powder.

The difference between the two above values could be due to that the laser light scattering technique, is a volume-weighted measurement technique, while with SEM images a number-weighted measurement of powder particle size was obtained.

3.3. Substrate characterization

In this work, coatings were deposited on both nonporous stainless steel substrates shown in Fig. 17(a) and porous alumina substrates shown in Fig. 17(b). Stainless steel substrate were used in preliminary experiments in order to find the best process window for deposition of the membrane and alumina substrates were used in order to produce the final membrane system that could be used in service performance tests. Description of the substrates are as follows:

a) Nonporous substrate: Square shaped 304 stainless-steel, 25.4 mm x 25.4 mm x 3 mm

b) Porous substrate: Disc shaped alumina (Kerafol, Germany), 48mm x 2mm, mean pore size of 2μm

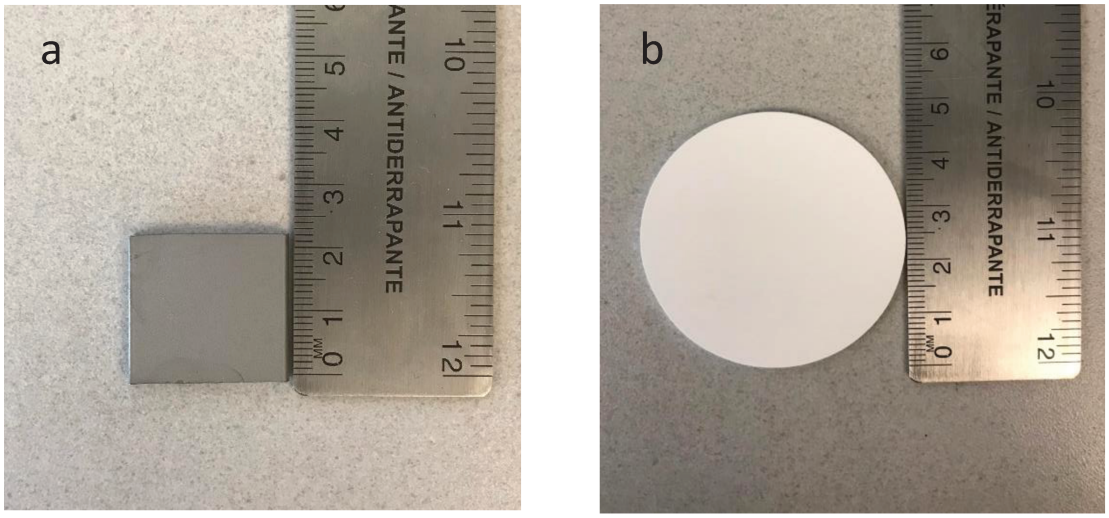

Fig. 17. a) Non porous stainless steel substrate, b) porous alumina substrate.

Porosity of the alumina substrate was measured as 36 % obtained with a mercury intrusion porosimeter (Micromeritics Autopore IV, USA) with a quite narrow pore size distribution. Figure. 18 shows the pore size distribution of the porous alumina substrate. Average pore size of the alumina substrate was 1190 nm with around 80% of the pores are in the range of 1000-3000 nm obtained with a mercury intrusion porosimeter (Micromeritics Autopore IV, USA), which is in agreement with data received from the manufacturer.

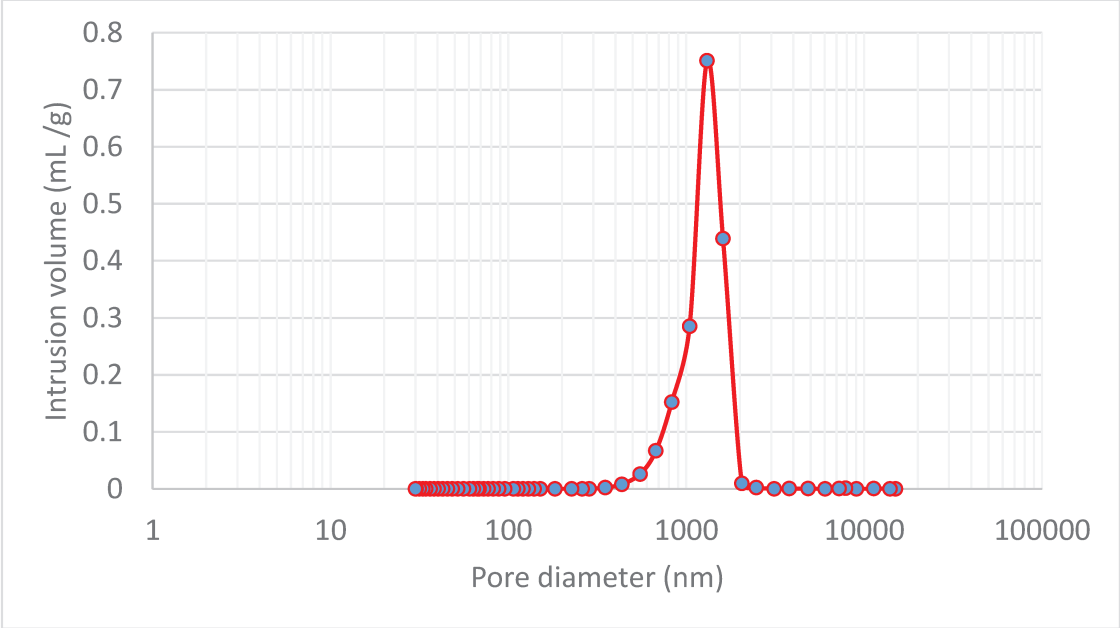

Fig. 18. Pore size distribution of porous alumina substrate.

Prior to coating on stainless steel substrates, they were grit-blasted using 80 grit Al_2O_3 particles, cleaned by compresses air jet to remove the embedded particles and ultrasonically cleaned in acetone in order to remove any residue from blasting.

Surface roughness of stainless steel substrate was obtained as Ra ~ 5.3 μm, measured with a 3D confocal laser microscope (Olympus OLS4000).

Porous alumina substrates were used in SPS process as purchased and without grit blasting. Before the coating deposition process, the surface of alumina substrates were cleaned by air blast. Surface roughness of porous alumina substrate was obtained as R_a ~ 0.9 μm, measured with a 3D confocal laser microscope (Olympus OLS4000).

3.4. Preliminary experiment

The preliminary experiment was based on the spray parameters and suspension composition borrowed from a previous work on TiO_2 hydrophobic coatings [67]. In order to prepare the suspension for spraying sample SPS-W-0, Polyacrylic acid (PAA) (Sigma-Aldrich, Oakville, Canada) was used as surfactant. Surfactant was added as 5% of the solid content of the suspension. Table 2 describes the suspension formulation and Table 3 describes the spray parameters of the preliminary sprayed coating, SPS-W-0. Spray parameters will be discussed in coming sections.

Table 2. Suspension formulation of sample SPS-W-0.

Sample	Solid content (%wt)	Spray distance (mm)	Solvent	Surfactant
SPS- W-0	20	50	Water	PAA 5% of solid content

Table 3. Spray parameters of sample SPS-W-0.

Ar (LPM)	H_2 (LPM)	Current (A)	Voltage (V)	Power (kW)	Spray velocity (m/s)	Injector diameter (mm)	Spray distance (mm)	No. of passes
60	2	500	50	25	1	0.2	50	75

Figure. 19 shows SEM micrograph of the polished cross- section of sample SPS-W-0, in which columnar features can be observed. In this work, one of the goals was to produce a membrane with a uniform microstructure. As a result, the columnar structure, which is one of the features that may appear in SPS coatings due to the shadow effect was not desirable. In addition, during spray process of SPS-W-0, sedimentation of the suspension occurred shown in Fig. 20. Therefore, a rigorous analysis, described in the following section, was dedicated to obtain a stable suspension throughout the spraying time.

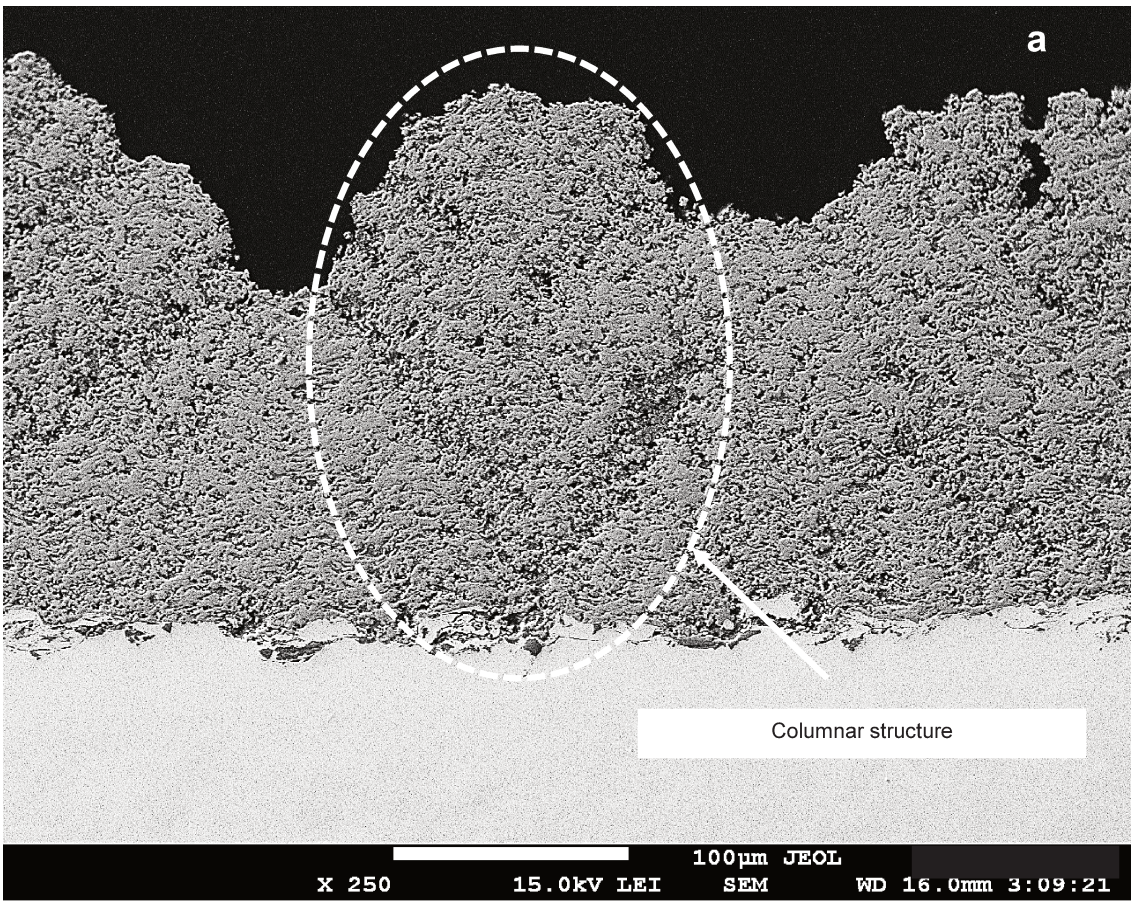

Fig. 19. SEM micrograph of the polished cross section of sample SPS-W-0.

Fig. 20. Sedimentation line marked on the container of suspension used in the spray process of SPS-W-0 at the end of the SPS process.

3.5. Suspension preparation and optimization

In order to delay the sedimentation of the suspension, a stable suspension without large agglomerates was essential in the first place. In order to find a stable suspension throughout the spray process in this work, an experiment with 8 types of suspensions according to Table 4, was performed. Polyacrylic acid (PAA) (Sigma-Aldrich, Oakville, Canada) was used as surfactant based on previous experiments on TiO_2 suspensions and added as a certain percentages of solid content. Ethylene glycol was used as a part of the solvent in order to increase the viscosity of the suspension and was added as 20% of the fluid content of the solvent.

In order to prepare the suspensions, for the cases with a surfactant, in the first step surfactant was added to the solvent gradually until completely dissolved and then TiO_2 powder was gradually added to the mixture. To provide an effective mixing and to avoid having large agglomerates, the process was carried out on a magnetic stirrer and an ultrasonic agitator was used during the whole suspension preparation process in order to break down the large powder lumps and the agglomerates in the suspension as much as possible. In the case of the suspensions containing

ethylene glycol, in the first step ethylene glycol was added to water and was stirred for one minute and the rest was according to the suspension preparation procedure.

Table 4. The formulation of 8 suspensions used for evaluation of the stability.

Suspension	a	b	c	d
Water based suspension with 20%wt TiO_2	0% surfactant or ethylene glycol	5% surfactant	10% surfactant	0% surfactant Solvent: 80% water + 20% ethylene glycol
Water based suspension with 10%wt TiO_2	0% surfactant or ethylene glycol	5% surfactant	10% surfactant	0% surfactant Solvent: 80% water + 20% ethylene glycol

In order to confirm the static stability, 100 mL of each of the eight suspension mentioned in Table 4 was prepared. In the next step, each suspension was poured in a separate vial and the opening of the vials were sealed completely. The vials were put on a stable surface and pictures were taken in intervals. Figure. 21 illustrates the level of sedimentation of the 8 suspensions mentioned above within two weeks.

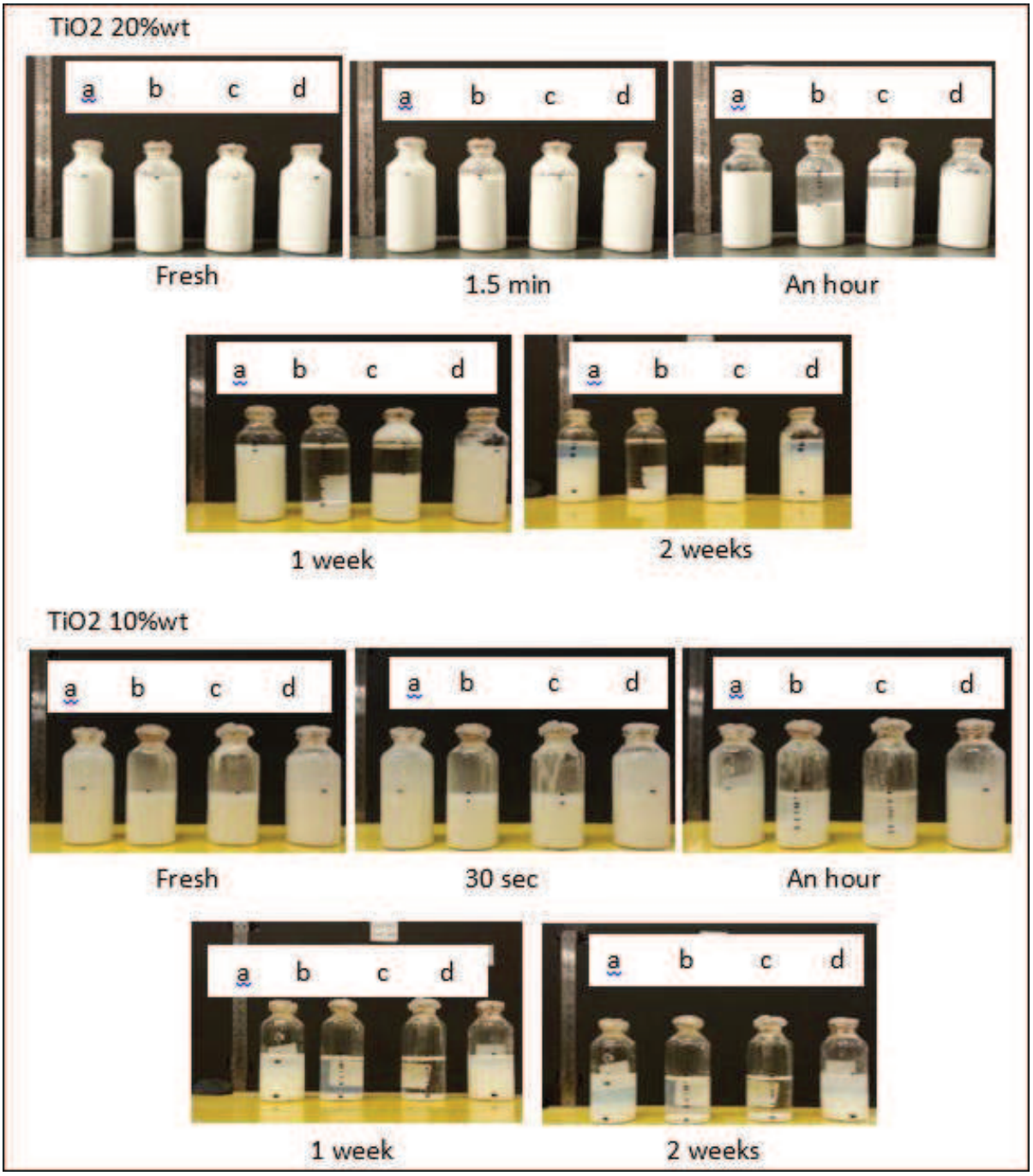

Fig. 21. Level of sedimentation of water based TiO_2 suspensions with TiO_2 20$wt\%$ and with TiO_2 10$wt\%$, a) without surfactant, b) 5% of solid content surfactant, c) 10% of solid content surfactant, d) without surfactant and the solvent contained 80% water + 20% ethylene glycol.

By observing these samples, in both suspensions with 10 wt% and 20 wt% solid content, suspensions without any surfactant and those in which the solvent was the mixture of water and ethylene glycol showed more stability.

It was observed that in suspension with 10 wt% solid content, sedimentation started within 30 sec in both surfactant concentrations and continued with almost the same rate. On the other hand, sedimentation in suspension without surfactant and the suspension with solvent containing ethylene glycol started within around two hours. After a week all these four suspensions were settled, although some suspended particles were still observable in the suspension without surfactant and in the suspension with solvent including ethylene glycol.

In the case of suspension with 20 wt% solid content, it was observed that sedimentation started within 1.5 min in both surfactant concentrations. However, the sedimentation continued with a higher rate in suspension with 5% of surfactant. Sedimentation in the suspension without surfactant and in the suspension with solvent including ethylene glycol was started at a small level within 48 hours. Sedimentation of suspension with 10% surfactant seemed to remain unchanged in two weeks. The three other suspensions were settled in two weeks.

The purpose of this experiment was not to deny the influence of surfactant in delaying the agglomeration. The obtained results regarding the stability of the suspensions is only reliable in the case of using the certain surfactant of choice, PAA, in this experiment. However, other authors also used both water based and ethanol based TiO_2 suspensions in SPS process without adding surfactant [40].

It has been confirmed that suspensions with lower viscosity values are easier to atomize in the plasma jet [82]. Suspension viscosity measurement on these 8 samples, based on table 4, was performed by automatic rheometer instrument (MCR Rheometer, Anton Paar, and CANADA). The results are illustrated in Fig. 22.

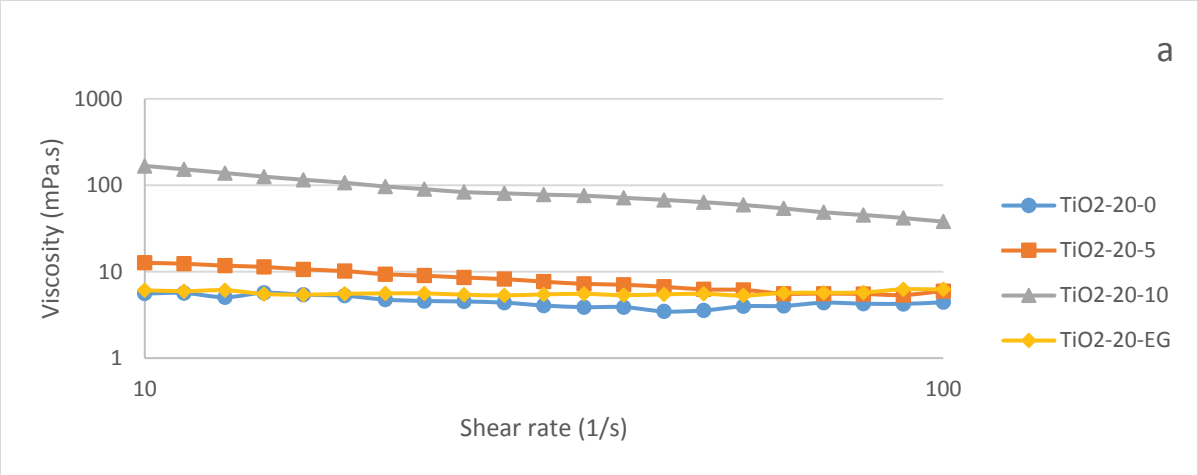

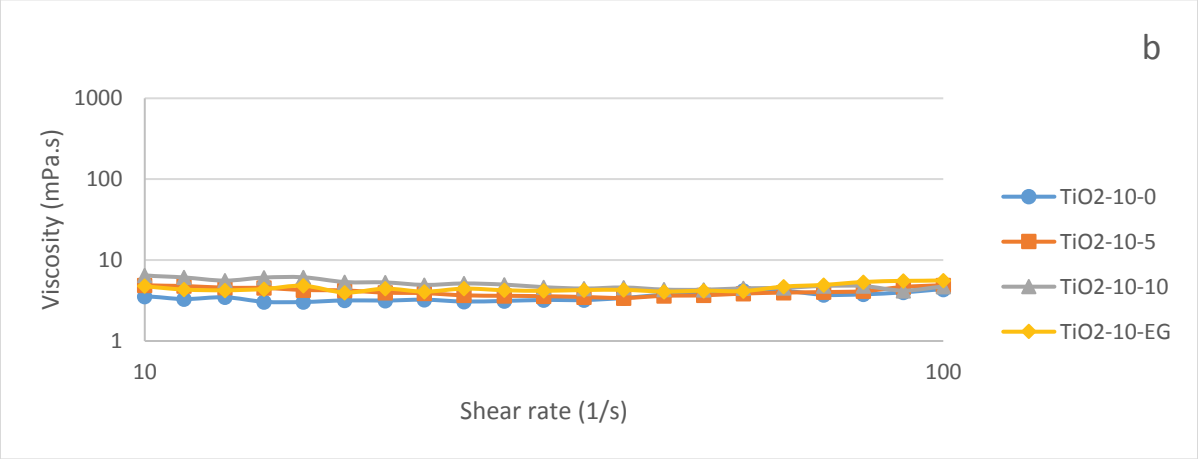

Fig. 22. Viscosity measurements of 8 samples based on suspensions in Table 5 for, a) four water based TiO_2suspensions with TiO_2 10$wt\%$ and; b) four water based TiO_2suspensions with TiO_2 20wt%.

It can be seen that in the case of TiO_2 20 wt% suspensions in Fig. 21(a), the lowest viscosity belongs to the suspension without surfactant and to the suspension with solvent containing 20% ethylene glycol. In Fig. 21(a), it can also be observed that results for suspension with 10% surfactant is significantly higher than the three other samples. This suspension did not fulfil the higher stability condition. Therefore, it was eliminated from the chosen suspensions and no further investigation was conducted regarding its viscosity.

In the case of TiO_2 10 wt% suspensions in Fig. 21(b), the results do not demonstrate a significant difference in viscosity.

Comparing the results on stability and viscosity measurements of the eight suspension, four suspensions that fulfilled both conditions of more stability and low viscosity were chosen to design the matrix of experiment as follows;

- TiO_2 10 wt% without surfactant
- TiO_2 10 wt% without surfactant and with solvent containing 20% ethylene glycol
- TiO_2 20 wt% without surfactant
- TiO_2 20 wt% without surfactant and with solvent containing 20% ethylene glycol

3.6. Design of experiment and spray conditions

Based on the results obtained from suspension stability measurement experiment and in order to examine the influence of different spray parameters on the TiO_2 SPS coatings, a matrix of experiments was designed in order to generate dissimilar TiO_2 coatings. Only one set of deposition parameters, which is summarized in Table 5, was used for deposition of the coating in all samples. Argon was used as primary gas with the flow rate set on 60 LPM. The hydrogen flow rate was chosen in order to have power equal to 25 kW.

Table 5. Deposition parameters of SPS titanium dioxide membranes.

Ar [LPM]	H_2 [LPM]	Current [A]	Voltage [V]	Power [kW]	Spray velocity [m/s]	Injector diameter [mm]
60	2	500	50	25	1	0.2

A full factorial matrix of experiments was designed for three variables at two levels, which resulted in eight samples based on the difference in their solid contents, solvent and the spray distance according to Table 6. Theses 8 samples were sprayed on stainless steel substrates.

Table 6. Matrix of experiments for SPS titanium dioxide membranes.

Sample	Solid content (%wt)	Spray distance (mm)	Solvent
SPS- W+E-1	10	50	Water+ 20% ethylene glycol
SPS- W-2	10	50	Water
SPS- W+E-3	10	30	Water+ 20% ethylene glycol
SPS- W4	10	30	Water
SPS- W+E-5	20	50	Water+ 20% ethylene glycol
SPS- W6	20	50	Water
SPS- W+E-7	20	30	Water+ 20% ethylene glycol
SPS- W8	20	30	Water

3.6.1. Coating deposition

In this work, the traverse of the plasma torch over the stationary substrate was carried out by a robot arm in a pattern with a meander-like movement as illustrated in Fig. 23.

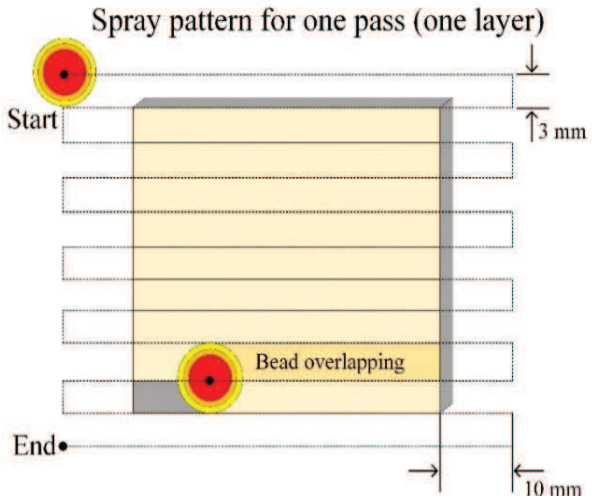

Fig. 23. Schematic description of torch raster pattern. Spray pattern for one coating pass used in this study [81].

The plasma torch was moved in the x-direction with a constant speed of 1 m/s and a specified stand-off distance (30 mm or 50 mm) with respect to the substrate surface. Once the torch reached the end of the length of the substrate in the x direction, it was indexed in the y-direction (3 mm) for the next adjacent bead. To cover the entire substrate surface, the torch scanned the surface with an additional tolerance of 10 mm in each horizontal displacement. The porous alumina substrate was fixed in a substrate holder, as shown in Fig. 24, for the SPS coating deposition process. In each spray process one SPS TiO_2 membrane could be produced. Titanium dioxide membrane was deposited on alumina substrate by 40 passes of spraying.

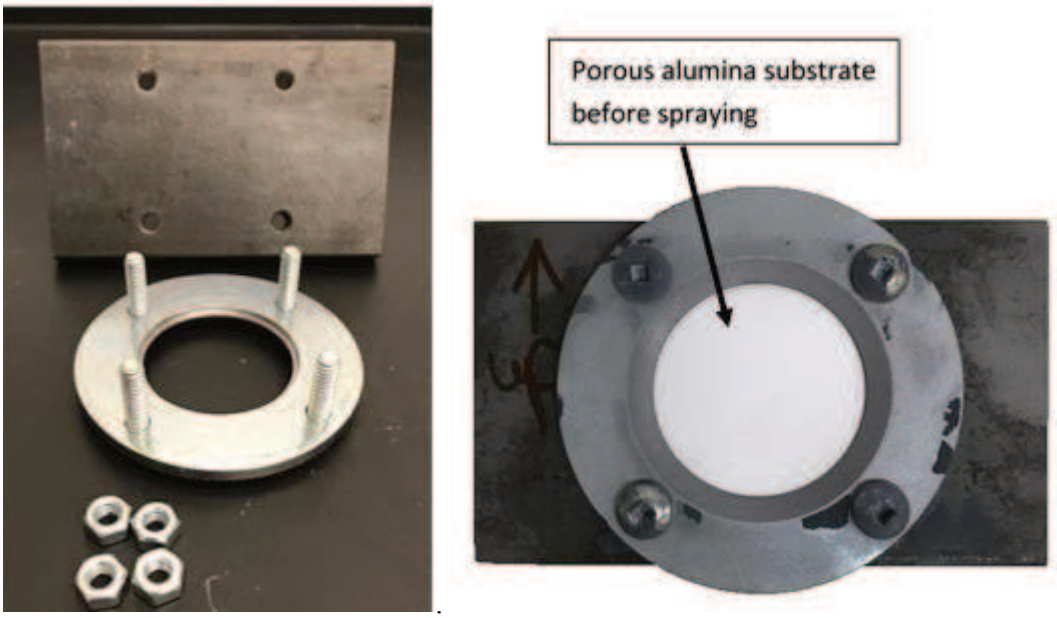

Fig. 24. Substrate holder used for alumina substrates in SPS coating deposition process.

3.6.2. Temperature measurement on the substrate

An infrared camera (A310, FLIR, US) was used to monitor the temperature of the substrate during the membrane deposition process on porous alumina substrates. Therefore, temperature of the ceramic substrate was held between 200 ± 15 °C. Completing one raster travel, the torch was stopped from starting the next pass for the substrate to cool down to the range of temperature mentioned above. Reaching the desired range of temperature, the next layer of coating was allowed to be deposited. The temperature was read when each raster pattern was completed and the surface

of the substrate was clear from the movement of the robot arm and torch, in a way that there was no interference for the infra-red camera to estimate the temperature.

3.7. Membrane characterization

3.7.1. Metallographic sample preparation process

The metallographic sample preparation of the sprayed samples included cold- mounting, sectioning, grinding and polishing.

Cold- Mounting: Samples were mounted with a mixture of cold- mounting resin and hardener (Epofix, Struers, USA) in order to facilitate their manipulation and safekeeping the deposited coating during sectioning and polishing process. A vacuum chamber (Cito Vac, Struers, USA) was used to enhance the epoxy infiltration through the pores in the coating for 10 minutes and at the pressure of 10 KPa.

Sectioning: Mounted samples were cut with a cut-off machine (Secotom-15, Struers, USA). In order to keep the coating intact from being damaged during the cutting process, the mounted samples were fixed in a way that the coating was under compressive stress applied by the cutting wheel. A compatible cutting wheel, (50A20, 200 × 0.8 × 22mm, Struers, USA), was used for the cutting process. The velocity of the cutting wheel and the feed rate were adjusted at 2000 rpm and at 0.5 mm/s respectively.

Grinding and Polishing: the mounted and sectioned samples were grinded- polished with an automatic polishing machine (Tegramin-25, Struers, USA), in order to obtain smooth surfaces suitable for metallographic observation. Samples were put in the sample holder in symmetrical positions and a continuous water flow was used during the process as a coolant and also to remove the debries from grinding of the surface. Summary of the grinding- polishing process is described in Table 7. The speed of the platen and the head was 300 rpm.

Table 7. Summary of grinding and polishing process.

Grinding and polishing	SiC (Grit 320)	SiC (Grit 500)	SiC (Grit 800)	Diamond suspension (9µm)	Diamond suspension (3µm)	Diamond suspension (1µm)
Time (min)	2	2	2	6	4	2

3.7.2. Microstructural evaluation

Scanning Electron Microscope (SEM): The microstructural observation of the samples was carried out with a field emission gun scanning electron microscope (JEOL JSM- 7600F). Samples were coated with carbon film in order to create an electrical conductive surface. Both backscatter electron and secondary electron detectors were used for the observations.

3.7.3. X Ray Diffraction

Phase composition of the feedstock powder and the SPS TiO_2 membranes was analyzed using XRD (X'Pert pro MRD, Malvern panalytical, UK). Measurements were carried out in the 2θ step scan mode from 20° to 90° using CuKα radiation and a step size of 0.02. Content of anatase in the feedstock powder and in the SPS membrane was measured using X'Pert pro software (Malvern panalytical, UK).

3.7.4. Porosity evaluation

Porosity evaluation of samples was performed with two analytical methods; gray scale image analyzing based on SEM images and mercury intrusion porosimetry.

Gray scale image analyzing: Gray scale image analyzing was performed with an image analyzing software (Olympus Stream basic, Canada) based on SEM images of the polished cross- sections of the samples obtained with backscatter electron detector and at the magnification of 2000X. In order to have consistent results, the images were captured in the same conditions regarding the voltage (15 kV), working distance (15 mm), contrast and brightness. The evaluation was carried out by adjusting the gray scale threshold, at the level that provided the best coverage of the pores. Figure. 25 shows an example of the adjusted threshold in an SEM image of the cross- section of SPS TiO_2

membrane, in which the porous area is marked in blue color. The evaluation was completed by calculation of the surface area of the colored sections (Porous surface area), by the software. The final result was reported as the average obtained from 10 SEM images.

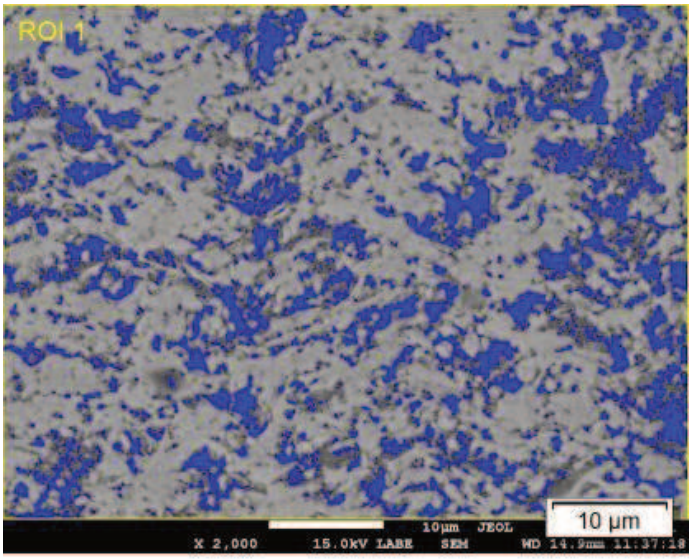

Fig. 25. Gray scale threshold adjustment in an SEM image of the cross- section of SPS TiO_2 membrane.

Mercury intrusion porosimetry: This technique is based on the fact that a non- wetting liquid such as mercury does not penetrate pores by capillary action. Thus, pressure is needed to be applied in order to force mercury to intrude the capillaries. The pressure is inversely proportional to the size of the pores. Large pores are intruded under lower pressure, while higher pressure is needed to intrude small pores. The relation between the capillary diameter and the pressure is described by equation (1), called Washburn equation [83].

$$P = \frac{-4\gamma \cos\theta}{d} \qquad (1)$$

Where p is pressure, γ is surface tension of the liquid (mercury), θ is Contact angle of the liquid, and d is diameter of the capillary.

As shown in Fig. 26, in general, pores can be classified in three major groups; closed pores, blind pores and open pores including cross-linked pores and through pores.

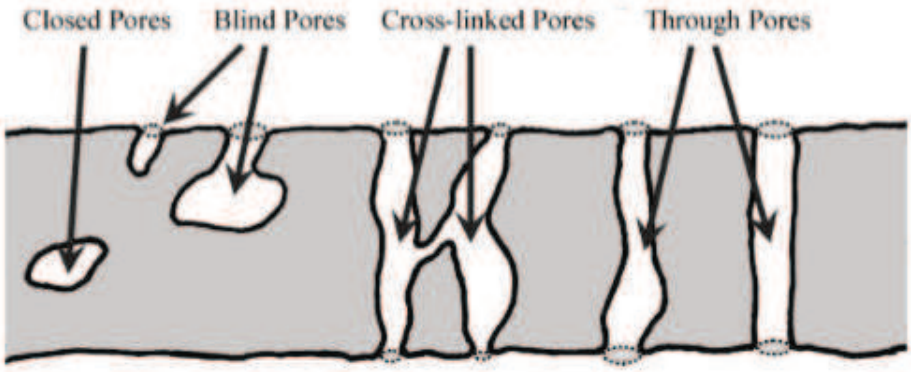

Fig. 26. Schematic of pore structure [102].

The pores that are filled with mercury are through pores, cross linked pores and blind pores.

In this study, an automatic mercury intrusion porosimeter (Autopore IV, Micrometric, USA) was used. The evaluation was performed on a free standing coating deposited on a stainless steel substrate. Dimensions of the sample was ~ 1.5 × 2.5 × 0.014 cm. In order to remove the coating, the substrate was bent mechanically resulting in delamination of the coating from the substrate. A solid sample penetrometer with the volume of 5 cm^3 and the stem volume of 0.392 cm^3 was used. Mercury contact angle and its surface tension were set at 130° [84] and at 485 dynes/cm respectively. The measurements were carried out in both low and high pressure range and the pressure was increases up to 60,000 psi (~ 414 MPa).

3.8. Evaluation of service performance of the membrane

3.8.1. Water permeation measurement

Clean water permeation measurement was performed with a dead end stirred cell (Sterlitech, HP4750, USA. The details of the cell is illustrated in Fig. 27. The pressure rate is up to 1000 psi and membrane discs with diameters between 47 mm and 50 mm can be fitted in this cell and the active membrane area is 14.6 cm².

The membrane was inserted in the bottom of the cylinder. The cell was closed and sealed with high pressure clamps and the cylinder was filled with deionized water. The water was forced to pass through the membrane by applying compressed nitrogen. The pressure used in this experiment

was between 2 psi and 40 psi. The volume of permeated water was measured at a constant time. In this work, the stir bar assembly and the magnetic stirring plate was not used, since the experiment was performed with clean deionized water.

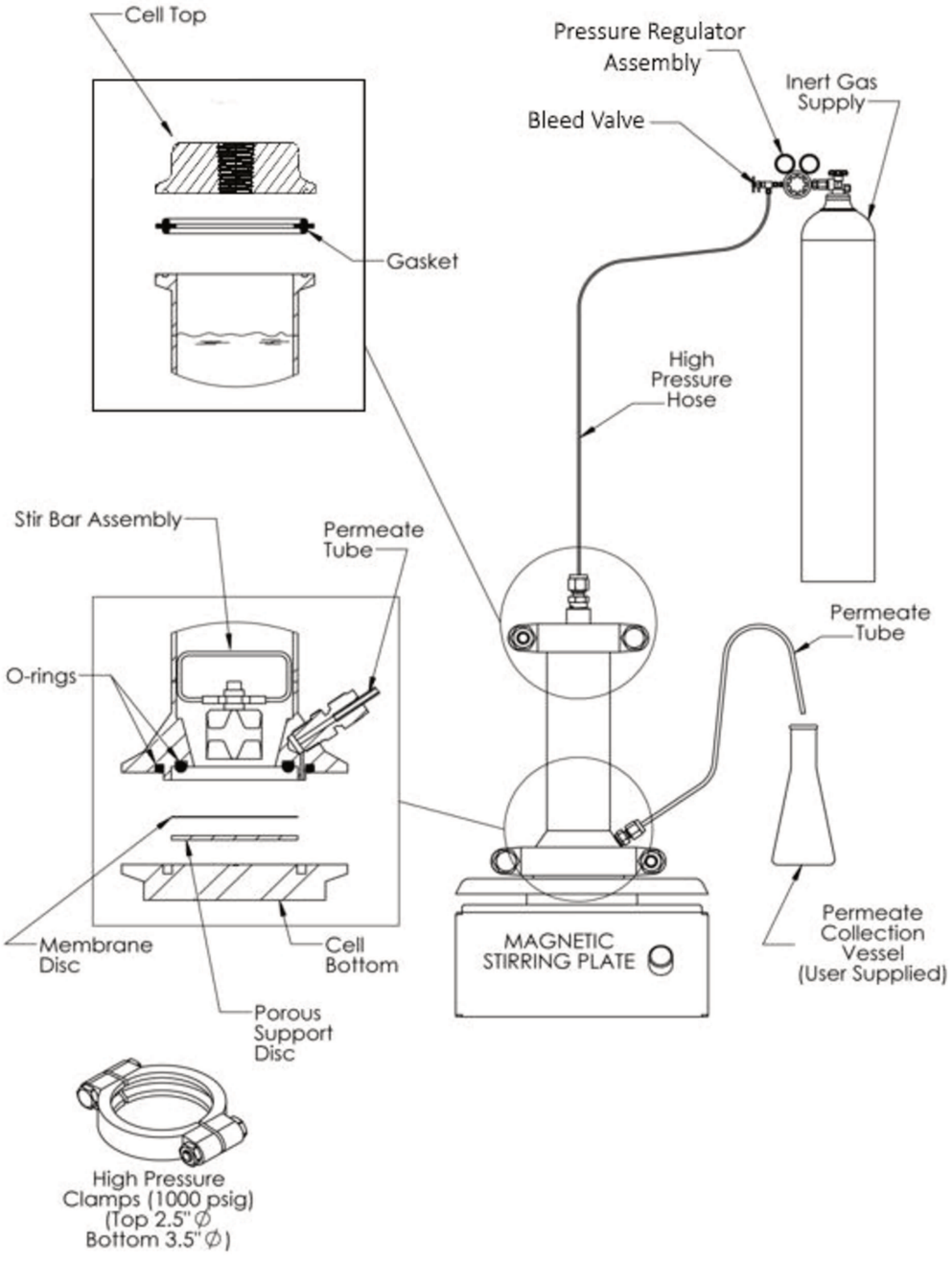

Fig. 27. Schematic of a standard HP4750 stirred cell system [85].

Water permeation flux was calculated according to equation (2) [86].

$$J = \frac{V}{t.A} \qquad (2)$$

Where J is the permeation flux ($L\,h^{-1}m^{-2}$), V is the volume (L), A is the active surface area of the membrane (m^2). The experiment was repeated three times.

3.8.2. Evaluation of photocatalytic activity of the membrane

The photocatalytic activity of the titanium dioxide membrane was evaluated by analyzing the degradation of an aqueous solution of an organic dye, methylene blue (Sigma- Aldrich, USA), under UVC illumination (100-280 nm).

The characteristics of the UVC lamp (Ster-L-Ray, Atlantic Ultraviolet co. USA) that was used for photodegradation of methylene blue aqueous solution in the presence of TiO_2 membranes, is summarized in Table 8.

Table 8. Characteristics of UVC light.

Lamp description	Length (mm)	Power (W)	Current (mA)	UV output (W)	UV output at 1meter (Micro watts)	Effective life (hours)
Ozone free	201	18.4	425	5.8	59	10000

Figure. 28 illustrates a schematic of the photoreactor that was used for this experiment. The photoreactor was a system made by a petri dish containing the membrane and the dye solution enclosed in a wooden box covered with aluminum foil to avoid interference from natural light and to block UVC irradiation. In order to generate some agitation in the solution system, a magnetic stirrer was used. Since the intensity of the UV light decreases by increasing the distance from the light source, the petri dish was mounted on an elevator to keep the surface of the membrane at a close distance to the UV light source. The distance between the top of the petri dish and the UV lamp was adjusted at 2 cm. Sampling was carried out with a pipet and through a sampling window on top of the box. The experiment was carried out under fume hood and at room temperature.

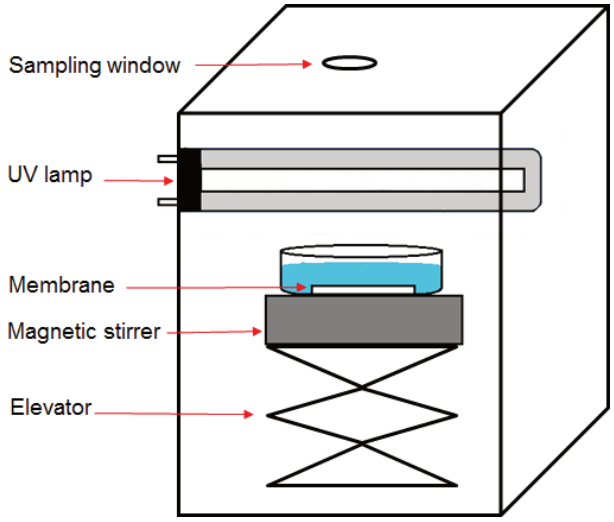

Fig. 28. Schematic of the photoreactor.

Methylene blue solutions for this experiment were diluted from an aqueous solution of 1000 ppm methylene blue in deionized water. The dilution was carried out in multiple steps respecting equation (3) [87].

$$C_1V_1 = C_2V_2 \quad (3)$$

Where, C_1 is the initial concentration, V_1 is the initial volume, C_2 is the final concentration and V_2 is the final volume.

Concentration of methylene blue solution used in this work was 100 ppm. Two membranes were attached to the bottom of the petri dish with double sided tape, as it is shown in Fig. 29(a). A 100 mL of methylene blue solution was added to the petri dish containing the membranes and was stirred on the magnetic stirrer in the dark for 30 minutes in order to reach Methylene blue absorption-desorption equilibrium to initiate the photocatalytic reaction [35]. Figure. 29(b) shows the position of the membranes under UV light.

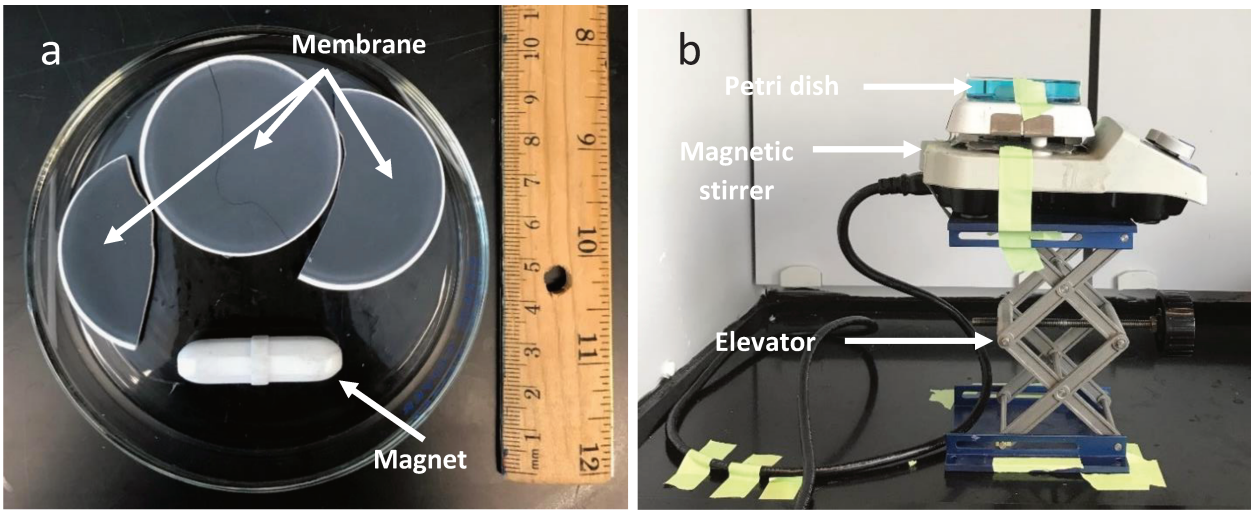

Fig. 29. a) Arrangement of titanium dioxide membranes in the petri dish and; b) under UV light for evaluation of photocatalytic behavior.

The UVC lamp was turned on after that and samples were taken with time intervals according to Table 9.

Table 9. Sampling time intervals for evaluation of photocatalytic activity of the membrane.

Sample number	1	2	3	4	5	6	7	8	9	10
Time (min)	0	15	30	40	50	55	60	65	70	80

The process of sampling stopped when the sample became completely clear and without traces of blue dye.

Degradation of methylene blue was analyzed by measuring the absorbance with a UV- Vis spectrometer (Cary 8454 UV– vis Spectrophotometer, Agilent technologies) at 660 nm, where the change in light absorbance with respect to the methylene blue concentration was the most significant for aqueous methylene blue solution.

In order to measure the absorbance of a solution of an unknown concentration, a six points calibration curve, shown in Fig. 30, was obtained for methylene blue samples with 10, 25, 50, 75, 100 and 125 ppm of concentration. The calibration curve was linear in the concentration range of

the experiment and the linear regression equation was y = 0.0082x+0.0039 with correlation coefficient 0.994.

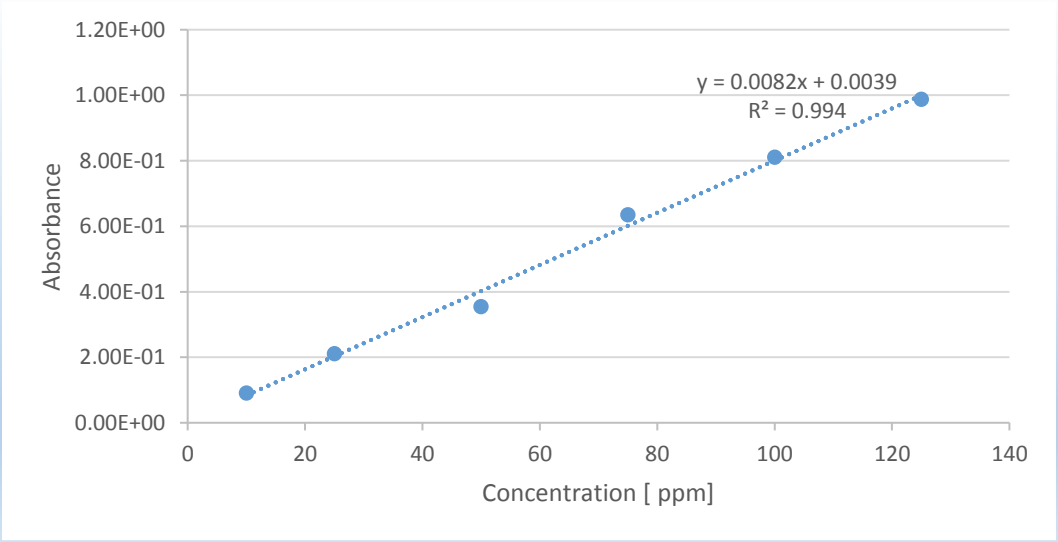

Fig. 30. Calibration curve for evaluation of photocatalytic behavior of titanium dioxide membranes.

In order to eliminate the error associated with the loss of light due to the reflection from the surface of the cuvettes containing the methylene blue samples, a reference measurement was made with a cuvette containing only deionized water (solvent). This experiment was repeated three times.

4. Results and discussion

As mentioned earlier, the objective of this work was to determine the possibility of manufacturing water permeable titanium dioxide membrane with suspension plasma spray technique. In this chapter first the microstructures SPS samples will be introduced in the following order. SPS TiO_2 coating on stainless steel substrate from preliminary experiment (SPS-W-0), eight SPS TiO_2 coatings on stainless steel substrate based on Table 6, SPS TiO_2 membrane on porous alumina substrate without and with cooling the substrate. In the next step the influence of spray conditions on microstructures of three samples (SPS-W-0, SPS-W6 on stainless steel substrate and SPS-W-6 on alumina substrate) will be discussed and their micro structures will be described in detail. The results of porosity measurement and XRD phase analysis will be presented and the results of experiments for evaluation of service performance of the suspension plasma sprayed TiO_2 membranes deposited on porous Al_2O_3 substrate including water flux and photocatalytical behavior will be discussed.

4.1. Microstructure of the SPS $\boldsymbol{TiO_2}$ coatings and membranes

4.1.1. Microstructure of the preliminary SPS $\boldsymbol{TiO_2}$ coating deposited on stainless steel substrate

The spray parameters used for deposition of sample SPS-W-0, which was the preliminary sample produced in this work, were summarized in Table 5 and the spray conditions was according to Table 10.

Table 10. Spray condition for preliminary experiment (sample SPS-W-0).

Sample	Substrate	Solid content (%wt)	Spray distance (mm)	Solvent	Surfactant
SPS-W-0	Stainless steel	20	50	Water	5% PAA

Coating was generated by 75 passes of spraying and the average thickness of the coating was 194 µm. Microstructure of SPS TiO_2 coating on stainless steel substrate obtained from the preliminary experiment is presented in Fig. 31.

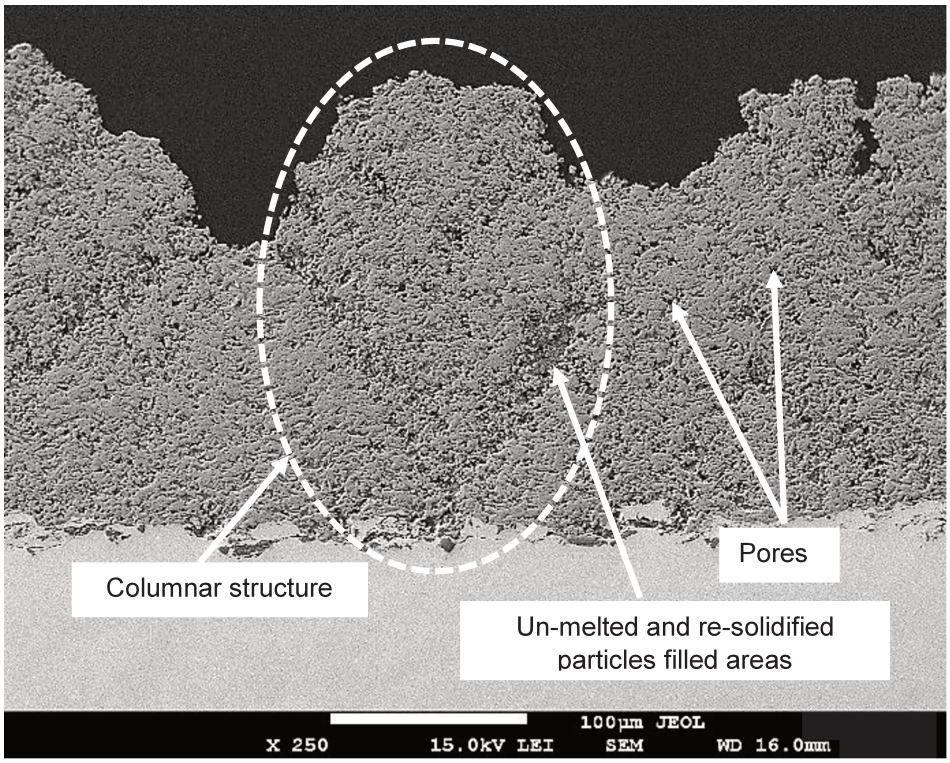

Fig. 31. SEM micrograph of the polished cross section of sample SPS-W-0.

As it can be seen in Fig. 31, at this point, a porous coating was generated. The light gray areas correspond to the areas formed by melted particles and the dark gray areas are the porosities filled with un-melted and/ or re-solidified particles. Also, the columnar features formed as the result of the shadow effect can be observed significantly. This sample will be discussed in more detail in the following sections.

4.1.2. Microstructure of eight SPS TiO_2 coatings deposited on stainless steel substrates based on matrix of experiment

Figure. 32 illustrates the low magnification optical microscope images of polished cross- sections of the eight coatings deposited on stainless steel substrates based on the matrix of experiments mentioned in Table 6.

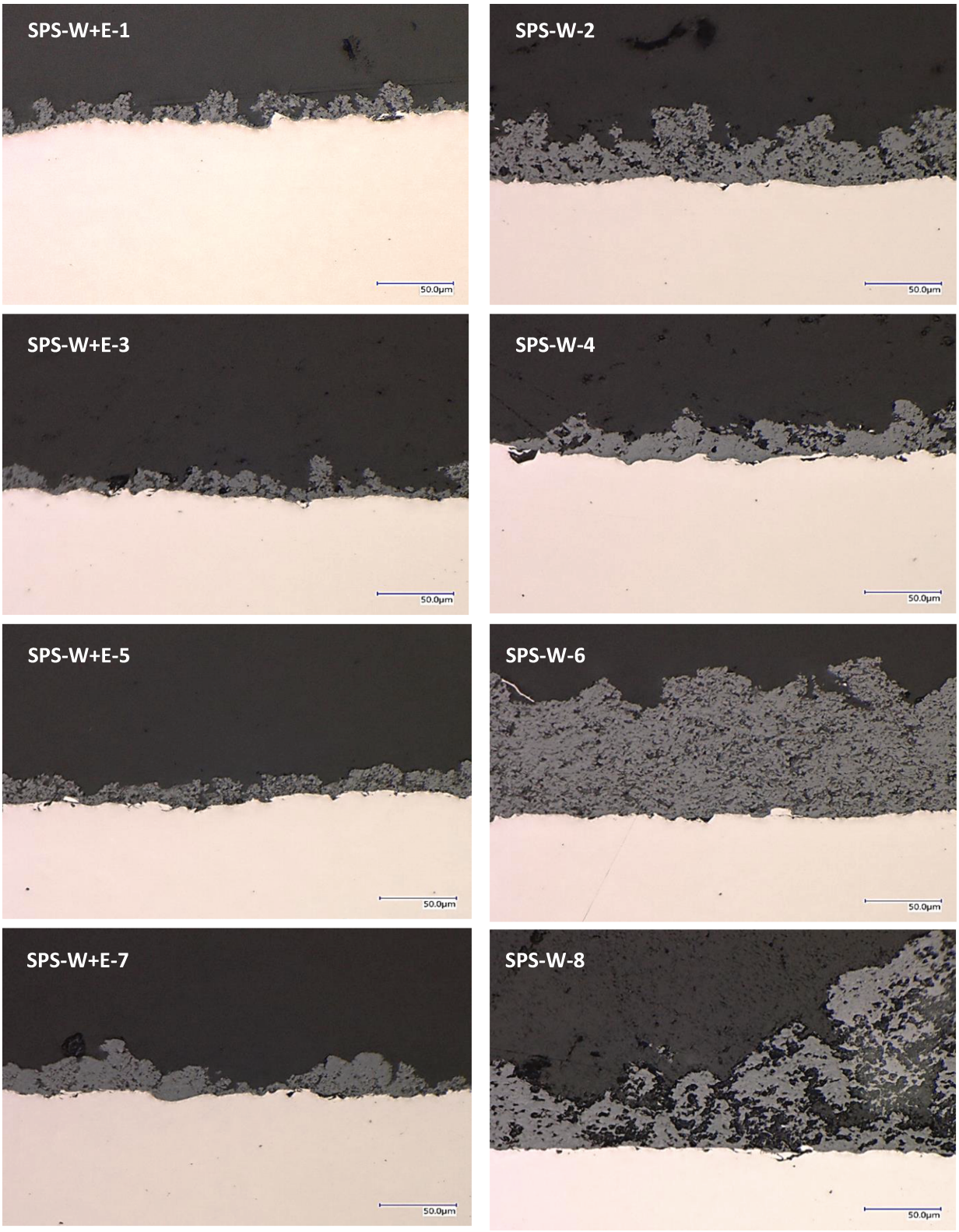

Fig. 32. Polished Cross- sectional view of SPS TiO_2 coating deposited on stainless steel substrates based on the designed matrix of experiments observed with optical microscope.

All these coatings were obtained after 40 passes of spraying. As mentioned before, the microstructure of the filtration membranes needs to be uniform. In addition, the membrane coating has to cover all surface of the porous substrate. It can be observed that only in the case of sample SPS-W-6 a relatively uniform coating covering all parts of the substrate with the average thickness of 96 µm was generated. Thus, sample SPS-W-6 was chosen to spray on porous ceramic substrate. The purpose of this experiment was to find process parameters for deposition of a coating with the characteristics mentioned above to spray on porous substrate. This sample will be discussed in more detail in the section 4.2.

4.1.3. Microstructure of SPS TiO_2 membrane deposited on porous alumina substrate

Figure. 33(a) shows the SPS TiO_2 membrane deposited on porous alumina substrate without cooling the substrate and Fig. 33(b) shows the SPS TiO_2 membrane deposited on porous alumina substrate with cooling the substrate. All the membranes sprayed without the substrate cooling cracked during the spay process. This could possibly be related to the decrease of thermal conductivity of alumina ceramics with porosity [88], which along with the low thickness of alumina substrates (2 mm), might have made it prone to cracking during the coating deposition process.

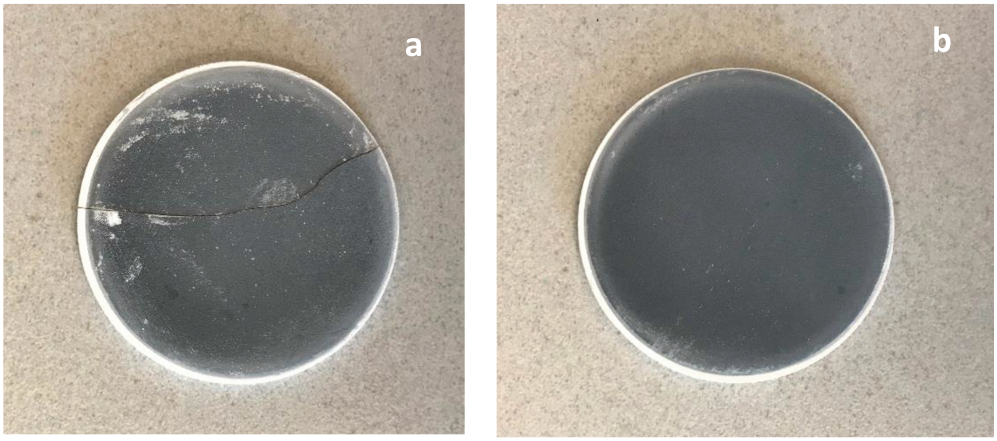

Fig. 33. SPS TiO_2 membrane deposited on porous alumina substrate a) without cooling and b) with cooling the substrate.

Figure. 34(a) shows the SEM images of the polished cross sections of SPS TiO_2 membrane deposited on porous alumina substrate without cooling the substrate and Fig. 34(b) shows the SEM images of the polished cross sections of SPS TiO_2 membrane deposited on porous alumina

substrate with cooling the substrate. As it can be observed at the first glance, these two images do not seem to significantly different from the microstructural aspect. However, results of porosity measurement and the XRD showed a slight difference between them. These results will be discussed in more detail in section 4.5.1.

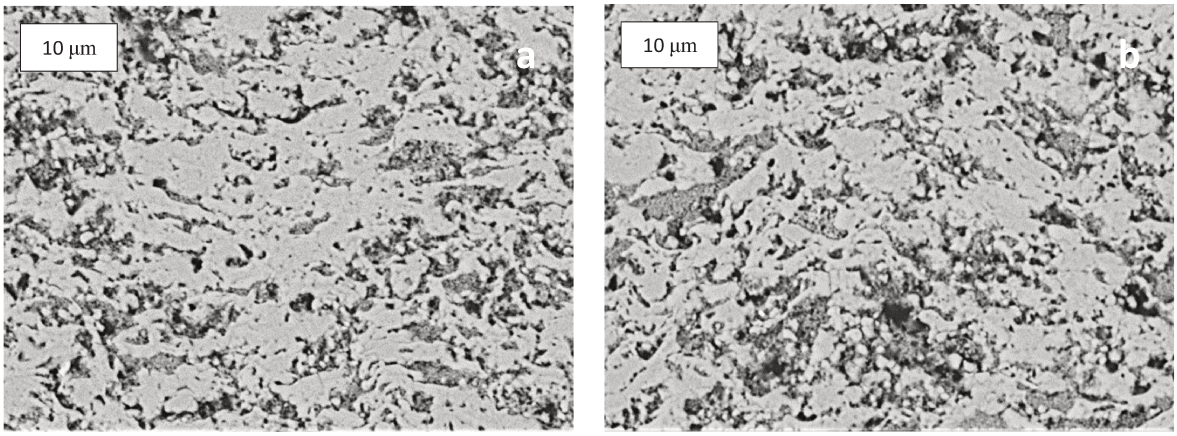

Fig. 34. SEM micrographs of polished cross sections of SPS TiO_2 membrane deposited on porous alumina substrate a) without cooling and b) with cooling the substrate.

Figure. 35 shows the low and high magnification images of SPS TiO_2 membrane. As it can be seen, a relatively uniform coating was generated on the porous substrate. The high magnification image reveals more details on the microstructure. This micro structure will be discussed in detail in section 4.3.

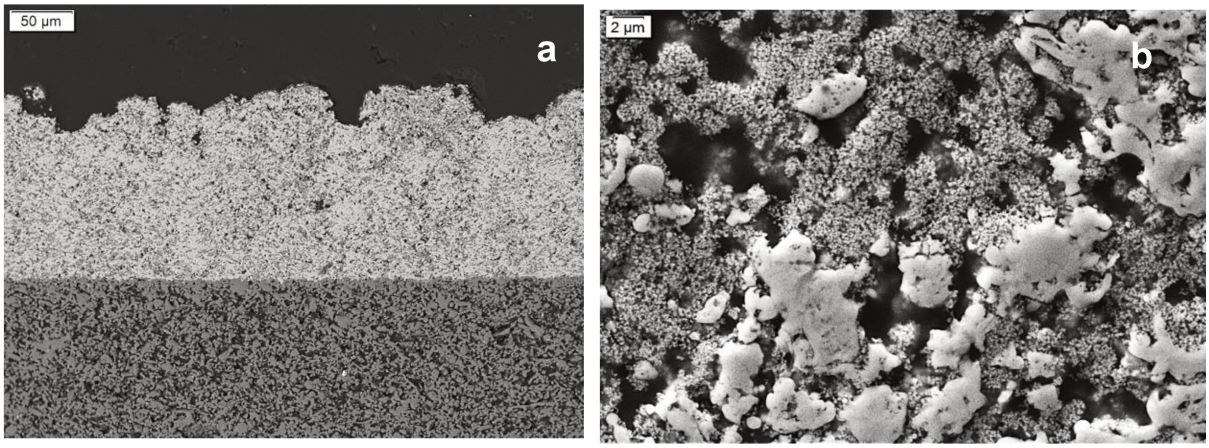

Fig. 35. a) Low magnification and; b) high magnification SEM micrograph of polished cross-sectional view of SPS TiO_2membrane deposited on porous alumina substrate.

4.2. Influence of spray conditions on coating structure

In this section the overall homogeneity of the SPS TiO_2 coatings on three samples (SPS-W-0 on stainless steel substrate, SPS-W-6 on stainless steel substrate and SPS-W-6 on porous alumina substrate) and the possible effect of two factors, namely the suspension stability and the roughness of the substrate on the uniformity of the coatings will be discussed.

Table 11 shows three SPS TiO_2 samples based on the difference in suspension recipes and in the substrates roughness. In order to identify the type of substrates used for each sample, two letters has been added to the name of the samples; SS stands for stainless steel and PA stands for porous alumina.

Table 11. Description of samples SPS-W-0, SPS-W-6 on stainless steel substrate and SPS-W-6 on alumina substrate.

Sample	Substrate	Substrate roughness R_a (µm)	Solid content (%wt)	Solvent	Surfactant	Spray distance (mm)	No. of passes
SPS-W-0-SS	Stainless steel	5.3	20	Water	5% of solid content PAA	50	75
SPS-W-6-SS	Stainless steel	5.3	20	Water	Non	50	40
SPS-W-6-PA	Porous alumina	0.9	20	Water	Non	50	40

Figure. 36, shows low magnification SEM micrographs of three coatings mentioned in Table 11. Considering that a filtration membrane is expected to be uniform, the columnar microstructure generated as a result of shadow effect in SPS coatings was considered an undesirable feature in the microstructure.

The columnar features in SPS-W-0-SS, SPS-W-6-SS and SPS-W-6-PA samples can be observed in Fig. 36 with various levels of severity. In this part, first samples SPS-W-0-SS and SPS-W-6-SS will be compared based on the suspension used and in the next step sample SPS-W-6-SS and sample SPS-W-6-PA will be compared based on the substrate they were sprayed on.

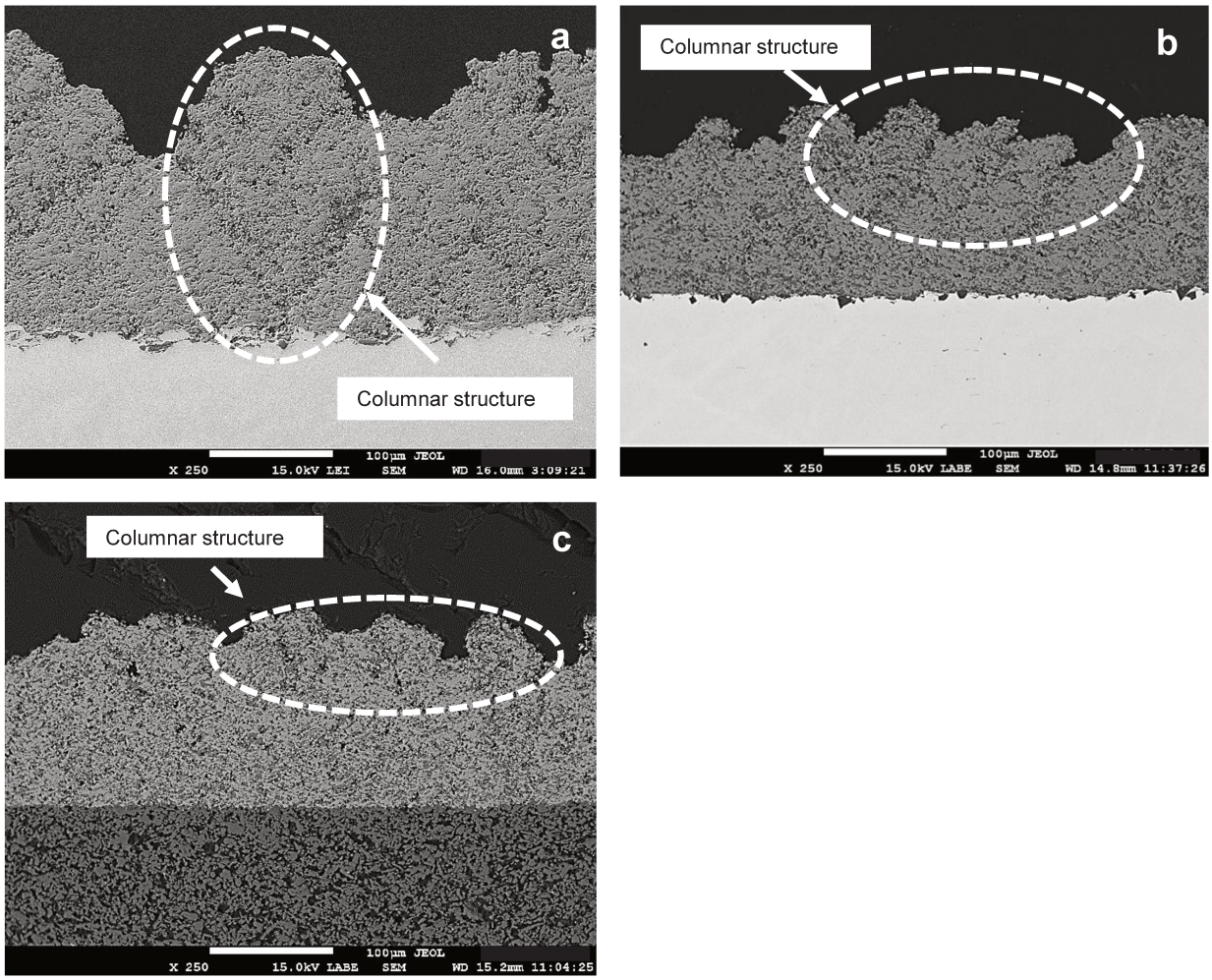

Fig. 36. SEM micrographs of SPS TiO_2 coating; a) SPS-W-0-SS, b) SPS-W-6-SS, c) SPS-W-6-PA.

Comparing Fig. 36(a) and Fig. 36(b), it can be seen that in the former, generation of columnar features in the coating has been started from the beginning of spray process. However, although the columnar features can be observed in Fig. 36(b), it can be seen that their formation has been started further during the spray process. In this case, about half of the coating thickness, corresponding to the layers deposited in the beginning of spray process, is free of these features

and shows a homogenous microstructure. The variable between samples SPS-W-0-SS and SPS-W-6-SS was the suspension used in the coating deposition process as it is mentioned in Table 11.

As mentioned before, sedimentation of the suspension occurred during the deposition process of samples SPS-W-0-SS. Meaning that the particles present in that suspension were more prone to agglomeration. It may be assumed that in the case of SPS-W-0-SS, impingement of the large agglomerates on the asperities of the stainless steel substrate may possibly promote the influence of shadow effect through creating larger asperities.

In the case of SPS-W-6-SS, presence of large agglomerations in the suspension was possibly less likely due to the more uniformity of the suspension. In this case, suspension contained more uniform particle size distribution without large agglomerates. Therefore, a more uniform coating compared to SPS-W-0-SS would have been generated in the beginning. However, by increasing the thickness of the coating, the effect of the surface asperities could have been resulted in generation of columnar features due to the shadow effect.

Comparing coatings illustrated in Fig. 36(b) and Fig. 36(c), effect of surface roughness of the substrate may be described. Suspension used in both these cases were the same and the variable was the difference in the substrates. Roughness value of stainless steel substrate was about 6 times more than porous alumina substrate. It can be seen that about two third of the coating in sample SPS-W-6-PA is homogenous and the non-uniformities are restricted to the top layers. It may be concluded that due to the lower roughness of the ceramic substrate, the effect of the surface asperities was eliminated by a higher level resulting in a more uniform microstructure with more thickness compared to SPS-W-6-SS. In fact, the smoother surface of the ceramic substrate might have possibly delayed the influence of large agglomeration within the suspension, which would generate the asperities on the coating.

4.3. Microstructural features of sample SPS-W-6 on porous alumina substrate

Figure. 37 demonstrates the details of SPS TiO_2 membrane deposited on porous alumina substrate, in the polished cross- sectional view. Features of microstructure have been marked on the SEM images. In this manuscript, sample SPS-W-6 deposited on porous alumina substrate, will simply be referred to as SPS TiO_2 membrane from now on.

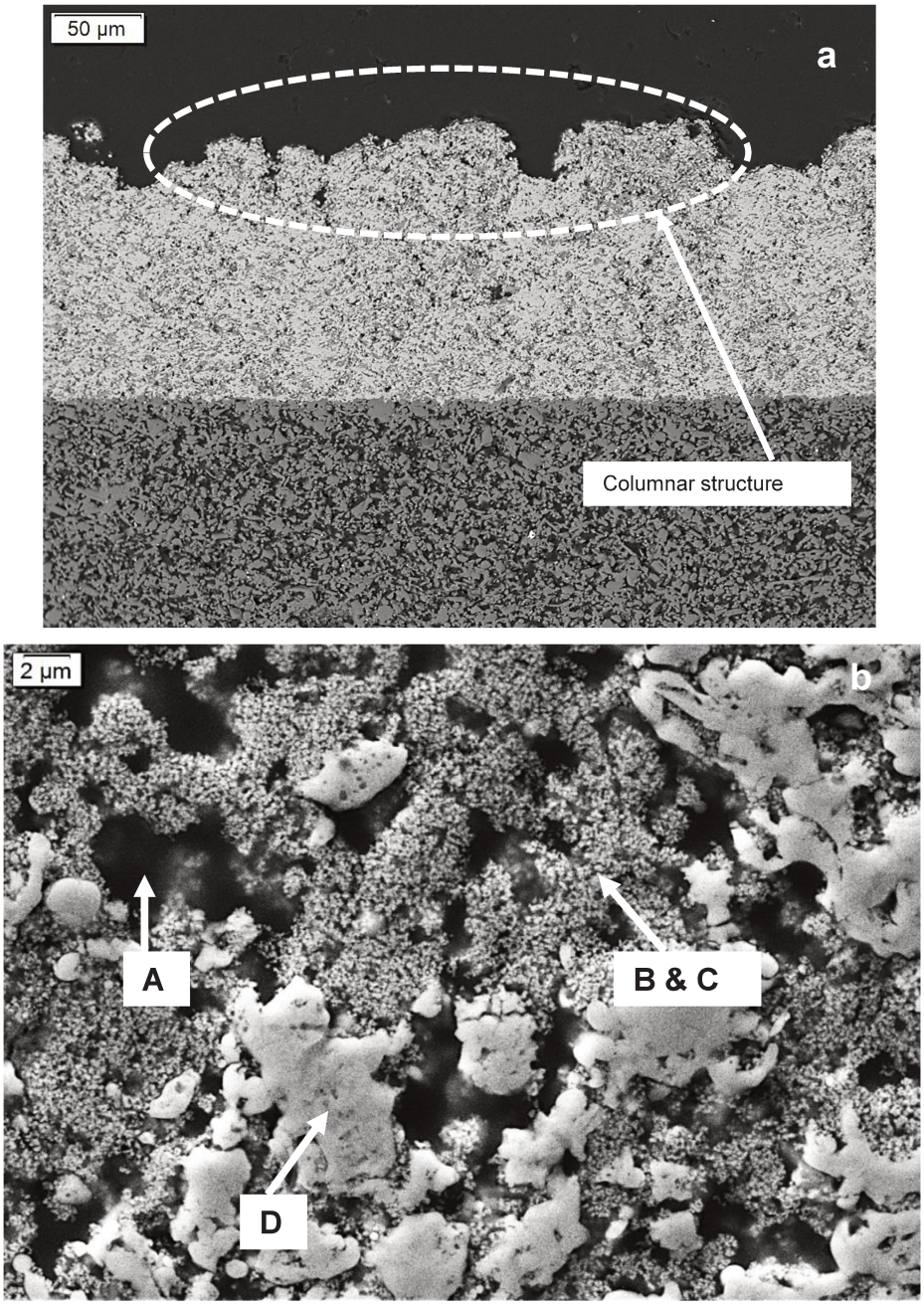

Fig. 37. a) Low magnification and; b) high magnification SEM micrograph of polished cross-sectional view of SPS TiO_2 membrane.

As it can be seen in the low magnification SEM micrograph of SPS TiO_2 membrane in Fig. 37(a), a relatively homogeneous porous coating with average thickness of 139 µm was generated with 40 passes of spraying, which gave around 3.5 µm of coating per each pass. The non- uniform features in the microstructure are limited to the top layers of the coating. The tops of the bumps that were seen in the cross sectional view of the membrane cab be observed in Fig. 38.

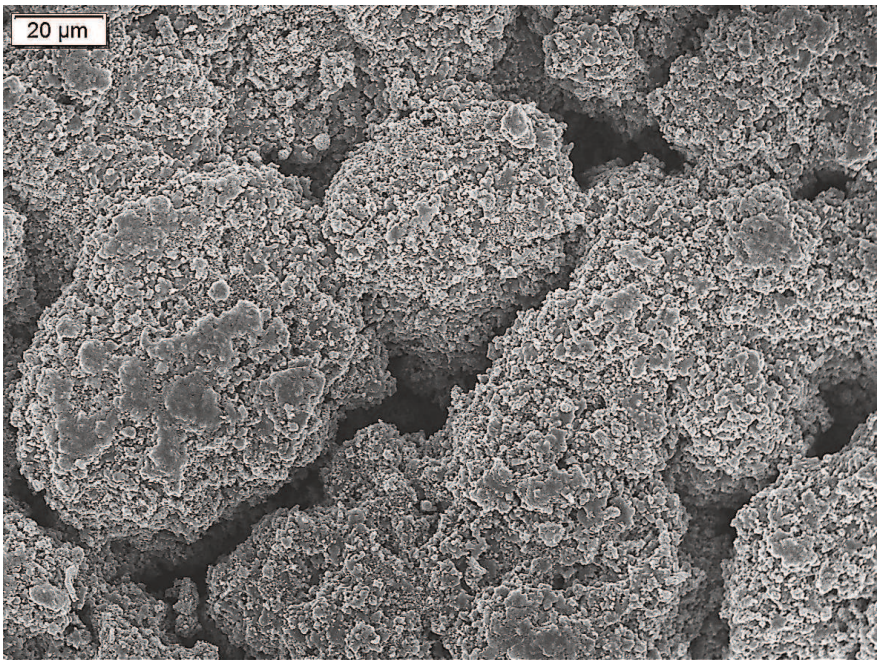

Fig. 38. SEM micrograph of columnar microstructure on the surface of SPS TiO_2 membrane.

Surface roughness of SPS TiO_2 membrane was measured as R_a equal to 8.8 µm.

As mentioned before, an ideal ceramic filtration membrane needs to have a porous uniform structure, which results in a stable filtering process. A uniform micro structure would also be advantageous since it is easy to be cleaned. The non- uniformities on the surface of SPS TiO_2 membrane could probably be eliminated by producing a thinner membrane layer. However, photocatalytic property would possibly decrease by the smoothness of the surface of the membrane due to the decrease of reactive surface area. In the case of SPS TiO_2 membrane, although the presence of columnar features on the top layer of membrane has a negative effect on homogeneity of the membrane, it could possibly perform in favor of photocatalytic behavior of the membrane due to the increased reactive surface area.

Different features of the polished cross-sectional microstructure in Fig. 37(b), include large porosities (A), areas include a mix of non-melted (B) and possibly re-solidified (C) particles and areas formed by fully melted particles (D). Figure. 39, demonstrates the microstructural features of SPS TiO_2 membrane on its fractured cross- section in a more detailed manner.

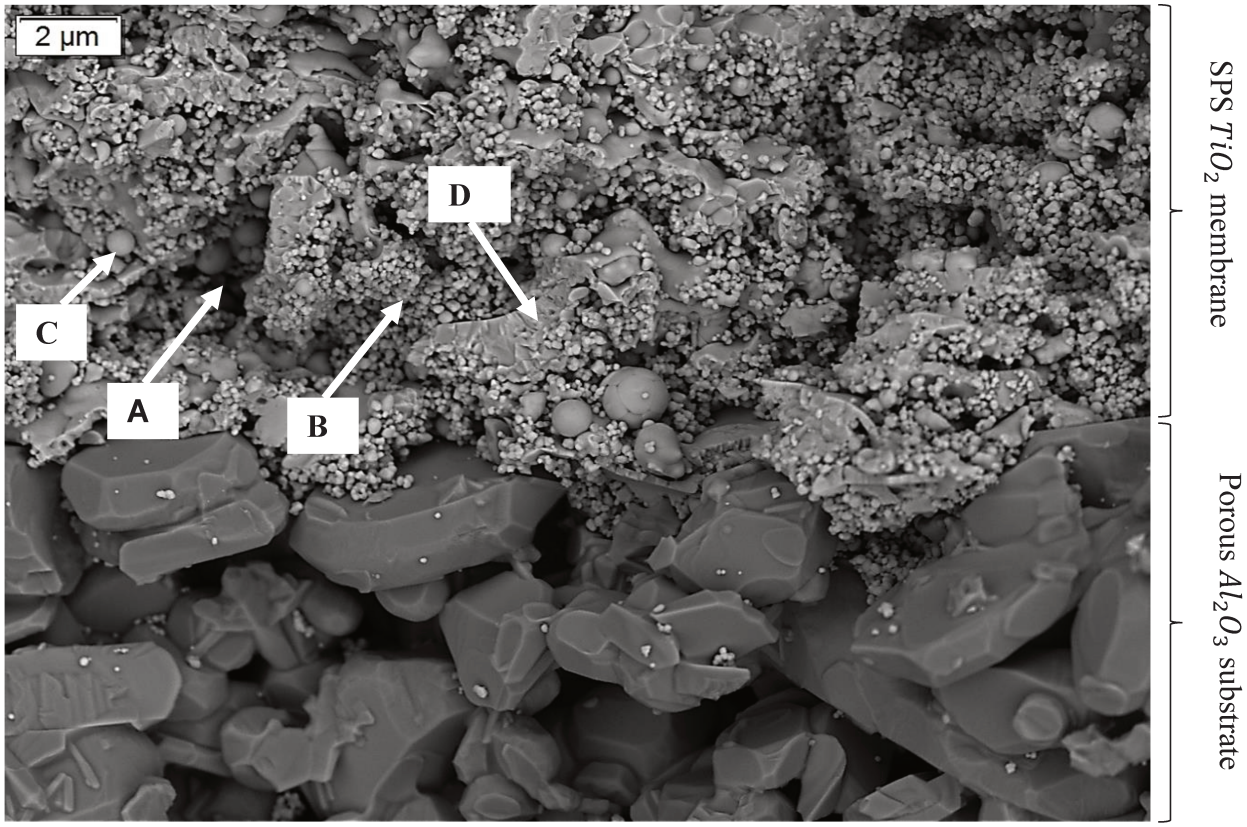

Fig. 39. SEM micrograph of fractured cross- section of SPS TiO_2 membrane.

Unlike conventional ceramic membranes, in which using binders is essential not only to attach the membrane particles together but also to attach the membrane to the substrate, it can be observed that in SPS TiO_2 membrane a unique network of fine pores was generated as a result of entrapment of un-melted and re-solidified particles within a matrix built by fully melted particles. Moreover, the adherence of the SPS TiO_2 membrane to the substrate occurs independent of any binder and only due to the mechanical bonds between the membrane and the substrate. Measurement of the particle diameters present in SPS TiO_2 membrane based on SEM micrographs of the coating showed an average particle size of 154 nm, which is in agreement with average starting feedstock powder particle size of 137 nm obtained from SEM micrographs of the TiO_2 powder.

Other than the microstructural features (A), (B), (C) and (D) mentioned above, with a closer look in the high magnification cross- sectional view of the fractured surface of SPS TiO_2 membrane shown in Fig. 40, areas of good (E) and poor (F) inter-splat bonding. Columnar grain growth of the splats (G), intra-lamellar cracks (H) and inter-splat cracks (I) can be observed [89].

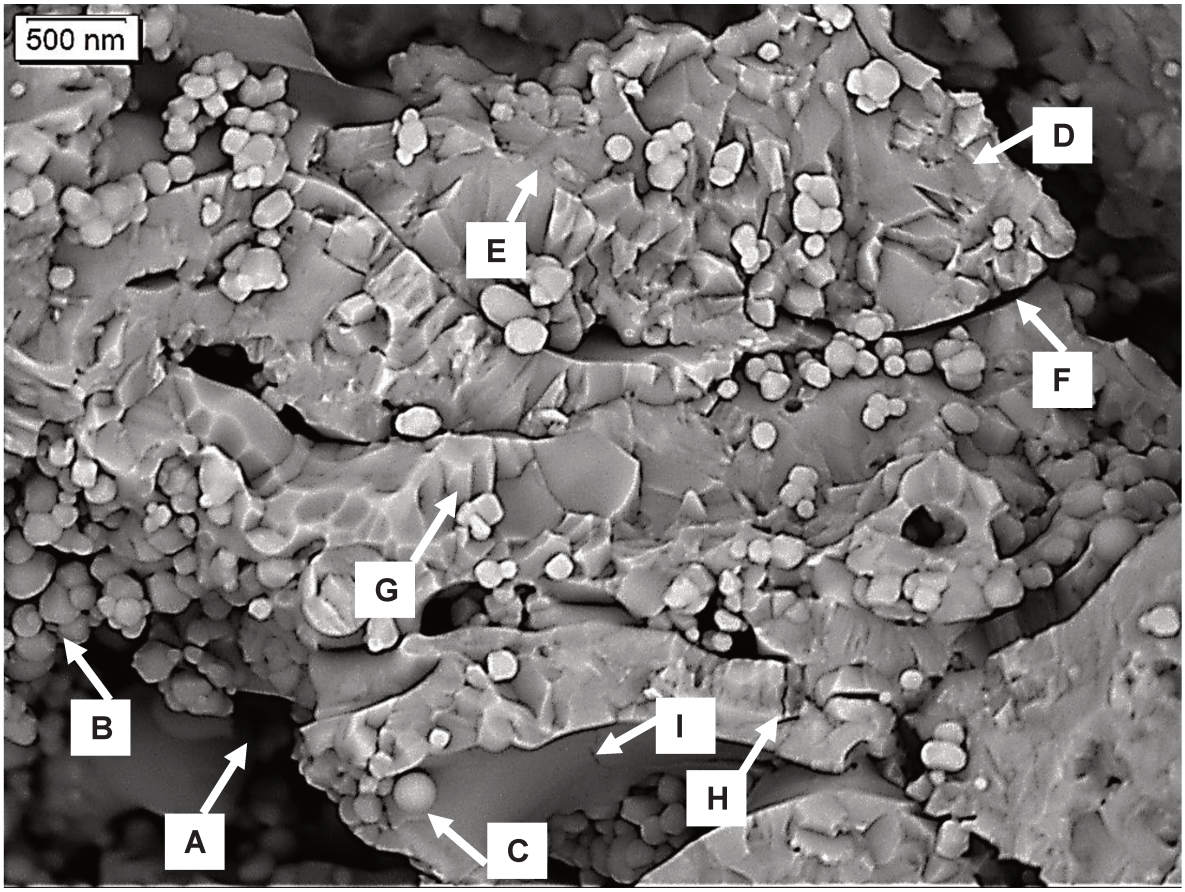

Fig. 40. High magnification SEM micrograph of fractured cross- section of SPS TiO_2 membrane.

4.4. XRD results

Figure. 41 shows the diffraction patterns of the TiO_2 powder used in the feedstock suspension and Fig. 42 shows the diffraction pattern in the SPS TiO_2 membrane. In these two images, A stands for anatase and R stands for rutile. XRD analysis results showed modifications in the crystalline composition of the SPS TiO_2 membrane with respect to that to the initial raw material feedstock.

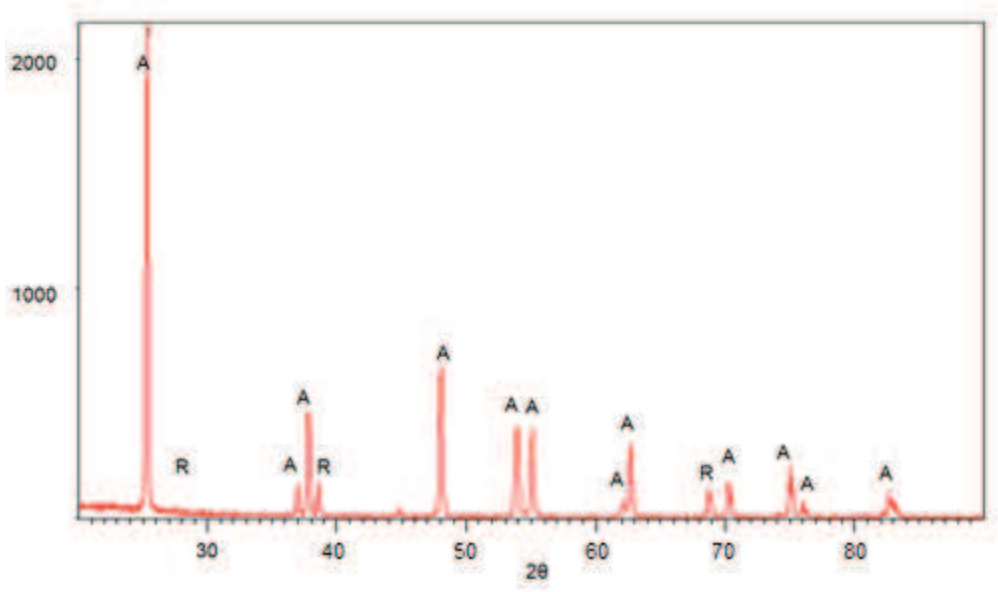

Fig. 41. X ray diffraction pattern of TiO_2 powder used in the feedstock suspension.

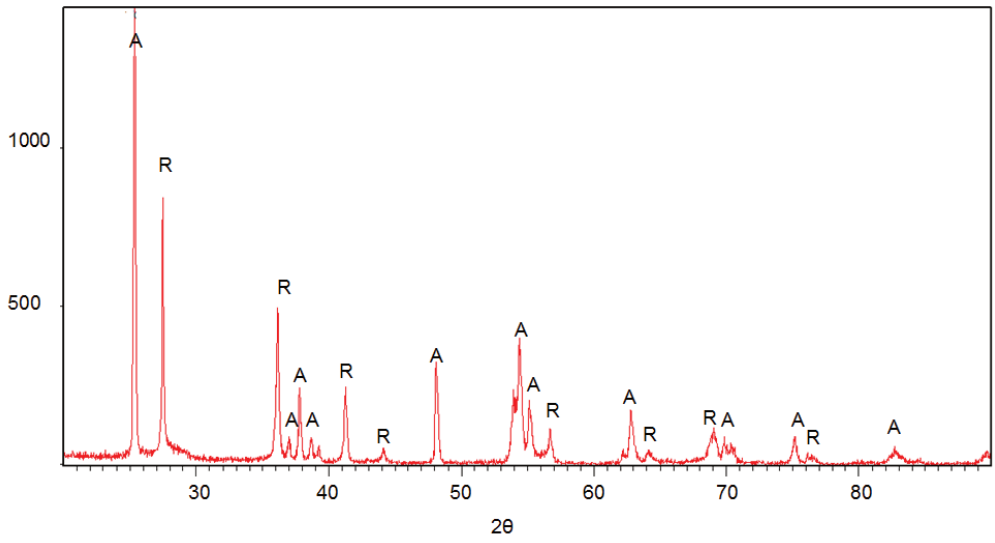

Fig. 42. X ray diffraction pattern of SPS TiO_2 membrane.

Figure. 43, compares the anatase and rutile contents in the feedstock powder and in the final membrane based on XRD results.

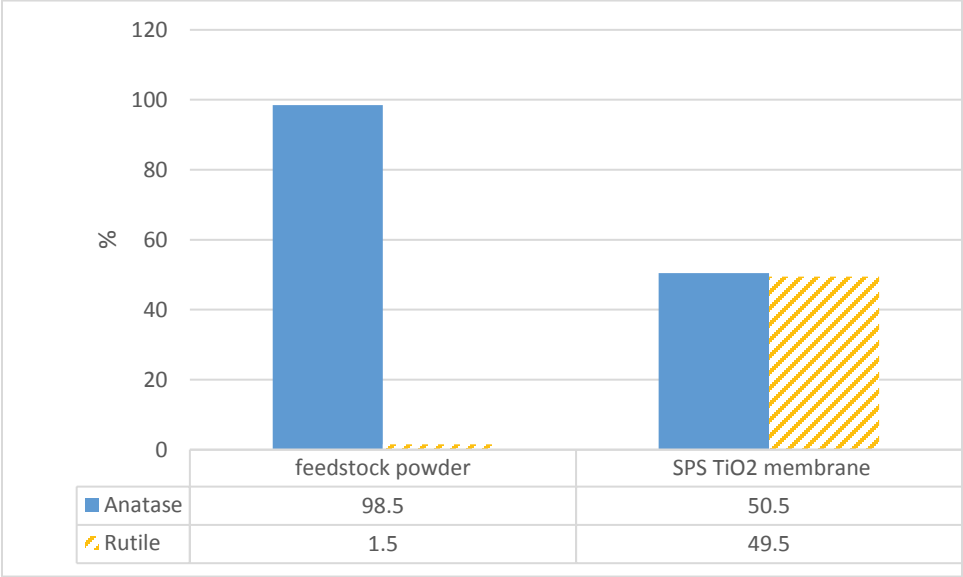

Fig. 43. Anatase and rutile contents in the feedstock powder and in the SPS TiO_2 membrane.

Since anatase transforms to rutile irreversibly at 900K, it may be concluded that the anatase content of SPS TiO_2 membrane was possibly a result of the presence of un-melted particles in the membrane. In the process of deposition of SPS TiO_2 membrane, due to the presence of water as a carrier for feedstock powder, the heat transfer between the plasma and the particles were lower. This could probably result in the presence of more number of un-melted particles with initial anatase phase in the final coating. The similarity of the size of the particles present in the coating and the size of those in the feedstock powder could also support this theory. In addition, looking at Fig. 37(b), by eliminating the porous area, it can be seen that approximately 50% of the surface corresponds to the particles and 50% to the melted zones, which seems to be in accordance with the XRD results showing the presence of 50% anatase in the membrane. However, In SPS nucleation of anatase from the melt is possible depending on the free energy of nucleation and interfacial energy between solid and liquid phase. In SPS process agglomerates of submicron to nano- sized particles are injected into the plasma jet. Some of these particles may melt or evaporate. Melted particles may then re-solidify during the flight or after impinging the substrate as metastable anatase forming nano-sized crystallites.

4.5. Porosity evaluation

In this part the results of porosity measurements obtained by two analytical methods and subsequently the possible origins of porosity generation in suspension plasma spray coatings mentioned in literature will be discussed. However, Since SPS TiO_2 membrane in this work was deposited based on one set of parameters, further investigation based on choosing different suspension and spray parameters is needed to study the effects of these parameters on pore generation in this type of membrane.

Results of image analyzing of SPS TiO_2 membrane showed 17% of porosity in the SPS TiO_2 membrane. Considering that this result was obtained based on a binary image of the cross section surface, it may take all types of pores including closed, blind, cross- linked and through pores in to account. The accuracy of the result may be limited regarding the areas containing non-melted particles shown in Fig. 44, since the adjustment of gray scale threshold in those areas could not be performed accurately. It can be seen that large pores have an anisotropic morphology, while the smaller pores were formed in a more regular shapes. Open and interconnected pores are probably the larger ones containing agglomerates of un-melted particles.

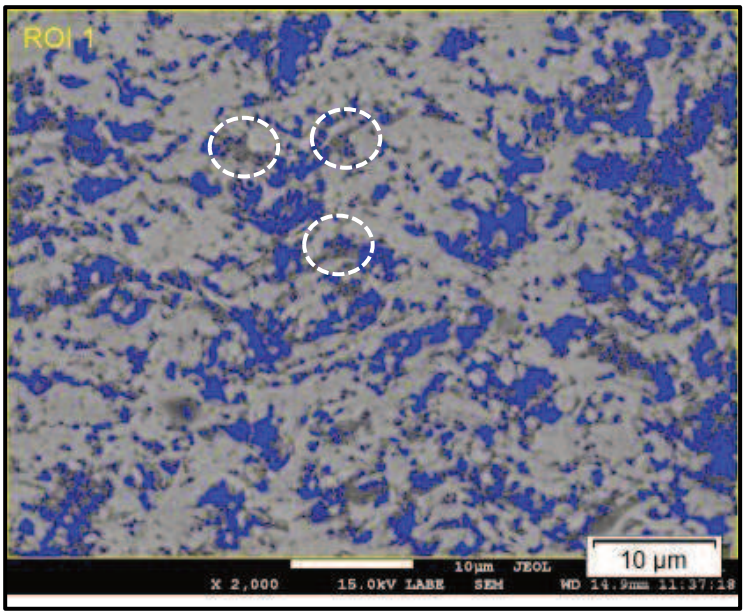

Fig. 44. Gray scale threshold adjustment for image analyzing of SPS TiO_2 membrane.Circled areas show the regions containing un-melted particles.

In order to gather complementary data concerning the bulk of the coating, mercury intrusion porosimetry was performed.

The results of porosity measurement in mercury intrusion porosimetry is based on the possibility of forcing mercury to fill the pores. Consequently, this method gives information on connected to the surface pores including blind pores, crosslinked pores and through pores.

Figure. 45, illustrates the mercury intrusion volume versus pressure in SPS TiO_2 membrane. It can be seen that the intrusion volume increases with increasing the pressure. Large pores in SPS TiO_2 membrane were filled in lower pressures, while higher pressure was needed to fill the small pores. All the connected to the surface pores were filled at 33000 psi.

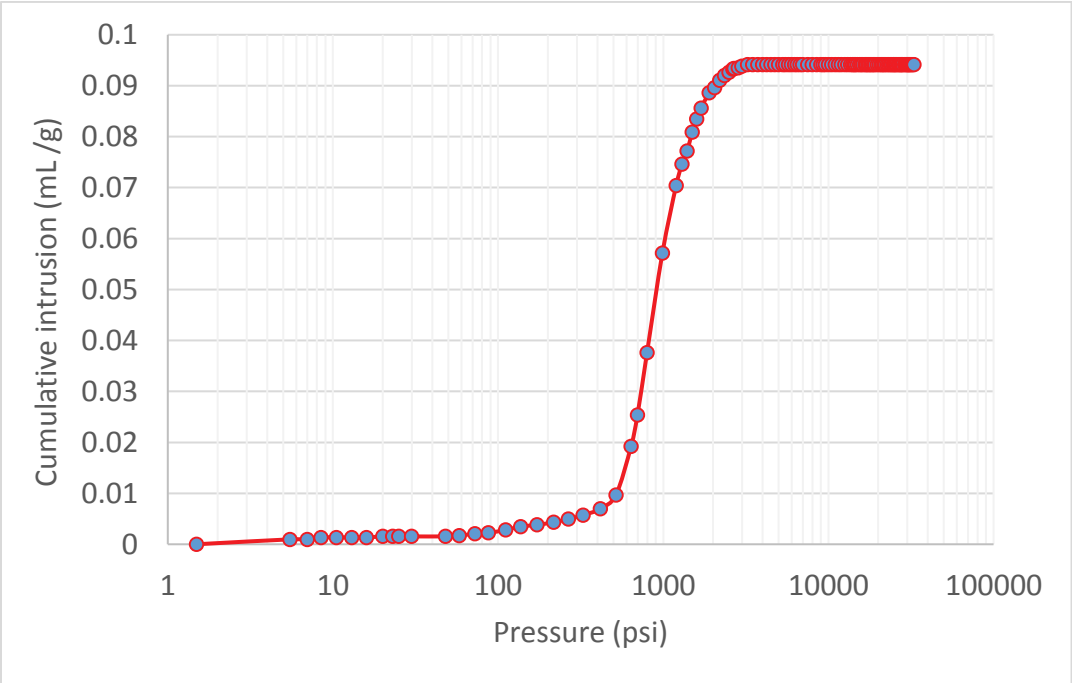

Fig. 45. MIP results of SPS TiO_2 membrane showing the intrusion vs pressure.

Pore size distribution of SPS TiO_2 membrane is illustrated in Fig. 46. A rather narrow pore size distribution can be observed between around 100 nm and 500 nm.

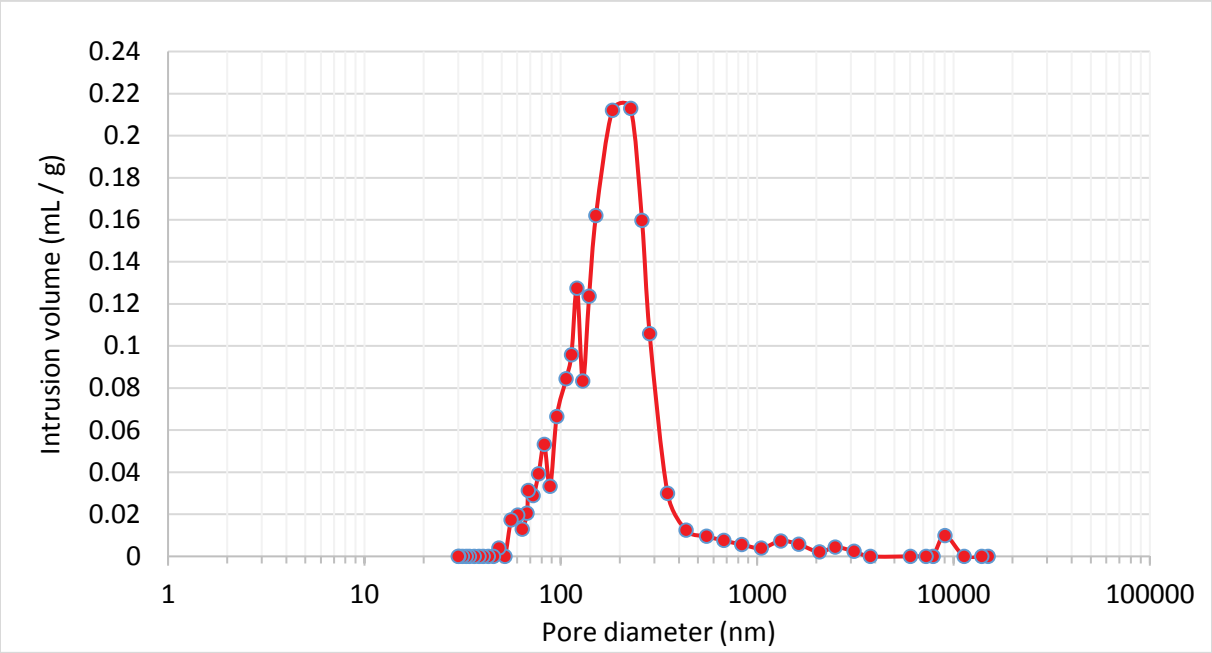

Fig. 46. MIP results of SPS TiO_2 membrane showing Pore size distribution.

Total porosity of SPS TiO_2 membrane measured by mercury intrusion porosimetry was 14%.

The classification of pore diameters illustrated in Fig. 47 shows about 90% of the pores to be in the range of 100- 10,000 nm, which according to Table 1 puts the SPS TiO_2 membrane in the category of microfiltration membranes. With about 86% of the pore sizes in the range of 100- 500 nm, the pore sizes in SPS TiO_2 membrane is close to the lower limit of microfiltration membranes. An average pore diameter of 184 nm was obtained for the membrane. It may be concluded that some of the larger pore sizes were probably corresponded to the columnar features on the surface of the membrane and to the voids between adjacent columns.

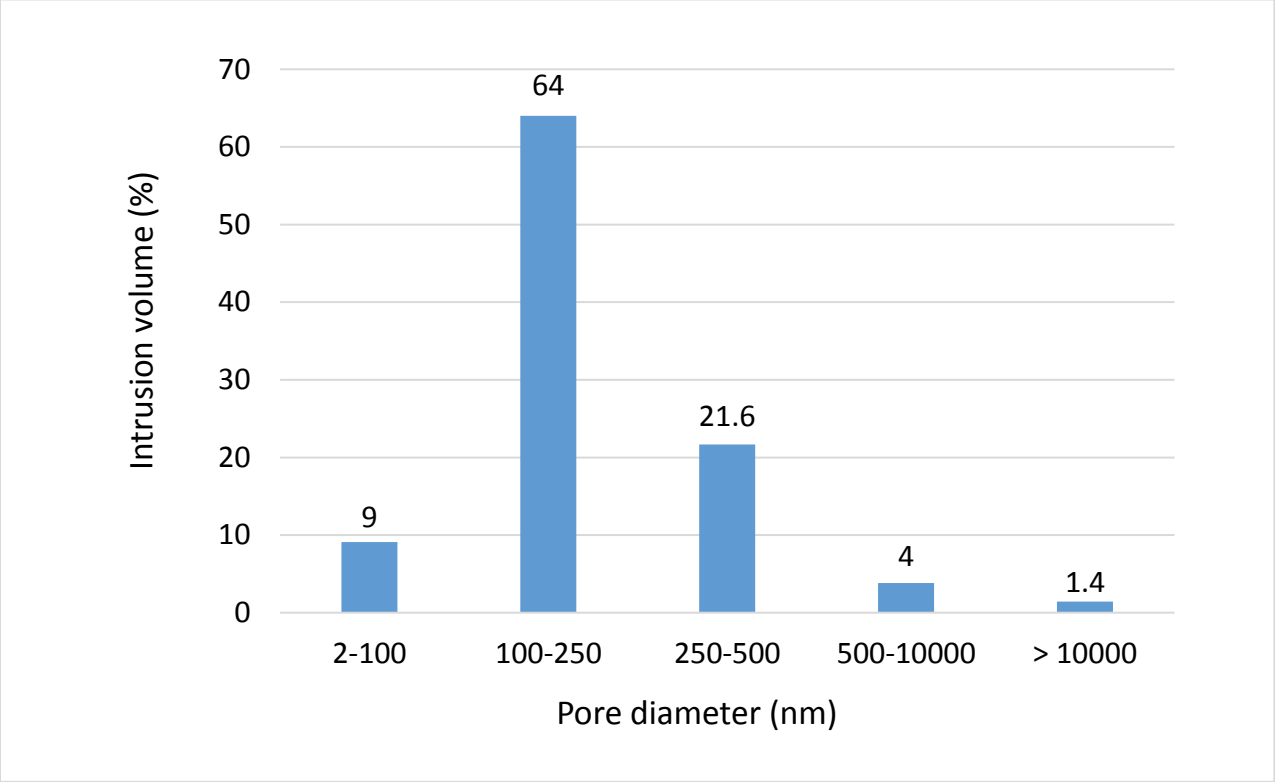

Fig. 47. Pore size classification in SPS TiO_2 membrane.

It needs to be mentioned that the precision on measurements may be limited due to the following factors. In mercury intrusion porosimetry, pore size is determind by converting the intrusion pressure to corresponding pore size based on Washburn equation. One of the most important limitations of mercury intrusion porosimetry is that based on Washburn equation, the pores are considered to be cylindrical. Thus, with this method it is the largest entrance to a pore from the surface of the sample that would be measured and not the actual inner size of a pore. This assumption may cause differences in the analytical results compared to reality, since in the case of this work the shape of the pore network is quite complex. In addition, because of the limitation in the size of the sample, the filled stem volume was less than recommended. However, since the results of total porosity from both analytical methods were not significantly different, it may be concluded that the results were not far from reality.

4.5.1. Effect of the temperature of the substrate

Substrate temperature is a parameter that can influence the deposition formation and the development of microstructure in plasma spraying [90].

Figure. 48 shows the microstructure of polished cross-section of SPS TiO_2 membrane on (a) not cooled and (b) cooled porous alumina substrate.

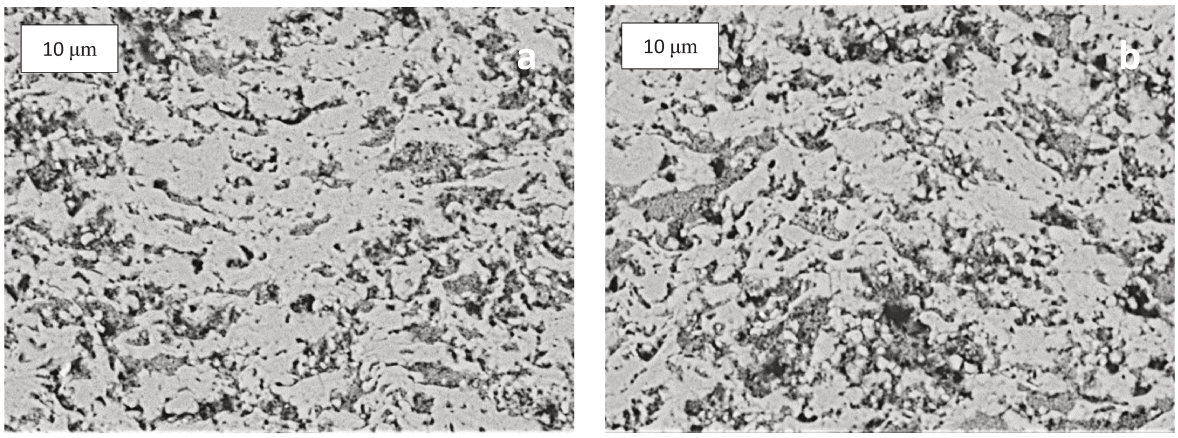

Fig. 48. SEM micrographs of polished cross sections of SPS TiO_2membrane deposited on porous alumina substrate a) without cooling and b) with cooling the substrate.

As it can be observed in Fig. 48, these two microstructures do not seem different. However, as it is summarized in Table 12, measuring the porosity with image analyzing method showed a slight increase of 1.5% in porosity in samples sprayed with cooling the substrate compared to that sprayed without cooling.

Table 12. Porosity measurement of SPS TiO_2 membrane deposited on cooled and not cooled substrates obtained with gray scale image analyzing method.

SPS TiO_2 membrane	Magnification	Porosity[%]
Cooled	2000	17
Not cooled	2000	15.5

The difference may be due to that when the particles impact a high temperature substrate, they deposit in the form of a disc with uniform heat conduction leading to a lower inter-lamellar porosity and enhanced contact between splats. On the other hand, impinging on a low temperature substrate,

particles deposit in the form of splashes, which by providing less contact to the previously deposited splat may result in forming porosity in the deposited coating.

It also can be assumed that the intervals between depositions of two successive layers could promote weaker adhesive bonds between the layers. Although from the cross- sectional view the membrane seems to be uniform, further experiments can be designed in order to evaluate the endurance of the membrane.

Cooling the substrate also influenced the crystalline phases present of the membrane that could influence the porosity content as well. Figure. 49 compares the anatase content and porosity content in membranes sprayed on cooled ant not cooled substrates. The anatase content of the membranes sprayed on cooled substrate was obtained around 10% higher than that in membranes sprayed on not cooled substrate. Considering that the anatase content in the coating could possibly be corresponded to the presence of un-melted anatase particles from the feedstock powder, one may conclude that the higher amount of anatse in the membrane could be interpreted as the presence of more porosity in the membrane deposited on cooled substrate.

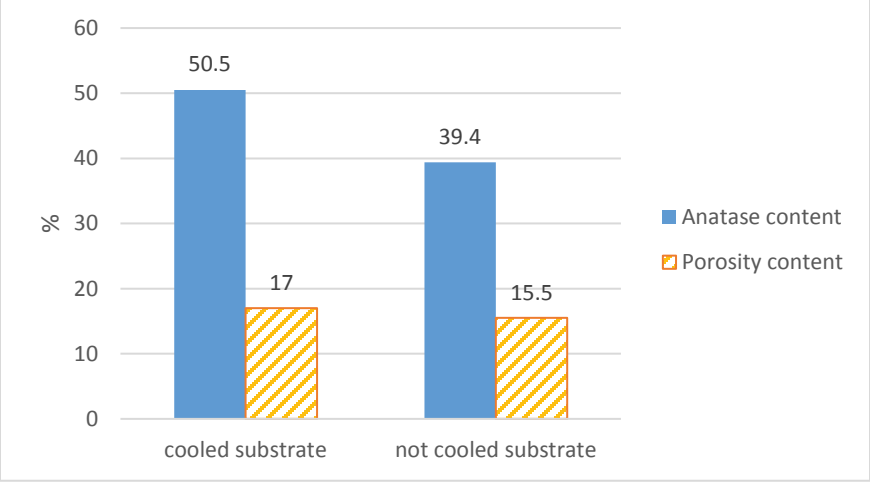

Fig. 49. Anatase content and porosity content in membranes sprayed on cooled ant not cooled substrates.

4.6. Water permeability of the membrane

Figure. 50 shows the experimental measurements of water flux of SPS TiO_2 membrane. Increase in water flux of the membrane showed a linear behavior by increasing the pressure. Clean water flux was obtained as 430 L/h/m²/bar.

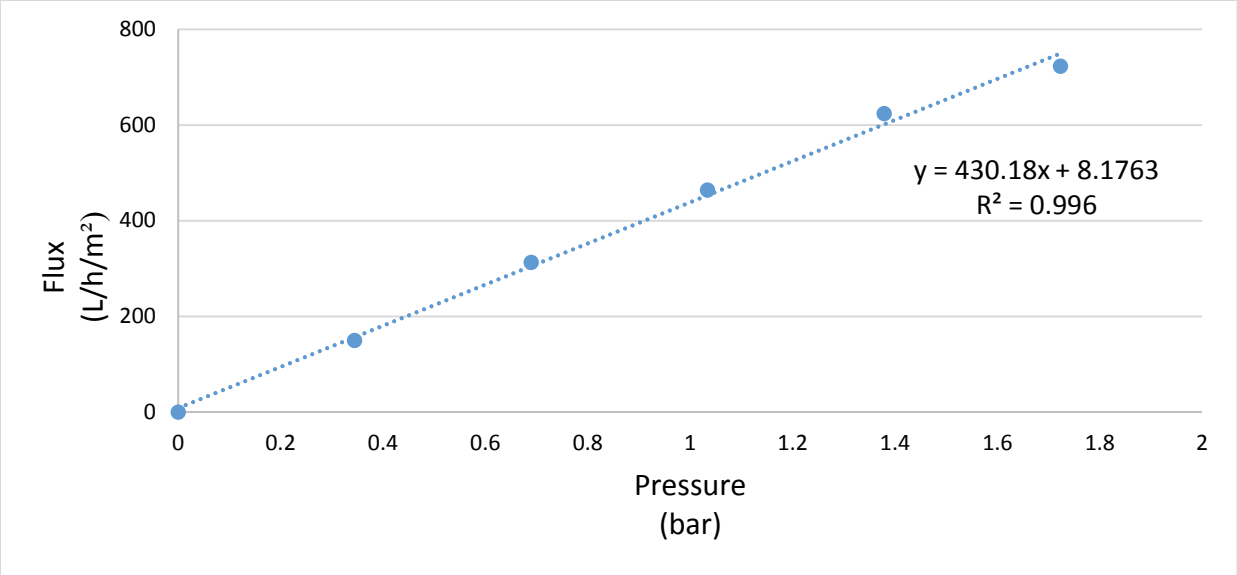

Fig. 50. Water permeability measurement on SPS TiO_2membrane.

The highest pressure applied on this membrane was 25 psi (1.72 bar). Permeation flux of SPS TiO_2membrane in presence of pollutants at constant pressure, which will provide a better understanding of the service operation of this membrane needs to be investigated.

According to the commercial data available on filtration membranes mentioned in Table 1, permeability of SPS TiO_2 membrane is lower than that of microfiltration membranes.

4.6.1. Effect of thickness

The low water permeability of the SPS TiO_2 membrane could be explained by its high thickness. Water permeability of a membrane is inversely proportional to its thickness [60]. Although a higher thickness may produce more porous layers in the SPS membrane, it also may cause the clogging of the pores on the bottom layers. Therefore, there would be no guarantee that the number of interconnected pores may be increased in a coating with higher thickness. Optimum thickness of the membrane needs to be chosen in order to ensure the optimum permeation flux as well as the optimum filtration process. The membrane needs to be thin enough to allow a high flux and to be thick enough to make the filtration process possible. As it was mentioned earlier, the thickness of the membrane was suggested to be considered 50 times more than the particle size. Considering the average feedstock particle size in this work as 137nm, gives the optimum membrane thickness of about 7 µm. The average thickness of SPS TiO_2 membrane was measured as 139 µm. The

thickness of the uniform section of the coating was around 100 µm, which gives a value around 14 times greater than that suggested in litrature. Thus, it may be concluded that by decreasing the membrane thickness the permeability would increase.

4.7. Photocatalytic activity of the membrane

Photocalitycal behavior of SPS TiO_2 membrane was evaluated through measuring the degradation of an aqueous solution of an organic dye, methylene blue, under UVC illumination. Figure. 51 illustrates the degradation of methylene blue within 80 min. The degradation can be observed by gradual change in the color of the solution from blue in sample number 1, to complete decoloration of the solution in sample number 9.

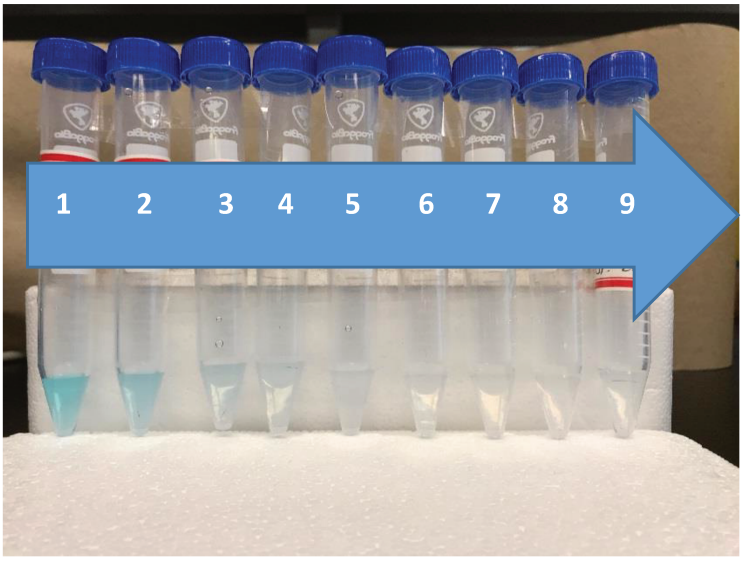

Fig. 51. Degradation of methylene blue by decoloration of the solution in the presence of SPS TiO_2 membrane.

Figure. 52 shows the degradation of methylene blue under UVC light with and without membrane. Although degradation of methylene blue aqueous solution occurred under UVC illumination and in the absence of membrane, addition of SPS TiO_2 membrane had a significant influence on increasing the degradation of the dye solution and almost total degradation occurred after 80 min.

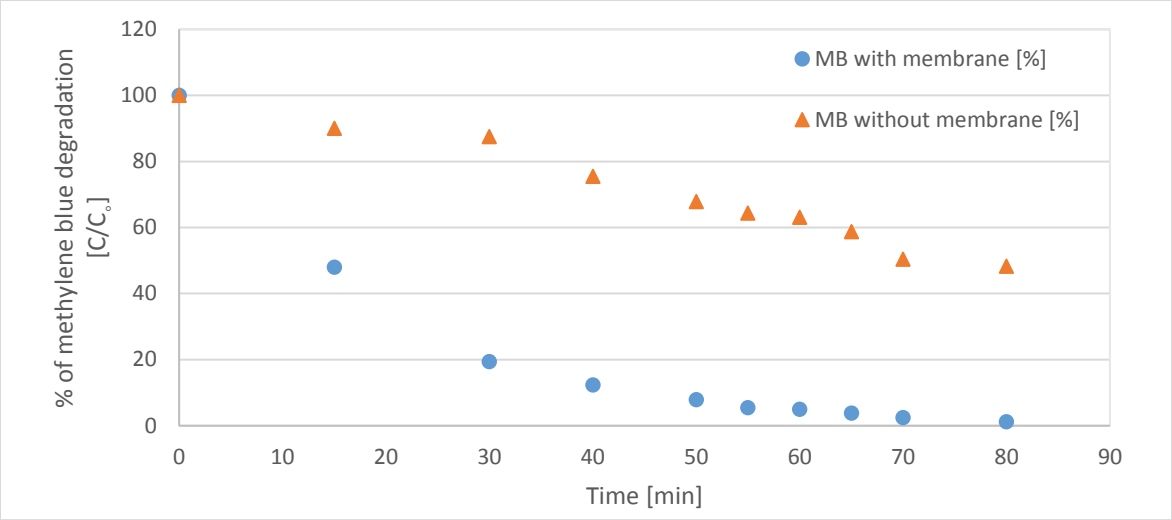

Fig. 52. Influence of SPS TiO_2 membrane on Photo degradation of methylene blue.

The variation in methylene blue concentration with time may be represented using equation (4)

$$\frac{-dC}{dt} = kC \tag{4}$$

Which after integration results in equation (5)

$$-\ln\frac{C}{C0} = kt \tag{5}$$

where C is the methylene blue concentration *(ppm)*, $C_\circ$ is the initial concentration of methylene blue, t is the irradiation time *(h)*, and k is the constant of photocatalytic activity (min^{-1}) [38].

Figure. 53, shows the plot of ln ($C_\circ/C$) against time, for methylene blue under UVC light with and without the membrane, in which the slope corresponds to k. higher values for k, corresponds to faster degradation of dye solution.

The rate constant for SPS TiO_2 membrane under UVC light was obtained as 0.053 min^{-1} with correlation coefficient of 0.993. The constant rate for UVC light and without the membrane was obtained as 0.0094 min^{-1} with correlation coefficient of 0.953. Therefore, it can be concluded that the presence of SPS TiO_2 membrane increases the rate constant by the factor of 5.7.

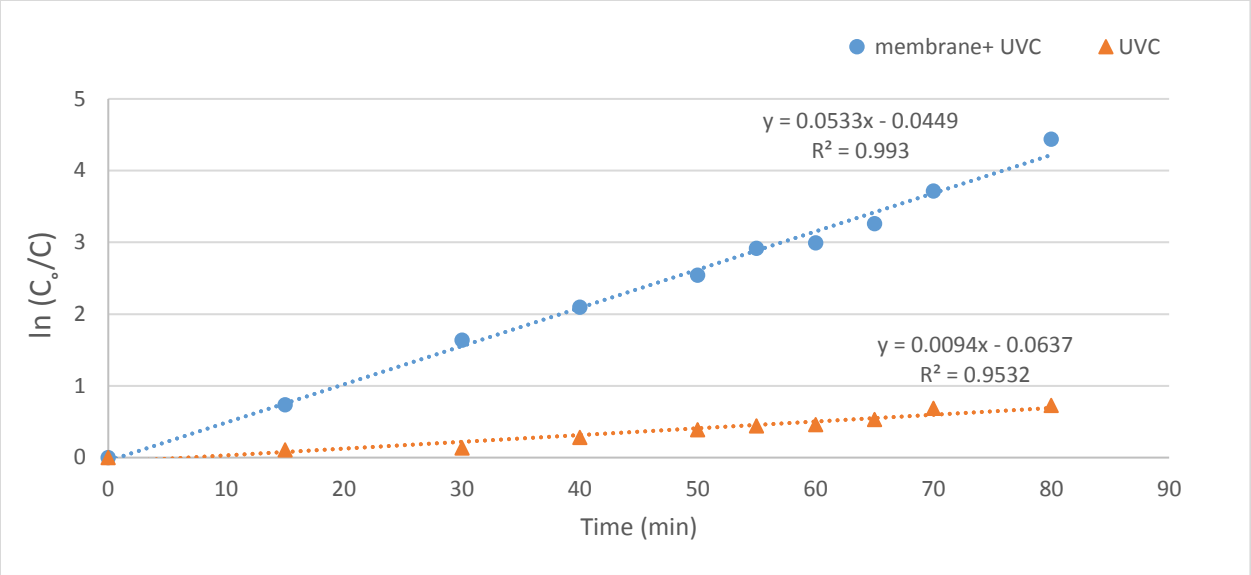

Fig. 53. Variation of ln (C_0/C) with irradiation time for SPS TiO_2 membrane+ UVC light and for UVC light.

Degradation of methylene blue aqueous solution with UVC light can be corresponded to the potential of UVC light to enable directs photolysis action on methylene blue and the fact that UVC photons can decrease the probability of recombination of electron-hole species due to the shorter penetration in catalyst particles resulting in higher photocataltytical activity [91].

4.7.1. Effect of porosity and surface roughness

As mentioned, a drawback of using catalysts in the form of membranes instead of powder was the decrease in their capacity of degrading organic contaminants due to the reduction of active surface area. In the case of SPS TiO_2 membrane, porous structure of the membrane as well as the presence of columnar structure on the surface of the membrane, showed in Fig. 54, may have been one of the parameters that acted in favor of the photo reactivity of the membrane by increasing the active surface area.

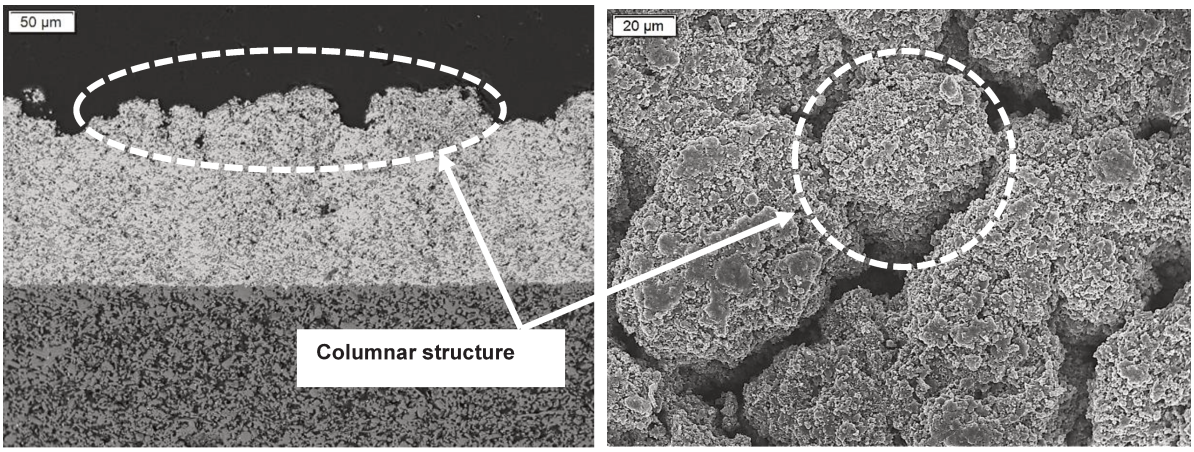

Fig. 54. Columnar structure on the surface of SPS TiO_2 membrane; left) cross- sectional view, right) top view.

5. Conclusion and future work

This study investigated, the capacity of suspension plasma spray process as an innovative technique to deposit sub-micron sized particles, in order to fabricate liquid permeable titanium dioxide membranes for filtration application for the first time.

SPS TiO_2 membrane was deposited on a porous alumina substrate in order to generate a hybrid microfiltration/ photocatalysis membrane. Generation of the porous water permeable membrane was carried out through controlling and optimization of some process parameters. In addition, controlling the ceramic substrate temperature during spray process was proved to be an essential factor in order to produce an intact membrane system.

SEM analysis of the membrane revealed a uniform porous coating with a unique complex microstructure, in which the network of open pores was built by un-melted and re-solidified particles entrapped in a body made by fully melted particles and the membrane coating was adhered to the porous substrate completely. Different microstructural features, including dense and porous regions and columnar features on the surface of the membrane were recognized. Porosity evaluation of the membrane confirmed the presence of 14% open porosity in the membrane with about 95% of the pore under 500 nm, which puts the SPS TiO_2 membrane in the class of micro filtration membranes. Clean water permeability of about 430 L/h/m²/bar was obtained for SPS TiO_2 membrane. Water permeability may be improved by decreasing the thickness of the membrane. Photocatalytical performance of SPS TiO_2 membrane demonstrated the capacity of the membrane to be used to degrade organic pollutants. This property would also be useful for defouling of the membrane surface. A more homogenous membrane could be obtained by polishing the columnar features observed on the top layer of the membrane or by depositing a thinner membrane coating.

While some of the trends described in this manuscript obviously require more detailed investigation, the results clearly showed the potential of suspension plasma spray for production of ceramic membranes. Further studies are needed for optimizing the spray parameters and the material combination to achieve better flux and filtration performance by these membranes.

The following lines of investigation can be proposed for further development of the application of suspension plasma spray technique for ceramic membrane manufacturing:

- Optimization of process parameters in order to improve the water flux of the membrane through increasing the porosity content or decreasing the membrane thickness. Effect of the membrane thickness can be evaluated by a layer by layer deposition approach by spraying multiple samples and each time increasing the coating thickness by deposition of one extra layer. In this case the critical thickness of the membrane after which the columnar structure would start to grow may also be determined.
- Fabricating membranes with various pore size and porosity by taking approaches such as designing proper spray parameters, controlling the pore size by the feedstock particle size and adding pore forming agents in the suspension.
- Investigation of the capacity of the SPS method for deposition of the membrane on substrates with complex shapes. The possibility of deposition of the membrane on metallic substrates may be advantageous since it can potentially decrease the price.
- Investigation of the rejection rate and photocatalytical behavior of the membrane with various contaminants in order to gather more information on the filtration performance of the membrane. In addition, the influence of parameters such as ph, temperature and concentration of the contaminant on the degradation process could be investigated.
- Investigating the development of SPS titanium dioxide membrane that could be used as a photocatalyst under visible light.

6. References

[1] D. Grey, D. Garrick, D. Blackmore, J. Kelman, M. Muller, and C. Sadoff, "Water security in one blue planet: twenty-first century policy challenges for science.," *Philos. Trans. A. Math. Phys. Eng. Sci.*, vol. 371, no. 2002, pp. 201-204, 2013.

[2] M. M. Pendergast and E. M. V. Hoek, "A review of water treatment membrane nanotechnologies," *Energy Environ. Sci.*, vol. 4, no. 6, p. 1946, 2011.

[3] M. M. Mekonnen and Y. A. Hoekstra, "Four Billion People Experience Water Scarcity," *Sci. Adv.*, vol. 2:e1500323, no. February, pp. 1–7, 2016.

[4] C. J. Vörösmarty, P.B. McIntyre, M. O. Gessner, D. Dudgeon, A. Prusevich, P. Green, S. Glidden, S. E. Bunn, C. A. Sullivan, C.R. Liermann, and P.M. Davies , "Global threats to human water security and river biodiversity," *Nature*, vol. 467, no. 7315, pp. 555–561, 2010.

[5] R. Herman, S. Sampath, and R. McCune,"Thermal Spray: Current Status and Future Trends," *MRS Bull.*, vol. 25, no. 7, pp. 17-25, 2000.

[6] J.V. Heberlein, P. Fauchais and M. Boulos, "Thermal Spray Fundamentals," New York: Springer, 2014.

[7] M. Mulder, "Basic principles of membrane technology," Dordrecht: Kluwer Acad. Publ., 2010.

[8] S. Alzahrani and A. W. Mohammad, "Challenges and trends in membrane technology implementation for produced water treatment: A review," *J. Water Process Eng.*, vol. 4, pp. 107–133, 2014.

[9] H. E. Johnson and B. L. Schulman, "Assessment of the potential for refinery applications of inorganic membrane technology: An identification and screening analysis. Final report ." No. DOE/FE/61680-H3. SFA Pacific, Inc., Mountain View, CA (United States), 1993.

[10] R. W. Baker, "Membrane Technology and Applications." Hoboken, N.J.: Wiley, 2013.

[11] R. Mallada and M. Menéndez, "Inorganic membranes: synthesis, characterization and applications." Amesterdam: Elsevier, 2013.

[12] B. Van Der Bruggen, C. Vandecasteele, T. Van Gestel, W. Doyen, and R. Leysen, "A review of pressure-driven membrane processes in wastewater treatment and drinking water production," *Environ. Prog.*, vol. 22, no. 1, pp. 46–56, 2003.

[13] M. Ulbricht, "Advanced functional polymer membranes," vol. 47, no. 7, pp. 2217–2262, 2006.

[14] R. W. Baker and B. T. Low, "Gas separation membrane materials: A perspective," *Macromolecules*, vol. 47, no. 20, pp. 6999–7013, 2014.

[15] A. Prakash Rao, N. V Desai, and R. Rangarajan, "Interfacially synthesized thin film composite RO membranes for seawater desalination," *J. Membr. Sci.*, vol. 124, no. 2, pp. 263–272, 1997.

[16] A. Sagle and B. Freeman, "Fundamentals of membranes for water treatment," *Futur. Desalin. Texas*, vol. 2, no. 137, pp. 1–17, 2004.

[17] J. Kim and B. Van Der Bruggen, "The use of nanoparticles in polymeric and ceramic membrane structures: Review of manufacturing procedures and performance improvement for water treatment," *Environ. Pollut.*, vol. 158, no. 7, pp. 2335–2349, 2010.

[18] A. Rahimpour, M. Jahanshahi, B. Rajaeian, and M. Rahimnejad, "TiO2 entrapped nano-composite PVDF/SPES membranes: Preparation, characterization, antifouling and antibacterial properties," *Desalination*, vol. 278, no. 1–3, pp. 343–353, 2011.

[19] L. Yan, Y. S. Li, and C. B. Xiang, "Preparation of poly(vinylidene fluoride)(pvdf) ultrafiltration membrane modified by nano-sized alumina (Al2O3) and its antifouling research," *Polymer.*, vol. 46, no. 18, pp. 7701–7706, 2005.

[20] M. Zargar, Y. Hartanto, B. Jin, and S. Dai, "Polyethylenimine modified silica nanoparticles enhance interfacial interactions and desalination performance of thin film nanocomposite membranes," *J. Memb. Sci.*, vol. 541, pp. 19–28, 2017.

[21] A. Bottino, G. Capannelli, and A. Comite, "Preparation and characterization of novel porous PVDF-ZrO2 composite membranes," *Desalination*, vol. 146, no. 1–3, pp. 35–40, 2002.

[22] L. Huang, S. Zhao, Z. Wang, J. Wu, J. Wang, and S. Wang, "In situ immobilization of silver nanoparticles for improving permeability, antifouling and anti-bacterial properties of

ultrafiltration membrane," *J. Memb. Sci.*, vol. 499, pp. 269–281, 2016.

[23] J. Finley, "Ceramic membranes: A robust filtration alternative," *Filtr. Sep.*, vol. 42, no. 9, pp. 34–37, 2005.

[24] T. Tsuru, "Inorganic Porous Membranes for Liquid Phase Separation," *J. Separation & purification methods,* vol. 30, no. 2, pp. 191- 220, 2001.

[25] M. M. Cortalezzi, J. Rose, A. R. Barron, and M. R. Wiesner, "Characteristics of ultrafiltration ceramic membranes derived from alumoxane nanoparticles," *J. Memb. Sci.*, vol. 205, no. 1–2, pp. 33–43, 2002.

[26] R. R. Bhave, J. Guibaud and R. Rumeau, "Inorganic Membranes Synthesis, Characteristics and Applications ," Dordrecht: Springer, 1991.

[27] X. Ding, Y. Fan, and N. Xu, "A new route for the fabrication of TiO2 ultrafiltration membranes with suspension derived from a wet chemical synthesis," *J. Memb. Sci.*, vol. 270, no. 1–2, pp. 179–186, 2006.

[28] Y. Lv, H. Liu, Z. Wang, L. Hao, Y. Sang, D. Liu, J. Wang, and R. Boughton, "Silver nanoparticle-decorated porous ceramic composite for water treatment," *J. Memb. Sci.*, vol. 331, no. 1–2, pp. 50–56, Apr. 2009.

[29] B.S. Karnik, S.H. Davies, M.J. Baumann, and S.J. Masten, "Fabrication of Catalytic Membranes for the Treatment of Drinking Water Using Combined Ozonation and Ultrafiltration." vol. 39, no. 19, pp. 7656- 7661, 2005.

[30] N. Ma, X. Quan, Y. Zhang, S. Chen, and H. Zhao, "Integration of separation and photocatalysis using an inorganic membrane modified with Si-doped TiO2 for water purification," *J. Memb. Sci.*, vol. 335, no. 1–2, pp. 58–67, 2009.

[31] "Wastewater UV Disinfection Systems - TrojanUV." [Online]. Acssessed on July, 05, 2018. Available: https://www.trojanuv.com/products/wastewater/.

[32] S. K. Sastry, A. K. Datta, and R. W. Worobo , "Ultraviolet Light," *J. Food Sci.*, vol. 65, no. 8, pp. 90–92, 2000.

[33] "Fresh-Aire UV." [Online]. Acssessed on July, 05, 2018. Available: https://www.freshaireuv.com/index.html.

[34] "Air Oasis UV PCO Air Purifiers, UV Air Cleaners Sanitizers." [Online]. Acssessed on July, 05, 2018. Available: https://www.air-oasis-uv-pco-sanitizers.com/.

[35] C. Ramli, Z. Amali, N. Asim, W.N. Isahak, Z. Emdadi, N. Ahmad-Ludin, M.A Yarmo, M.A. and K. Sopian, "Photocatalytic degradation of methylene blue under UV light irradiation on prepared carbonaceous TiO2.," *ScientificWorldJournal.*, 2014.

[36] C. G. Joseph, Y. H. Taufiq-Yap, G. Li Puma, K. Sanmugam, and K. S. Quek, "Photocatalytic degradation of cationic dye simulated wastewater using four radiation sources, UVA, UVB, UVC and solar lamp of identical power output," *Desalin. Water Treat.*, vol. 57, no. 17, pp. 7976–7987, 2016.

[37] C. Xu, G. P. Rangaiah, and X. S. Zhao, "Photocatalytic Degradation of Methylene Blue by Titanium Dioxide: Experimental and Modeling Study." *J. Ind & Eng Chemistry research*, vol. 53, no. 38, pp. 14641- 14649, 2014.

[38] E. Bannier, G. Darut, E. Sánchez, A. Denoirjean, M.C. Bordes, M. D. Salvador, E. Rayón, E. and H. Ageorges, "Microstructure and photocatalytic activity of suspension plasma sprayed TiO2 coatings on steel and glass substrates," *Surf. Coatings Technol.*, vol. 206, no. 2–3, pp. 378–386, 2011.

[39] S. Kozerski, F. L. Toma, L. Pawlowski, B. Leupolt, L. Latka, and L. M. Berger, "Suspension plasma sprayed TiO2 coatings using different injectors and their photocatalytic properties," *Surf. Coatings Technol.*, vol. 205, no. 4, pp. 980–986, 2010.

[40] F.-L. Toma, G. Bertrand, D. Klein, C. Coddet, and C. Meunier, "Nanostructured photocatalytic titania coatings formed by suspension plasma spraying," *J. Therm. Spray Technol.*, vol. 15, no. 4, pp. 587–592, 2006.

[41] J. H. Carey, J. Lawrence, and H. M. Tosine, "Photodechlorination of PCB's in the Presence of Titanium Dioxide in Aqueous Suspensions." *Bull. of Environmental Contamination and Toxicology*, vol.16, no. 6, pp. 697-701, 1976.

[42] E. Friedler and Y. Gilboa, "Performance of UV disinfection and the microbial quality of greywater effluent along a reuse system for toilet flushing," *Sci. Total Environ.*, vol. 408, no. 9, pp. 2109–2117, Apr. 2010.

[43] C. Sattler, L. de Oliveira, M. Tzschirner, and A. E. H. Machado, "Solar photocatalytic water

detoxification of paper mill effluents," *Energy*, vol. 29, no. 5–6, pp. 835–843, Apr. 2004.

[44] M. R. Hoffmann, S. T. Martin, W. Choi, D. W. Bahnemannt, and W. M. Keck, "Environmental Applications of Semiconductor Photocatalysis," *Chem. Rev*, vol. 95, no.1, pp. 69–96, 1995.

[45] F.L. Toma, L.M, Berger, I. Shakhverdova, B. Leupolt, A. Potthoff, K. Oelschlägel, T. Meissner, J. Gomez, and Y. Miguel, "Parameters Influencing the Photocatalytic Activity of Suspension-Sprayed TiO2 Coatings," *J. Therm. Spray Technol.*, vol. 23, no. October, pp. 1–17, 2014.

[46] K. Madhusudan Reddy, S. V Manorama, and A. Ramachandra Reddy, "Bandgap studies on anatase titanium dioxide nanoparticles," *Mater. Chem. Phys.*, vol. 78, no. 1, pp. 239–245, 2003.

[47] Y. Ao, J. Xu, D. Fu, L. Ba, C. Yuan, "Deposition of anatase titania onto carbon encapsulated magnetite nanoparticles," *Nanotechnol.*, vol. 19, no. 40, pp.405604, 2008.

[48] R. Molinari, M. Mungari, E. Drioli, A. Paola, and V. Loddo, "Study on a photocatalytic membrane reactor for water purification," *Catal. Today*, vol. 55, no. 1–2, pp. 71–78, 2000.

[49] R.-X. Zhang, L. Braeken, P. Luis, X.-L. Wang, and B. Van Der Bruggen, "Novel binding procedure of TiO 2 nanoparticles to thin film composite membranes via self-polymerized polydopamine," *J. Memb. Sci.*, vol. 437, pp. 179–188, 2013.

[50] S. S. Chin, K. Chiang, and A. G. Fane, "The stability of polymeric membranes in a TiO2 photocatalysis process," *J. Memb. Sci.*, vol. 275, no. 1–2, pp. 202–211, Apr. 2006.

[51] H. Choi, E. Stathatos, and D. D. Dionysiou, "Sol-gel preparation of mesoporous photocatalytic TiO2 films and TiO2/Al2O3 composite membranes for environmental applications," *Appl. Catal. B Environ.*, vol. 63, no. 1–2, pp. 60–67, 2006.

[52] F. L. Toma, L. M. Berger, C. C. Stahr, T. Naumann, and S. Langner, "Microstructures and functional properties of suspension-sprayed Al 2O 3 and TiO 2 coatings: An overview," *J. Therm. Spray Technol.*, vol. 19, no. 1–2, pp. 262–274, 2010.

[53] E. S. C. Fan and O. Kesler, "Deposition of Lanthanum Strontium Cobalt Ferrite (LSCF) Using Suspension Plasma Spraying for Oxygen Transport Membrane Applications," *J.*

Therm. Spray Technol., vol. 24, no. 6, pp. 1081–1092, 2015.

[54] A. Killinger, R. Gadow, G. Mauer, A. Guignard, R. Vaßen, and D. Stöver, "Review of New Developments in Suspension and Solution Precursor Thermal Spray Processes." *J. Therm. Spray Technol.*, vol. 20, no.4, pp.677, 2011.

[55] O. Kesler, "Plasma Spray Processing of Solid Oxide Fuel Cells," *Mater. Sci. Forum*, vol. 539, pp. 1385–1390, 2007.

[56] P. Fauchais, M. Vardelle, A. Vardelle, and L. Bianchi, "Plasma Spray: Study of the Coating Generation," *Ceram. Int. Publ. bv Elsevier Sci. Ltd. Techna S.r*, vol. 221, no. 95, pp. 295–303, 1996.

[57] G. Ramakrishnan, G. Dwivedi, S. Sampath, and A. Orlov, "Development and optimization of thermal sprayed ceramic microfiltration membranes," *J. Memb. Sci.*, vol. 489, pp. 106–111, Sep. 2015.

[58] X. Ma, J. Dai, H. Zhang, J. Roth, T. D. Xiao, and D. E. Reisner, "Solid Oxide Fuel Cell Development by Using Novel Plasma Spray Techniques," *J. Fuel Cell Sci. Technol.*, vol. 2, no. 3, p. 190, 2005.

[59] A. A. Kulkarni, S. Sampath, A. Goland, and H. Herman, "Plasma spray coatings for producing next-generation supported membranes," *Top. Catal.*, vol. 32, no. 3–4, pp. 241–249, 2005.

[60] S. S. Madaeni, M. E. Aalami-Aleagha, and P. Daraei, "Preparation and characterization of metallic membrane using wire arc spraying," *J. Memb. Sci.*, vol. 320, no. 1–2, pp. 541–548, 2008.

[61] K. L. Tung, C. Hsiung, T.C. Ling, K.S Chang, T. Wu, and Y.L. Li,, "Preparation and characterization of aluminum oxide cermet microfiltration membrane using atmospheric plasma spraying," *Desalination*, vol. 245, no. 1–3, pp. 408–421, 2009.

[62] F. L. Toma, A. Potthoff, L. M. Berger, and C. Leyens, "Demands, Potentials, and Economic Aspects of Thermal Spraying with Suspensions: A Critical Review," *J. Therm. Spray Technol.*, vol. 24, no. 7, pp. 1143–1152, 2015.

[63] R. Vaßen, H. Kaßner, G. Mauer, and D. Stöver, "Suspension Plasma Spraying: Process

Characteristics and Applications." *J. Therm. Spray Technol.*,, vol.19, no. 1-2, pp. 219- 225, Jan. 2010.

[64] L. Pawlowski, "Suspension and solution thermal spray coatings," *Surf. Coatings Technol.*, vol. 203, no. 19, pp. 2807–2829, 2009.

[65] P. Fauchais, V. Rat, C. Delbos, J. F. Coudert, and T. Chartier, "Understanding of Suspension DC Plasma Spraying of Finely Structured Coatings for SOFC."*Trans. on Plasma Sci*., vol. 33, no. 2, pp. 920- 930, 2010.

[66] P. Fauchais, R. Etchart, and C. Delbos, "Suspension and solution plasma spraying of finely structured layers: potential application to SOFCs," *J. Phys. D Appl. Phys*, vol. 40, pp. 2394–2406, 2007.

[67] N. Sharifi, M. Pugh, C. Moreau, and A. Dolatabadi, "Developing hydrophobic and superhydrophobic TiO 2 coatings by plasma spraying," *Surf. Coat. Technol.*, vol. 289, pp. 29–36, 2016.

[68] A. Vardelle, C. Moreau, N. J. Themelis, and C. Chazelas, "A Perspective on Plasma Spray Technology." Plasma Chem. and Plasma Process., vol.35, no. 3, pp.491-509, May. 2015.

[69] P. Fauchais, V. Rat, J. F. Coudert, R. Etchart-Salas, and G. Montavon, "Operating parameters for suspension and solution plasma-spray coatings," *Surf. Coatings Technol.*, vol. 202, no. 18, pp. 4309–4317, 2008.

[70] P. Fauchais and A. Vardelle, "Solution and Suspension Plasma Spraying of Nanostructure Coatings," *Adv. Plasma Spray Appl.*, no. March 2012, pp. 149–188, 2012.

[71] P. Fauchais, R. Etchart-Salas, V. Rat, J. F. Coudert, N. Caron, and K. Wittmann-Ténèze, "Parameters controlling liquid plasma spraying: Solutions, sols, or suspensions," *J. Therm. Spray Technol.,* vol. 17, no. 1, pp. 31-59, Mar. 2008.

[72] J. O. Berghaus, J.-G. Legoux, C. Moreau, F. Tarasi, and T. Chráska, "Mechanical and Thermal Transport Properties of Suspension Thermal-Sprayed Alumina-Zirconia Composite Coatings." *J. Therm. Spray Technol.,* vol. 17, no.1 pp. 91 104, 2008.

[73] K. Vanevery, M. Krane, R.W. Trice, and, H. Wang, "Column Formation in Suspension Plasma-Sprayed Coatings and Resultant Thermal Properties." *J. Therm. Spray Technol.,*

vol. 20, no. 4, pp. 817- 828, 2011.

[74] F. L. Toma, L. M. Berger, D. Jacquet, and D. Wicky, "Comparative study on the photocatalytic behaviour of titanium oxide thermal sprayed coatings from powders and suspensions," *Surf. Coatings Technol.*, vol. 203, no. 15, pp. 2150–2156, 2009.

[75] F. L. Toma, G. Bertrand, D. Klein, C. Meunier, and S. Begin, "Development of photocatalytic active Tio2 surfaces by thermal spraying of nanopowders," *J. Nanomater.*, vol. 2008, no. 1, p. 58, 2008.

[76] E. Bannier, G. Darut, E. Sánchez, A. Denoirjean, M.C. Bordes, M. D. Salvador, E. Rayón, E. and H. Ageorges, "Microstructure and photocatalytic activity of suspension plasma sprayed TiO2 coatings on steel and glass substrates," *Surf. Coatings Technol.*, vol. 206, no. 2–3, pp. 378–386, 2011.

[77] D. A. H. Hanaor and C. C. Sorrell, "Review of the anatase to rutile phase transformation." *J. Material Sci.,* vol. 46, no. 4, pp. 855- 874, 2011.

[78] G. Mauer, A. Guignard, and R. Vaßen, "Plasma spraying of efficient photoactive TiO2 coatings," *Surf. Coatings Technol.*, vol. 220, pp. 40–43, 2013.

[79] E. S. C. Fan and O. Kesler, "Deposition of Lanthanum Strontium Cobalt Ferrite (LSCF) Using Suspension Plasma Spraying for Oxygen Transport Membrane Applications," *J. Therm. Spray Technol.*, vol. 24, no. 6, pp. 1081- 1092, Aug. 2015.

[80] M. C. Bordes, M. Vincent, A. Moreno, and R. Moreno, "Microstructure and photocatalytic activity of APS coatings obtained from different TIO2 nanopowders," *Surf. Coatings Technol.*, vol. 220, pp. 179–186, Apr. 2013.

[81] O. Rezania, "Anelastic Behavior of Suspension Plasma Sprayed Ceramic Coatings," Master, Concordia University, 2016.

[82] R. Rampon, O. Marchand, C. Filiatre, and G. Bertrand, "Influence of suspension characteristics on coatings microstructure obtained by suspension plasma spraying," *Surf. Coatings Technol.*, vol. 202, no. 18, pp. 4337–4342, Jun. 2008.

[83] A. B. Abell, K. L. Willis, and D. A. Lange, "Mercury Intrusion Porosimetry and Image Analysis of Cement-Based Materials." *J. Colloid & Interface Sci.*, vol. 211, no. 1, pp. 39-

44. Mar. 1999.

[84] S. hee Kim and C. C. Chu, "Pore structure analysis of swollen dextran-methacrylate hydrogels by SEM and mercury intrusion porosimetry," *J. Biomed. Mater. Res.*, vol. 53, no. 3, pp. 258–266, 2000.

[85] "HP4750 assembly; operational manual." Sterlitch corp., 2018. Accessed on July, 5, 2018, [Online].Available:https://www.sterlitech.com/media/wysiwyg/Manual2018/Manual_HP4750.pdf

[86] K. Fischer, M. Grimm, J. Meyers, C. Dietrich, R. Gläser, and A. Schulze, "Photoactive microfiltration membranes via directed synthesis of TiO 2 nanoparticles on the polymer surface for removal of drugs from water," *J. Membrane Sci.,* vol. 478, pp. 49- 57, 2015.

[87] D. J. Udonne, N. A. Folami, "Treatment of Industrial Waste Effluent Using Treated Bagasse," *Int. J. Sci. Eng. Res.*, vol. 7, no. 3, pp. 389- 397, 2016.

[88] Z. Živcová, E. Gregorová, W. Pabst, D. S. Smith, A. Michot, and C. Poulier, "Thermal conductivity of porous alumina ceramics prepared using starch as a pore-forming agent," *J. Eur. Ceram. Soc.*, vol. 29, no. 3, pp. 347–353, Feb. 2009.

[89] H. Kassner, R. Siegert, D. Hathiramani, R. Vassen, and D. Stoever, "Application of suspension plasma spraying (SPS) for manufacture of ceramic coatings," *J. Therm. Spray Technol.*, vol. 17, no. 1, pp. 115–123, 2008.

[90] S. Sampath, X. . Jiang, J. Matejicek, A. . Leger, and A. Vardelle, "Substrate temperature effects on splat formation, microstructure development and properties of plasma sprayed coatings Part I: Case study for partially stabilized zirconia," *Mater. Sci. Eng. A*, vol. 272, no. 1, pp. 181–188, Nov. 1999.

[91] C. G. Joseph, Y. H. Taufiq-Yap, G. Li Puma, K. Sanmugam, and K. S. Quek, "Photocatalytic degradation of cationic dye simulated wastewater using four radiation sources, UVA, UVB, UVC and solar lamp of identical power output," *Desalin. Water Treat.*, vol. 57, no. 17, pp. 7976–7987, 2016.